UNIVERSITY OF OKLAHOMA

GRADUATE COLLEGE

UNDERSTANDING CATALYTIC STRATEGIES FOR BIO-OIL UPGRADING: MODEL COMPOUND STUDIES

A DISSERTATION

SUBMITTED TO THE GRADUATE FACULTY

in partial fulfillment of the requirements for the

Degree of

DOCTOR OF PHILOSOPHY

By

MIGUEL ANGEL GONZALEZ BORJA
Norman, Oklahoma
2014

UNDERSTANDING CATALYTIC STRATEGIES FOR BIO-OIL UPGRADING:
MODEL COMPOUND STUDIES

A DISSERTATION APPROVED FOR THE
SCHOOL OF CHEMICAL, BIOLOGICAL AND MATERIALS ENGINEERING

BY

_____
Dr. Daniel Resasco, Chair

_____
Dr. Robert White

_____
Dr. Friederike Jentoft

_____
Dr. Steven Crossley

_____
Dr. Richard Mallinson

To my Father in Heaven, for it is Him who gives me the ability to produce wealth. *Deut. 8:18*

To my parents, Luis and Clara, for this is the fruit of the seeds they planted and watered during the last 25 years. I love you very much daddy and mommy. I thank God for your lives and the sacrifices you made so that I could be where I am today. Thank you for not giving up on my siblings and I.

Acknowledgements

First of all I would like to acknowledge my Lord Jesus Christ, for He has given me abundant life and strength to overcome every obstacle since the moment I decided to follow Him. He is the most outstanding thing that happened to me during my doctoral studies and I am graceful for the way He pursued me and found me. I thank Him for his love, unconditional like no one in this world could offer.

The second most important thing I found at OU was the woman that makes my heart beat faster and who has the ability to steal a smile from my mouth even in hard moments. I thank my fiancée Dianita because she believed in me, even in times when I did not think I could do it. Her support was indispensable for me to be able to achieve this goal, and has had an eternal impact in my life.

I am immensely thankful with Dr. Daniel Resasco, my advisor and mentor during the last six years. He saw in me talents and abilities that at times not even I could see in myself, and he spoke them out so that I could gain confidence in who I am. He was always encouraging and willing to listen to me; he edified me with his words and also offered great support for the dreams I had about my future. Furthermore, he is a very wise person and I had the privilege to learn from his knowledge and experiences. I want to thank Dr. Resasco for opening his door to me, and for walking this path along my side.

I also want to acknowledge Dr. Friederike Jentoft, Dr. Rolf Jentoft, Dr. Richard Mallinson, Dr. Steven Crossley, Dr. Lance Lobban and Dr. Robert White for his expertise and scientific advice.

Furthermore, I want to thank my friends and colleagues who shared with me an office, a lab space, and a time in life. I specially thank Stefano Cosma, Amalia Botero and Paula Zapata, for their mentoring when I started to work as a researcher and their support when the hard times came. I am also thankful for Manish Budhathoki, Felipe Anaya, Hernando Delgado, Taiwo Omotoso, and every person in our research group; their friendship and presence made the days of my doctoral studies filled with happiness and love.

I thank the National Science Foundation (NSF EPSCoR Award EPS0814361) and the Department of Energy (DE-FG36GO88064 and DE-SC0004600 grants) for their financial support.

This is not an individual success, but the result of all of your support, and I don't have enough words to thank you for what you have helped me achieve.

Table of Contents

Acknowledgements iv

List of Tables xi

List of Figures xiii

Abstract xix

1. Introduction 1

    1.1. Biomass conversion 1

    1.2. Bio-oil upgrading 2

        • Acetic acid upgrading 3

        • Furfural upgrading 5

        • Phenolics upgrading 6

    1.3. Kinetic studies of catalytic reactions 8

2. Bio-oil upgrading strategy and selected model reactions 14

3. Vapor phase upgrading: Phenolics hydrodeoxygenation 19

    3.1. Introduction 19

    3.2. Objectives 21

        • General 21

        • Specific 21

    3.3. Experimental methods 21

        • Thermodynamic calculations 21

        • Materials 22

        • Catalyst synthesis 22

- Catalyst characterization 25
- Catalytic reaction 27

3.4. Results and discussion 27

- Thermodynamic calculations 27
- Inconel supported catalysts characterization 28
- Cordierite supported catalyst characterization 35
- Guaiacol deoxygenation on Inconel supported monometallic and bimetallic catalysts 37
- Comparison of guaiacol and anisole deoxygenation on Inconel supported bimetallic catalyst 42
- Inconel supported catalyst regeneration. 49
- Cordierite supported catalysts activity tests. 50

3.5. Conclusions 52

3.6. Remarks for future work 52

- Catalyst deactivation and regeneration 52
- Synthesis of monolithic catalysts 53
- Catalyst characterization 53
- Other metals for the active phase 53

4. Liquid phase upgrading: Phenolics alkylation with short oxygenates 54

4.1. Introduction 54

4.2. Objectives 56

- General 56
- Specific 56

4.3. Experimental methods 57
- Thermodynamic calculations 57
- Materials 58
- Catalytic reaction 58
- Transport limitations test 59

4.4. Results and discussion 60
- Thermodynamic calculations 60
- Product distribution from alkylation of m-cresol with isopropanol . 61
- Verification of the absence of mass transport limitations 66
- Conversion of isopropyl-methylphenol (thymol) and isopropoxybenzene 68
- Effect of alkylating agent 72
- Reaction pathways and kinetic model 78
- Validating model by independent rate measurements and added constrains 82
- Kinetic modeling results 86

4.5. Conclusions 93

4.6. Remarks for the future 94
- Extension of kinetic modeling to variable temperatures, solvents and catalysts 94
- Experimental setup 95

5. Liquid phase upgrading: water effect on hydrophilic and hydrophobic zeolites for phenolics alkylation 96

5.1. Introduction 96

5.2. Objectives 100

- General 100
- Specific 101

5.3. Experimental methods 101

- Hydrophobic zeolite synthesis 101
- Catalytic reactions 102

5.4. Results and discussion 103

- Phase selectivity in alkylation of m-cresol with isopropanol 108

5.5. Conclusions 110

5.6. Remarks for the future 111

- Deactivation function 111

6. Liquid phase upgrading: water effect on hydrogenation of furfural 112

6.1. Introduction 112

- Water effect on hydrogenation reactions 112
- Solvent effects in liquid phase reactions 113
- Furfural polymerization 114

6.2. Objectives 116

- General 116
- Specific 116

6.3. Experimental methods 116

- Thermodynamic calculations 116
- Materials 117

- Catalyst synthesis and characterization 117
- Catalytic reaction 118

6.4. Results and discussion 119

- Thermodynamic calculations 119
- Thermal stability of furfural in water 119
- Catalysts dispersion 121
- Reactivity and product selectivity in different solvents 123
- Evaluation of transport limitations 132
- Kinetic model of furfural hydrogenation 135

6.5. Conclusions 138

6.6. Remarks for the future 138

- DFT calculations 138
- Experimental data collection 139

7. References 140

List of Tables

Table 3.1. Catalysts metal loading and initial activity 39

Table 4.1. Acid site density of zeolites used for mass transport limitations test. Original zeolite was an HY with Si/Al=30 (first row) 67

Table 4.2. Adsorption constants of reactants and products on HY zeolite in the reaction of m-cresol with isopropanol using two different kinetic models. Units are [l mol^{-1}] 86

Table 4.3. Rate constants for dehydration and polymerization in the reaction of m-cresol with isopropanol using two different kinetic models. Units are [mol l^{-1} h^{-1} $gcat^{-1}$] 88

Table 4.4. Rate constants for alkylation and ether decomposition in the reaction of m-cresol with isopropanol using a Langmuir-Hinshelwood kinetic model. Units are [mol l^{-1} h^{-1} $gcat^{-1}$] 90

Table 4.5. Rate constants for alkylation and ether decomposition in the reaction of m-cresol with isopropanol using an Eley-Rideal kinetic model. Units are [$(h*g\ cat)^{-1}$] for alkylation and [mol l^{-1} h^{-1} $gcat^{-1}$] for ether decomposition 91

Table 4.6. Deactivation parameters in the reaction of m-cresol with isopropanol 92

Table 5.1. Specific Area (S_{BET}) and Micropore Volume (V_{micro}) of silane-functionalized H-USY zeolites compared to the untreated H-USY zeolite before and after reaction for 22 h at 200°C and 700 psi in He. Feed: isopropanol/m-cresol (3/1 molar ratio); total molar concentration: 2 M 98

Table 5.2. Kinetics analysis of the m-cresol and 2-propanol reaction with the proposed reaction pathway 103

Table 5.3. Reaction and deactivation constants obtained at 200°C and 700psi of He over untreated and functionalized HY zeolite (Si/Al molar ratio: 30). Feed: isopropanol/m-cresol moar ratio:4; total molar concentration: 2.5M 106

Table 6.1. Dispersion of a series of Pd/C catalysts measured by two different methods 122

Table 6.2. Turnover frequency for furfural conversion over different Pd/C catalysts 132

List of Figures

Figure 2.1. Integrated strategy for catalytic upgrading of bio-oil fractions 15

Figure 3.1. Concentrations at equilibrium for reactant and products of guaiacol hydrodeoxygenation at 1 atm 27

Figure 3.2. (a) Cylindrical shape Inconel monolith, (b) SEM picture showing monolith structure..... 28

Figure 3.3. SEM pictures of monolithic catalysts: (a) Blank/Inconel, (b) and (c) CNF/Inconel (d) High magnification image to show the CNF 29

Figure 3.4. Energy dispersive X-ray spectroscopy (EDS) analysis of a Cu-Inconel sample covered with carbon nanofibers 29

Figure 3.5. Carbon-nanofibers burn off profile in CNF/Inconel catalyst..... 30

Figure 3.6. TEM pictures of carbon nanofibers: (a) Before impregnation with Pt-Sn (b) After impregnation with Pt-Sn and calcination 31

Figure 3.7. TPR profiles for catalyst supports, monometallic catalysts and bimetallic catalysts 34

Figure 3.8. (a) Honeycomb geometry cordierite monolith, (b) SEM picture showing morphology of the channel wall's surface 35

Figure 3.9. Nickel concentration along the walls of cordierite monolith synthesized with vacuum oven drying. Top: SEM photographs showing morphology of the wall. Bottom: EDS map for the element nickel (purple) 36

Figure 3.10. Nickel concentration along the walls of cordierite monolith synthesized with freeze-drying. Top: SEM photographs showing morphology of the wall. Bottom: EDS map for the element nickel (purple)..... 36

Figure 3.11. SEM pictures of monolithic catalysts: (a) Bare cordierite, (b) Al_2O_3/Cordierite (c) CNF/ Al_2O_3/Cordierite 37

Figure 3.12. Guaiacol conversion over monometallic catalysts. Conditions: P=1atm, T=400°C, W/F=3.4 g catalyst/(g reactant/h), H_2/feed molar ratio=30 38

Figure 3.13. Guaiacol conversion and product yields over mono- and bimetallic catalysts: (a) Sn/Inconel, (b) Pt/Inconel, (c) Pt-Sn/Inconel, and (d) Pt-Sn/CNF/Inconel. Conditions: P=1atm, T=400°C, W/F=3.2 g catalyst/(g reactant/h), H_2/feed molar ratio=30 39

Figure 3.14. Pt-Sn/CNF/Inconel catalyst deactivation for two different reactants: (a) Anisole, and (b) Guaiacol. W/F is g catalyst/(g reactant/h). Conditions: P=1atm, T=400°C, H_2/feed molar ratio=30..... 43

Figure 3.15. Product yields over Pt-Sn/CNF/Inconel catalyst for different reactants: (a) Anisole TOS 45 min, (b) Anisole TOS 125 min, (c) Guaiacol TOS 45 min, (d) Guaiacol TOS 125 min. W/F is g catalyst/(g reactant/h). Conditions: T=400°C, and P=1atm, H_2/feed molar ratio=30 44

Figure 3.16. Gas chromatography analysis of non-condensable gases from anisole hydrodeoxygenation 45

Figure 3.17. Reaction scheme for guaiacol deoxygenation on Pt-Sn/CNF/Inconel catalyst. 47

Figure 3.18. Reaction scheme for anisole deoxygenation on Pt-Sn/CNF/Inconel catalyst 49

Figure 3.19. Regeneration of a Pt-Sn/CNF/Inconel catalyst using hydrogen flow at high temperature. Reaction conditions: Conditions: P=1atm, T=400°C, W/F=0.39 g catalyst/(g reactant/h), H_2/feed molar ratio=30 50

Figure 3.20. Activity and product yields for cordierite supported catalysts. Conditions: P=1atm, T=400°C, W/F=1.1 g catalyst/(g reactant/h), H_2/feed molar ratio=30, time on stream=85min 51

Figure 4.1. Concentrations at equilibrium for reactant and products of m-cresol alkylation at 47.6 atm 61

Figure 4.2. Product distribution from alkylation of m-cresol with isopropanol. (a) Dehydration/oligomerization products. (b) Alkylation products. Conditions: isopropanol/m-cresol=3.8, T=473K, P=4.8MPa, catalyst mass=50mg HY 62

Figure 4.3. Products from alkylation of m-cresol with isopropanol..... 63

Figure 4.4. MS fragmentation pattern for methyl-isopropoxybenzene from the reaction mixture 64

Figure 4.5. MS fragmentation pattern for isopropylmethylphenol from the reaction mixture 65

Figure 4.6. GC-MS chromatogram with products from alkylation of m-cresol with isopropanol over a HY zeolite. Column was Rtx-1701 with mid-polarity 65

Figure 4.7. Initial alkylation rates for catalysts with different acid site concentration. Conditions: IPA/m-cresol=3.8, T=473K, P=4.8MPa, reaction: 1h 67

Figure 4.8. Product distribution from alkylation of thymol (IMP) with isopropanol. (a) Dehydration/oligomerization products. (b) Alkylation products. Conditions: isopropanol/thymol=3.8, T=473K, P=4.8MPa, catalyst mass=50mg HY 68

Figure 4.9. Possible routes of conversion for methyl-isopropoxybenzene 69

Figure 4.10. Alkylation of methoxybenzene with isopropanol as a function of time. Conditions: isopropanol/methoxybenzene=4:1, temperature=200°C, pressure=700psi 70

Figure 4.11. Product distribution from decomposition of isopropoxybenzene. Conditions: initial concentration=0.51M, T=473K, P=4.8MPa, catalyst mass=50mg 71

Figure 4.12. Isopropoxybenzene decomposition and subsequent alkylation 72

Figure 4.13. Electrophilic substitution of m-cresol with isopropanol and propylene 73

Figure 4.14. Effect of isopropanol/m-cresol molar ratio and conversion on the selectivity to etherification products. Conditions: T=473K, P=4.8MPa 74

Figure 4.15. Alkylated and ether product yields for alkylation of m-cresol with propylene and isopropanol. Conditions: isopropanol or propylene/m-cresol=3.8, T=473K, P=4.8MPa, catalyst mass=20mg HY, reaction time=1h 75

Figure 4.16. Rate of dehydration and alkylation during reaction of isopropanol with m-cresol over a HY zeolite. Conditions: T=473K, P=4.8MPa 76

Figure 4.17. Alkylation via an oxonium and a carbenium ion 77

Figure 4.18. Product yields for alkylation of m-cresol with n-propanol. Conditions: n-propanol/m-cresol=3.7, T=473K, P=4.8MPa, catalyst mass=50mg HY, reaction time=1h 77

Figure 4.19. Reaction scheme for the reaction of m-cresol with isopropanol in the presence of HY zeolite. C_3H_8O: isopropanol. C_3H_6: propylene 80

Figure 4.20. Rate of isopropanol dehydration measured at different isopropanol concentrations and short reaction time. Conditions: T=473K, P=4.8MPa, catalyst mass=10mg HY, reaction time=0.2h 83

Figure 4.21. Rate of isopropoxybenzene decomposition measured at different isopropoxybenzene concentrations and short reaction time. Conditions: T=473K, P=4.8MPa, catalyst mass=20mg HY, reaction time=0.5h 84

Figure 4.22. Effect of m-cresol on the rate of isopropanol dehydration. Conditions: T=473K, P=4.8MPa 87

Figure 4.23. Langmuir-Hinshelwood kinetic model results 92

Figure 4.24. Eley-Rideal kinetic model results 93

Figure 5.1. Evolution of zeolite crystallinity as a function of reaction time at 200°C and 700 psi in He in an emulsion system. Feed: isopropanol/m-cresol (3/1 molar ratio); total molar concentration: 2 M 98

Figure 5.2. SEM images of the untreated H-USY zeolite (Si/Al = 30) after 22h reaction of m-cresol and isopropanol at 200°C and 700 psi of He in an emulsion system. Feed: isopropanol/m-cresol (3/1 molar ratio); total molar concentration: 2 M 100

Figure 5.3. SEM images of the OTS-functionalized H-USY zeolite after 22 h reaction of m-cresol and isopropanol at 200°C and 700 psi of He in an emulsion system. Feed: isopropanol/m-cresol (3/1 molar ratio); total molar concentration: 2 M 100

Figure 5.4. Kinetic fitting results for alkylation of m-cresol with isopropanol in 4 different systems (catalyst: untreated and OTS-functionalized H-USY; solvents: decalin single phase and water/decalin emulsion) 104

Figure 5.5. Comparison of measured product concentrations and calculated concentrations based on the fittings using the simplified kinetics model described in Table 5.2 for the four cases investigated (catalyst: untreated and OTS-functionalized H-USY; solvents: decalin single phase and water/decalin emulsion) 105

Figure 5.6. Deactivation function according to the expression $k_i = k_i^0 e^{-\tau t}$ 107

Figure 5.7. Product yield from alkylation of m-cresol with isopropanol in two different systems: HY indicates a hydrophilic zeolite in single decalin phase; OTS Biphasic indicates a hydrophobic zeolite in a biphasic water/decalin phase. (a) Mono-alkylated products. (b) Di-alkylated products 109

Figure 5.8. Ratio of ether to ring-alkylated products over two different systems: HY indicates a hydrophilic zeolite in single decalin phase; OTS Biphasic indicates a hydrophobic zeolite in a biphasic water/decalin phase 110

Figure 6.1. Concentrations at equilibrium of reactant and products of hydrogenation of furfural and furfuryl alcohol at 20.4 atm..... 119

Figure 6.2. Furfural disappearance at different temperatures in an aqueous environment under pressurized hydrogen (500psi). Test time: 3h. 120

Figure 6.3. Products from furfural thermal stability test. Temperature of the test, from left to right, was: 50°C, 150°C and 250°C. 120

Figure 6.4. Particle size distribution for a series of Pd/C catalysts, measured by TEM..... 121

Figure 6.5. Furfural conversion in different solvents. Conditions: initial concentration=0.1M, T=323K, P=2.1MPa, catalyst mass=20mg 5%Pd/C (commercial), reaction time=1h 124

Figure 6.6. Furfural hydrogenation products at mild conditions..... 125

Figure 6.7. Product yield for furfural ring hydrogenation (Ring HYD), aldehyde hydrogenation (Aldehyde HYD) and other products in different solvents. Conditions: initial concentration=0.1M, T=323K, P=2.1MPa, catalyst mass=20mg 5% Pd/C (commercial), reaction time=1h..... 126

Figure 6.8. Product yield in different solvents at the same level of furfural conversion (41%). Conditions: initial concentration=0.1M, T=323K, P=2.1MPa, catalyst mass=20mg 5%Pd/C (commercial)..... 127

Figure 6.9. Furfuryl alcohol conversion in different solvents. Conditions: initial concentration=0.1M, T=323K, P=2.1MPa, catalyst mass=20mg 5%Pd/C (commercial), reaction time=0.33h 130

Figure 6.10. Product yield for furfural ring hydrogenation (Ring HYD) and other products in different solvents. Conditions: initial concentration=0.1M, T=323K, P=2.1MPa, catalyst mass=20mg 5%Pd/C (commercial), reaction time=1h 131

Figure 6.11. Variation of turnover frequency for furfural hydrogenation as a function of catalyst metal loading 133

Figure 6.12. Conversion of furfural and product yields at different stirring speeds. Conditions: initial concentration=0.1M, T=323K, P=2.1MPa, catalyst mass=50mg 1.0%Pd/C, reaction time=1h 135

Figure 6.13. Reaction scheme for furfural hydrogenation in liquid phase 136

Figure 6.14. Conversion and product evolution as a function of time in hydrogenation of furfural, furfuryl alcohol and a mixture of furfural and furfuryl alcohol. Conditions: initial concentration=0.1M, T=323K, P=2.1MPa, catalyst mass=50mg 1.0%Pd/C 137

Abstract

In light of the awareness about climate change and the role that non-renewable sources of energy have had on this issue, there has been a notable effort in the last decades to develop alternative sources of energy. Conversion of ligno-cellulosic biomass has been of special interest because of its potential to produce liquid bio-fuels for direct use in the existing transportation infrastructure. The raw product from ligno-cellulosic biomass thermal processing is bio-oil, an unstable liquid with high content of oxygen. Upgrading the properties of this liquid is challenging, but indispensable in order to make it a suitable transportation fuel or even a source of fine chemicals. The approach for such upgrading has been to use catalytic processes that can selectively remove oxygen while maximizing the carbon retention in the liquid product. The aim of this work is to propose strategies for bio-oil upgrading and provide a fundamental understanding of the phenomena involved in such processes. Since bio-oil is a complex mixture, a set of model reactions was selected for this study. This allowed to understand the simplest cases, and is expected to serve as a foundation for the study of more complex systems, as they get closer to the real bio-oil.

The first stage in the upgrading scheme was proposed to be a vapor phase upgrading stage, and the model reaction studied was hydrodeoxygenation of methoxyphenols over a monolithic catalyst. It was shown that a bimetallic monolith supported catalyst could remove significant amounts of oxygen from guaiacol and anisole under mild reaction conditions. The products from this

initial upgrading could then be condensed and undergo liquid phase reactions such as alkylation or hydrogenation; these reactions comprised the second upgrading stage.

Alkylation of phenolics with short alkyl alcohols (both originated from bio-oil) is beneficial because it retains the short compounds in the liquid product as opposed to producing light gases. A kinetic study for alkylation of m-cresol with isopropanol (both model compounds) using a HY zeolite revealed that both ether and ring alkylated products could be obtained and their selectivity could be correlated to factors such as the type of alkylating agent, degree of alkylation, time of reaction, among others. In addition to these, the presence of water had important effects on catalyst activity and therefore its effect was subject of further study. Hot liquid water can severely degrade acidic solids such as the zeolites used for alkylation leading to dramatic deactivation during reaction. A plausible solution is to use a hydrophobic catalyst that could prevent the contact of the solid with liquid water and preserve catalytic activity. With this in mind, it was possible to synthesize and measure the rate of deactivation of a hydrophobic HY zeolite, probing its tremendous advantages over regular zeolites.

As opposed to the alkylation reaction, water may have a positive effect in reactions such as hydrogenation, which are key for bio-oil upgrading. The role of water was then studied using hydrogenation of furfural as a model reaction. Furfural is another product obtained in bio-oil that evolves from the hemicellulose fraction in biomass. It was shown that water could significantly increase the rate of furfural hydrogenation in liquid phase as well as

dramatically change the product selectivity. Based on previous studies about the role of water on hydrogenation reactions, it was proposed that water could decrease activation barriers for hydrogenation by shuttling hydrogen atoms from the surface to the furfural molecule as well as stabilizing particular transition states through hydrogen bonding interactions. A future kinetic model for this system could provide further proof of this hypothesis.

1. Introduction

1.1. Biomass conversion

The use of biomass for the production of fuels and chemicals has been extensively investigated in the last years.[1-7] It has been proposed that biomass in the form of wood, grass, crops or agricultural waste could be treated by pyrolysis or gasification in order to produce bio-oil or synthesis gas, respectively. One advantage of these processes is that usually no chemical pretreatment of the feed is required, but only a few physical operations (i.e. drying, grinding) should be performed before the biomass can be fed into a pyrolyzer or a gasifier. On one hand, pyrolysis bio-oil could potentially be refined to produce transportation fuels or chemicals. On the other hand, synthesis gas could and has been used for Fischer-Tropsch synthesis, as well as methanol and dimethyl ether production. Special emphasis has been given to the upgrading of bio-oil obtained from fast pyrolysis because it is a liquid product readily obtainable in large scale, but highly susceptible to degradation with time and temperature. Upgrading and stabilization of bio-oil is a challenging task because of its chemical complexity; it contains hundreds of compounds with multiple functional groups, most of them oxygenated.[8,9] Recently, it was proposed that direct production of bio-oil fractions containing specific groups of compounds, as opposed to production of whole bio-oil could be beneficial for upgrading.[10,11] By following this approach, a particular strategy for improving the properties of each fraction could be developed and the complexity due to the presence of multiple functional groups in the reaction system be significantly reduced. Fractionation of

bio-oil is achieved either by a step-wise condensation of pyrolysis vapors or by a multi-stage pyrolysis process, in which each fraction is obtained from treating biomass at different temperatures and times. In this way, separate fractions with high concentration of light oxygenates (acids, aldehydes, ketones), sugar derived compounds, and phenolics can be obtained, respectively.

An alternative for the utilization of biomass, as opposed to processing it as a whole, is to separate it into its main components, i.e. cellulose, hemicellulose and lignin. Each of these fractions could then be treated individually in order to obtain either fuels or chemicals. This approach somehow resembles the scheme of a conventional refinery, where crude oil is first separated into different fractions and then each fraction is further processed in order to maximize the yield of desired products. Because of this conceptual similarity, some authors have referred to this approach for processing biomass as a biorefinery.[12]

1.2. Bio-oil upgrading

Bio-oil obtained from fast pyrolysis has high oxygen content, which makes the product unsuitable for transportation fuels. This inadequacy of bio-oil creates the need for novel catalytic processes to upgrade the pyrolysis products with the required stability and fuel properties.[13,14] The compounds present in bio-oil (besides water) can be grouped in three families: short oxygenates, sugar-derived and phenolic compounds. Upgrading of this oxygenated mixture has been carried out over different types of catalysts. Several studies during the 90's used zeolites to convert oxygenated model compounds as well as whole bio-oil.[15-17] At the same time, motivated by the obvious advantage of co-processing bio-oil in existing

refinery operations, deoxygenation studies of bio-oil model compounds over conventional hydrotreating (HDT) catalysts have been conducted.[7,18,19] More recently, supported platinum catalysts have been investigated in the upgrading of model bio-oil mixtures.[20]

Model compound studies have been crucial for proposing and understanding strategies for bio-oil upgrading. Although they focus on a single reactant and reaction (at most two or three reactants), they provide valuable information regarding potential catalysts, product distributions, and reaction mechanisms, among others. Some examples of representative molecules for model studies are acetic acid (small oxygenate), furfural (sugar-derived), and guaiacol/cresols (phenolics), and some of the recent work on upgrading these compounds is presented next.

• *Acetic acid upgrading*

Acetic acid is the most abundant short oxygenate compound present in bio-oil and it contributes to the corrosiveness and instability of the same. A promising route for the elimination of acetic acid and other carboxylic acids from bio-oil is ketonization. This reaction has been conventionally carried out over metal oxide catalysts at relatively high temperatures in the vapor phase. However, as mentioned before, it would be advantageous for this upgrading step to take place in the liquid phase, in order to avoid the problem of vaporizing bio-oil. Pham et al. studied in detail the ketonization of acetic acid in the liquid phase.[21] They showed that a $Ru/TiO_2/C$ catalyst could successfully yield acetone in an aqueous environment at temperatures below 200°C. Furthermore they proposed that a Ti^{3+} species, whose formation was

possible in the presence of water, was responsible for the ketonization reaction, and the hydrophobic nature of the carbon prevented inhibition of the reaction by water molecules. The production of acetone in bio-oil increases its stability, however this molecule still has a short carbon chain and might be lost during hydrodeoxygenation processes. With this in mind, it is desirable to couple acetone with other molecules in bio-oil in order to increase carbon chain length, and thus liquid yield. A simple way of doing this is turning acetone into an alkylating agent such as isopropanol, which can easily undergo dehydration and alkylate phenolic compounds. Nie et al. used a two-bed flow reactor (vapor phase) in order to consecutively hydrogenate acetone and alkylate m-cresol with the in-situ produced isopropanol, proving the feasibility of this strategy.[11] The catalysts used in their tests were Cu/SiO_2 and Pt-Fe/ SiO_2 for hydrogenation and zeolite Hβ for alkylation.

Another way to couple short oxygenates with other fractions of bio-oil is through esterification reactions. Furfural can be easily hydrogenated to furfuryl alcohol, which is able to undergo esterification with acetic acid. Yu et al. studied this conversion route using a bifunctional Pd/Al-SBA-15 catalyst that could simultaneously perform hydrogenation and esterification. They demonstrated that a catalyst with medium Si/Al ratio (22) could successfully perform the reaction, yielding esters and alcohols as the upgrading products.[22] Furthermore, some studies have focused on the effect other bio-oil components have on acetic acid upgrading reactions. Hakim et al. looked at the rate of ketonization of acetic on a ceria-zirconia mixed oxide in the presence of furfural and acetol.[23] Furfural significantly reduced the rate of acetic acid conversion but its effect was reversible

and the original activity could be recovered after removing furfural from the feed. On the contrary, acetol did not affect the ketonization rate, and in turn was active in the formation of pyruvaldehyde and 1,2 propylene glycol. Lohitharn et al. studied the effect of aldehydes in the esterification of acetic with ethanol.[24] They observed that at high temperatures the rate of esterification was not influenced by the presence of aldehydes. However, as the reaction temperature was decreased, the effect of aldehydes became significant, and the conversion of acetic acid decreased up to 28%. This was attributed to a competition between esterification and acetalization, since the latter is faster at lower temperatures.

• *Furfural upgrading*

Two main routes have been proposed for conversion of furfural. The first one is condensation with short oxygenates also present in bio-oil, particularly acetone, that as mentioned before, is a direct product from acetic acid ketonization. Zapata et al. investigated the liquid phase aldol-condensation of furfural with acetone in a biphasic system using nanohybrid catalyst particles. These particles were composed of basic oxide nanoparticles joined to carbon nanotubes.[25] They demonstrated that the biphasic system was successful for the production of C_8-C_{10} oxygenated compounds, which could further be hydrogenated to produce long chain alkanes.

The second route for furfural conversion involves hydrogenation as well, but without previous condensation reactions. Sitthisa et al. looked at the hydrogenation of furfural in vapor phase and the effects of different metal catalysts on activity and product selectivity.[26] For example, they compared Cu/SiO_2 and Pd/SiO_2 catalysts and found that on copper furfuryl alcohol was the preferred product whereas on

palladium furan and tetrahydrofuran were dominant. This change in product selectivity was due to the adsorption mode that furfural takes on each of the metal surfaces, which determines the favored reaction pathway. Furthermore, they proposed the use of bimetallic catalysts such as Pd-Cu and Pd-Fe. The latter had an outstanding selectivity towards 2-methylfuran, a product that is a good candidate for gasoline blend due to its high octane number. Hydrogenation of furfural has also been carried out in the liquid phase, where the product selectivity is significantly different from the vapor phase. Zhou et al. looked at the hydrogenation of furfural in aqueous phase using different catalysts, i.e. Ni/CNT and CuMgAl hydrotalcites.[27,28] Working at relatively mild conditions (temperature around 100 °C), they were able to produce cyclopentanol with selectivity up to 95%. Water appeared to play a key role in the reaction mechanism, as it was able to promote ring opening of furfuryl alcohol, which was rapidly obtained from furfural hydrogenation.

• *Phenolics upgrading*

Among the phenolics, guaiacols and cresols are the most abundant compounds. Guaiacols have one or several methoxy groups, which decompose at high temperatures and can adsorb strongly on the catalyst surface. For this reason they can quickly deactivate both acid and metal catalysts (as demonstrated in Chapter 2). In this regard, Boonyasuwat et al. investigated a series of supported ruthenium catalysts for the conversion of guaiacol (2-methoxyphenol).[29] Among the different supports used by them, titanium oxide showed the highest activity and selectivity towards aromatic compounds, resulting in fully deoxygenated products.

It was proposed that a synergy between ruthenium and titanium oxide allowed for an enhanced performance as compared to the other supports. Most likely, ruthenium served as a promoter for titanium oxide reduction, thus generating new active acids on the oxide surface or at the interface with the metal particles. In a similar study, Guo et al. investigated the hydrogenation of eugenol over a Ru/SBA-15 catalyst in the liquid phase.[30] The upgrading reaction was carried out in different polar solvents and isopropanol resulted in the higher activity for eugenol conversion. The final products were saturated alcohols and in some cases hydrocarbons. No severe deactivation of the catalyst was observed with single model compounds, however significant coke formation was detected when the catalyst was tested with real bio-oil. Besides conversion of methoxyphenols (guaiacols), hydrodeoxygenation of cresols has also been studied over metal supported catalysts. Recently, Nie et al. studied this system over bimetallic catalysts, namely Ni-Fe metal alloys.[31] A comparison between mono- and bimetallic catalysts depicted that nickel alone favored the formation of ring-saturated oxygenated molecules such as methylcyclohexanone and methylcyclohexanol (to a lesser extent). On the other hand, the metal alloy selectively produced toluene, showing the superior performance of the bimetallic catalyst. The enhanced properties of this catalyst were attributed to its higher ability to hydrogenate the carbonyl group of a proposed ketone intermediate as opposed to hydrogenating the aromatic ring.

Alkylation of phenolics with long-chain olefins has also been studied as a strategy for bio-oil upgrading. Yang et al. investigated alkylation of phenol, catechol and guaiacol with 1-octene using a heteropolyacid catalyst [$Cs_{(2.5)}H_{(0.5)}PW_{(12)}O_{(40)}$/K-10]

in the liquid phase.[32] They monitored the selectivity towards O-alkylated products and found that it was favored at a 1:1 molar ratio of phenol to 1-octene and at lower temperatures (both with phenol and catechol), whereas the presence of the methoxy group in guaiacol inhibited the rate of alkylation at the oxygen atom. In another study Zhang et al. also looked at this alkylation reaction, evaluating a series of solid acid catalysts (Amberlyst 15, Dowex50WX2 and Dowex50WX4) and the effect of water in product selectivity.[33] They found that overall activity towards alkylation was high up to 120 °C and that the presence of water enhanced the selectivity towards O-alkylation products.

1.3. Kinetic studies of catalytic reactions

Most of the studies mentioned in the previous section involved the use of kinetic modeling and therefore a description of the importance and applications of this tool is to follow. A kinetic model is a representation that describes the mechanism of a chemical reaction and provides information about how the experimental conditions, e.g. temperature, concentrations, etc., affect the rate of reaction. In a typical kinetic model, a series of elementary steps are used to show how the reactants transform into the products at the molecular level. These steps can be used to derive a rate expression, which dictates the rate of reaction as a function of concentration of species involved in the reaction, thermodynamic equilibrium (if present), temperature and molecular interactions (both implicit in the rate constant), and in the presence of a catalyst, also as a function of the interaction between chemical species and catalyst surface (implicit in the adsorption constants). Many of the reactions for bio-oil upgrading are carried out in the presence of a catalyst; therefore

any kinetic model for such reactions should consider all of the parameters just mentioned.

A catalyst is a material that accelerates the progress of a reaction towards the chemical equilibrium. Therefore, before trying to explain the effect of a catalyst in any reaction, one should be aware of what the equilibrium state is at the reaction conditions. It is also important to consider the transport phenomena that are present in catalytic reaction systems.[34] When a porous solid particle is used as the catalyst, transport limitations may be introduced in the reaction system. In this type of fluid-solid system, the reactants need to diffuse from the bulk phase (gas or liquid) to the catalyst surface (external diffusion), and from the catalyst surface to the interior of the pores (internal diffusion); if these diffusional processes are not fast enough the reaction rate measured experimentally may be a combination of diffusion and reaction rates. Furthermore, if there is not an effective heat transfer from the active sites of the catalyst to the bulk phase or vice versa, the measured reaction rate may not correspond to the working temperature. This is especially important for exothermic reactions where a local temperature increase can greatly increase reaction rates.

There are several methods to evaluate whether a reaction system is under the influence of mass transfer limitations.[35,36] Consider first internal diffusion processes. The Thiele modulus and the Weisz-Prater parameter are good indicators for the magnitude of the rate of diffusion relative to the rate of reaction. Thiele modulus can be calculated if the geometry of the catalyst particle and the true rate constant are known. Weisz-Prater parameter is obtained from easily measured

quantities such as the radius of the catalyst particle and concentration of reactants at the surface. Effective diffusivity inside the pores is needed as well, and it can be estimated from molecular theory. In addition to these parameters, an experimental test to investigate internal diffusion could also be performed. If the reaction rate does not change when the size of the catalyst pellets is changed, then it is probable that internal diffusion limitations are not present. Consider now external diffusion limitations in liquid phase reactions. A simple experimental test to evaluate this effect is to measure the rate of reaction as a function of stirring speed; an invariant rate is an indication for the absence of such effects. One should be careful with this test because some reactors, specially laboratory scale ones, operate at low particle Reynolds numbers, which makes the diffusion at the external surface of the particle not dependant on the stirring speed. Madon and Boudart proposed a method to experimentally determine the presence of transport limitations in a reaction system.[36] This method is based on the statement that under the kinetic regime (i.e. no artifacts present) the rate of reaction is directly proportional to the concentration of active sites in the catalyst. This statement is known as the Koros-Nowak criterion. It can be proven that if the natural logarithm of the concentration of active sites is plotted against the natural logarithm of the reaction rate, a straight line with slope of one will result if there are not any internal or external mass transfer limitations. The test can be performed at different temperatures and if the slope remains to be one then heat transfer limitations are not present. The advantage of applying this methodology is that every kind of artifact, i.e. transport limitations and poisoning of catalyst, can be evaluated with the same set of experimental data. This

data set is simply the rate of reaction measured over a series of catalyst with different concentration of active sites (e.g. different metal loading). It should be noticed that, if dealing with a structure sensitive reaction, the dispersion of the active phase should be kept constant over the different catalyst samples; otherwise the test would not be valid.

Once the thermodynamic equilibrium of a reactive system has been determined and the effects of mass and heat transfer been evaluated, it is possible to collect relevant kinetic data. This data can then be used to find the kinetic model that best describes the system. As mentioned before, a kinetic model contains parameters that account for the effect of temperature and molecular interactions (between chemical species and with the surface) on the reaction rate. These parameters are the rate constant and the adsorption constant. When these constants are evaluated at different temperatures, it is possible to estimate changes in enthalpy and entropy for both reaction and the adsorption processes. Consider a system where reactants can go to products through different pathways, which are characterized by a particular molecular configuration. There is one pathway which possesses a potential energy that is lower than the other ones, therefore being the favored when going from reactants to products. In this pathway of minimum potential energy there is a point where the energy of the system reaches a maximum and then decreases to give the products of reaction. This energetic state with the maximum potential energy in the minimum potential energy pathway is called the transition state. The configuration of the molecules at the transition state is called the activated complex.

A study of the transition state based on quantum mechanics principles allows expressing the rate constant in terms of the partition function of reactants and activated complex.[34] These partition functions (Q's) are a representation of the energy state of each of the species. For a reaction where A ⇔ B, the rate constant can be expressed as:

$$k = \frac{k_B T}{h} \frac{Q^{\neq}}{Q_A Q_B} e^{-E_0/RT} = A e^{-E_0/RT} \qquad (1.1)$$

Here k is the rate constant, k_B is the Boltzman constant, T is the reaction temperature, h is the Planck constant, Q is the partition function for the activated complex, and species A and B respectively, E_0 is the activation energy, R is the gas constant and A the pre-exponential factor. Notice the second part of the equation is the known Arrhenius Equation that is useful to calculate activation energies. A thermodynamic analysis of the transition state is also possible, and this one provides a way for the calculation of not only activation energy but also the change in entropy between reactants and the transition state.

$$k = \frac{k_B T}{h} e^{-\Delta G^0_{\neq}/RT} = \frac{k_B T}{h} e^{\Delta S^0_{\neq}/R} e^{-\Delta H^0_{\neq}/RT} = A e^{-\Delta H^0_{\neq}/RT} \qquad (1.2)$$

In solid and liquid phase reactions the change in enthalpy between the reactants and the transition state can be assumed, to a good approximation, to be the activation energy. The above equation shows that the probability for a reaction to take place depends not only on the energy barrier that needs to be overcome but also in the entropic changes between reactants and transition state. For example, a reaction with high activation energy could still be favorable if the change in entropy is relatively large.

The adsorption-desorption equilibrium of a molecule can be described in terms of an equilibrium constant K. This equilibrium constant can be written as a function of thermodynamic quantities as follows,

$$K_{Ads} = e^{-\Delta G^0_{Ads}/RT} = e^{\Delta S^0_{Ads}/R} e^{-\Delta H^0_{Ads}/RT} \quad (1.3)$$

Therefore, it is also possible to estimate changes in entropy and enthalpy for adsorption of molecules on the catalyst surface.

The equations presented here provide a powerful tool for estimation of activation energies, activation entropies, and enthalpies and entropies of adsorption from experimental reaction data and therefore it is important to understand where they come from.

2. Bio-oil upgrading strategy and selected model reactions

It is evident from the previous chapter that the problem of bio-oil upgrading is not an easy one. The high diversity of families of compounds present in bio-oil demands an upgrading strategy able to carry out consecutive and even simultaneous reactions that increase the stability of crude bio-oil and brings its properties as close as possible to the desired final product. In this work, the proposed strategy involves both vapor and liquid phase upgrading and it is believed to be beneficial because it takes advantage of the various physical states of bio-oil during its processing while seeking to minimize the consequences of degradation in the overall process. Figure 2.1 shows a general schematic of such strategy. A multi-stage thermal treatment of biomass generates three main streams rich in a particular functional group, although lesser amounts of other functionalities are observed within all fractions. Due to the higher temperature of this thermal processing, most compounds exit the torrefaction unit as vapors. Since bio-oil degradation is believed to start right after the products are condensed into liquids, it would be advantageous to perform an initial stabilization in the vapor phase, before condensing the products. This would allow obtaining pseudo-stabilized oil that is easier to handle. It is to be expected that each torrefaction stream would require a different type of catalyst, according to their composition.

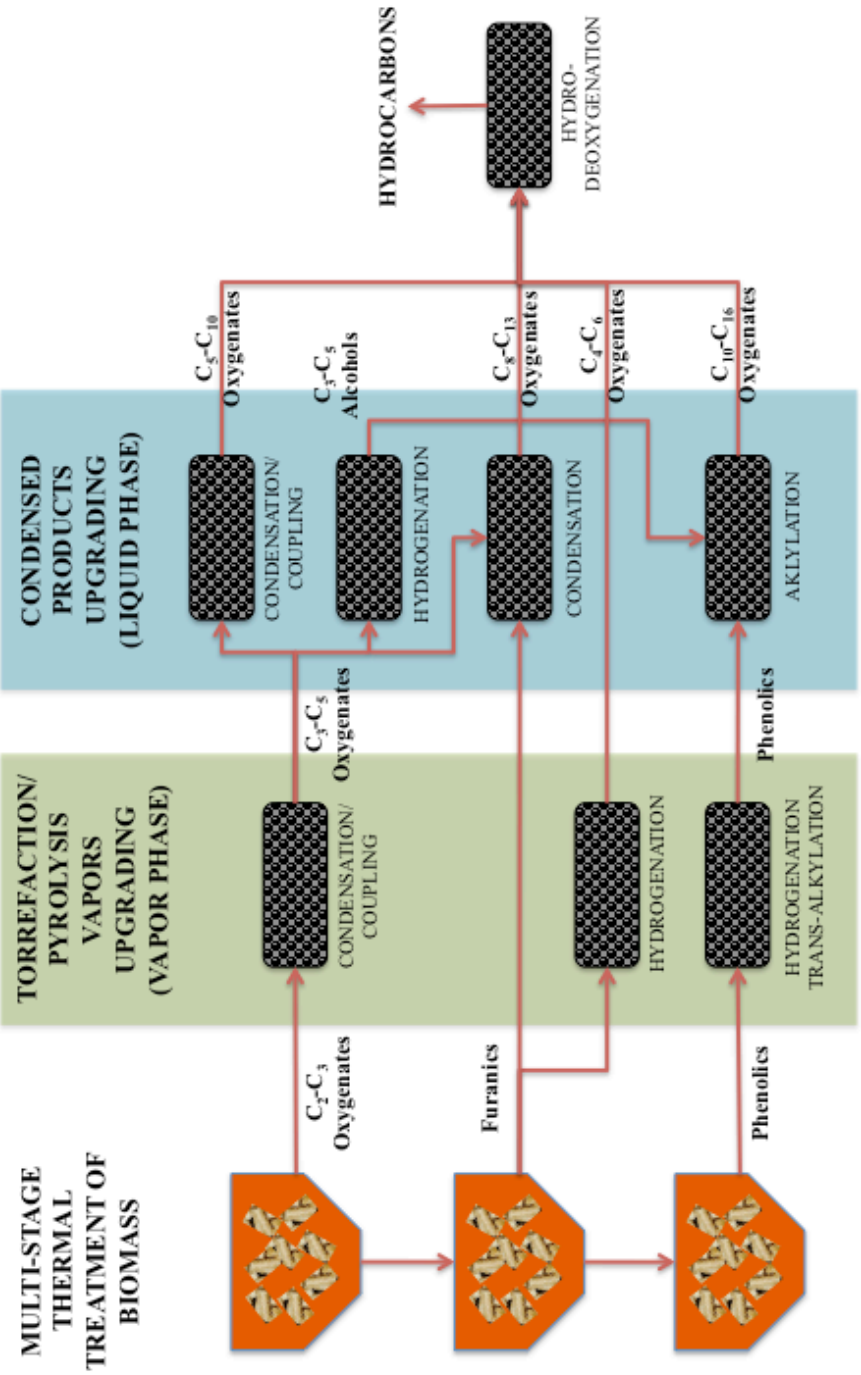

Figure 2.1. Integrated strategy for catalytic upgrading of bio-oil fractions

Thus it is proposed that short oxygenates undergo condensation reactions that can increase the carbon number and reduce the acid content of the torrefaction products. Furanics and phenolics could undergo mild hydrogenation reactions that partially reduce the oxygen content and increase stability of the condensed product. After this initial vapor phase upgrading, the liquid product from each fraction could then undergo further conversions in the liquid phase. Vapor phase upgrading is not likely to produce a fully stable liquid and there might still be complications while trying to vaporize these liquids. Therefore working in the liquid phase after the initial upgrading stage seems to be a better alternative. On top of this, liquid phase reactions, and particularly biphasic systems, offer additional advantages such as in situ separation of products from reactants and the possibility of performing phase-selective reactions; both of these are dependent on the partition of reactants and products between the two liquid phases. Most of the liquid phase reactions in the scheme from Figure 2.1 are related to coupling and carbon chain growth because, as mentioned before, it is desired to minimize the loss of carbon yield in the liquid as much as possible. Short oxygenates could undergo multiple condensation steps, or be combined with furanics or phenolics for aldol-condensation or alkylation reactions, respectively. Finally, the products from these condensation reactions, which would still have moderate oxygen content, could be fully deoxygenated in order to produce liquid hydrocarbons. This deoxygenation step could be in vapor or liquid phases.

With this upgrading scheme in mind, the next step is to look into the specific reactions that would take place and gain in-depth understanding of the catalyst and

reaction mechanisms involved. This will allow predicting outcomes under certain reaction conditions as well as proposing improvements and new alternatives for the upgrading strategy.

In the following chapters a study of three different reactions systems (model compounds reactions) will be presented.

- Vapor phase upgrading: Phenolics hydrodeoxygenation. A monolithic catalyst offers the advantage of a low-pressure drop while handling high gas flow rates. Therefore it is an attractive approach for the initial vapor phase upgrading stage. The model reaction studied here was hydrodeoxygenation of methoxyphenols, which requires the use of a metal catalyst. This study focused on the synthesis of a monolithic catalyst, its characterization and ability to decrease the oxygen content from the feed. Ideally the same type of catalyst support (monoliths) could be used for upgrading the vapors from other torrefaction streams. (Chapter 3)
- Liquid phase upgrading: Phenolics alkylation with short oxygenates. This reaction allows coupling of short alcohols and olefins with phenolic compounds, producing higher carbon number oxygenate molecules. There are several aspects of the reaction mechanism for alkylation of phenolics that were not well understood and this study sought to give answers to these questions and provide tools that would allow tailoring the product selectivity of the system. Additionally, the effect that water has on catalyst activity was investigated. (Chapters 4 and 5)

- Liquid phase upgrading: Water effect on hydrogenation of furfural. If the expectation from bio-oil upgrading is to have an oxygen-free liquid product, eventually hydrogenation will have to be considered in the upgrading scheme. At the same time, water is very likely to be present in most upgrading steps. Thus it is critical to understand the role of water in the different reactions. This study focused on how water affects the hydrogenation of furfural, looking at the mechanistic aspects and the implications of the presence of the water molecule on the catalyst surface. (Chapter 6)

3. Vapor phase upgrading: Phenolics hydrodeoxygenation

3.1. Introduction

It has been recognized that hydrodeoxygenation catalysts face the challenge of a fast deactivation in the presence of phenolic compounds, which can only be slowed down by using high hydrogen pressures. High-pressure post-pyrolysis hydrotreating processes cannot be easily integrated with conventional pyrolysis reactors, since the latter operate at near atmospheric pressure. The only option is therefore to condense the pyrolysis vapors and feed the liquid bio-oil to the hydrotreating units. The great challenge in doing this in large scale is the low chemical and thermal stability of bio-oil. A more desirable option would be to directly feed the vapors coming out of the pyrolysis unit into an upgrading reactor, or a cascade of reactors. Therefore, it is highly advantageous to find a catalyst system that can work efficiently in the presence of bio-oil vapors, particularly the severely deactivating phenolic compounds, at atmospheric pressure. An aspect that must be taken into account is the unwanted effect of pressure buildup in the upgrading reactor that might upset the stable operation of the pyrolysis reactor. In this regard, monolithic supports appear as an attractive option since they typically generate minimum pressure drops during operation, even at high flow rates.[37] Thus, we have focused on using monolithic catalyst supports for the proposed upgrading cascade of pyrolysis vapors.

It is well known that monolithic catalyst supports can be synthesized with low or high surface areas. High-surface-area monoliths are a better choice for catalytic reactions as they allow higher dispersion of the active material and provide higher

contact area between the catalyst and the gas. However, the synthesis of high-surface-area monoliths is rather expensive and their mechanical resistance is much lower than that of low-surface-area monoliths.[38] The disadvantages of a low-surface-area monolith can be overcome by coating the substrate with an overlayer of high-surface area. For example, washcoating is a widely used method for increasing the surface area of monoliths. Silica and alumina have been commonly used for this purpose by formation of a thin oxide layer onto the monolith walls, providing a suitable, high-surface-area material for incorporation of the active phase. Carbon has also been used as high-surface-area coating for monoliths and it presents good advantages since it is generally inactive for most secondary reactions that may occur on other catalyst supports.[39] For example, the behavior of platinum and palladium catalysts supported on carbon-nanofiber-coated cordierite monoliths was compared to that of catalysts supported on alumina-washcoated monoliths.[40] It was found that the surface area was doubled when carbon nanofibers were grown. Also, the adsorption of water on the support (and catalyst deactivation) was reduced due to the higher hydrophobicity of carbon when compared to alumina.

In the area of biomass utilization, monolithic catalyst supports have been used in the production of hydrogen gas from pyrolysis oil,[41-43] and in the cleaning of syngas from biomass gasification.[44,45] However, they have not been used yet in the upgrading of pyrolysis vapors. In this contribution, we have investigated Pt-Sn catalysts supported on carbon-nanofiber-coated monoliths as a novel catalytic upgrading system for the deoxygenation of anisole and guaiacol, chosen as model

molecules because they are among the most abundant phenolic compounds derived from lignin pyrolysis.[46]

3.2. Objectives

- *General*
  - To study the synthesis and reactivity of monolithic metal catalysts for use in hydrodeoxygenation of phenolic compounds present in pyrolysis oil vapors.
- *Specific*
  - To synthesize metal catalysts supported on different monolithic structures and evaluate their physical and chemical properties.
  - To determine the ability of the monolithic catalysts to perform deoxygenation of phenolic compounds under mild reaction conditions.
  - To evaluate the stability of the monolithic catalysts.
  - To propose a reaction scheme for hydrodeoxygenation of guaiacol and anisole.

3.3. Experimental methods

- *Thermodynamic calculations*

The concentration of each species at equilibrium was calculated using ASPEN software, with Peng-Robinson as the preferred model for estimation of thermodynamic properties. A simulation was setup with a stream of reactants (H_2 and guaiacol in a molar ratio 30:1) going into an equilibrium reactor held at 1 atm and 400 °C (this value was varied to study the equilibrium at different temperatures). The two effluents from this reactor (vapor and liquid phase) were combined in a mixer and the molar flows of each species at the exit of the mixer

were reported. The following reactions were allowed to take place inside the equilibrium reactor:

$$\text{Guaiacol} + H_2 \Leftrightarrow \text{Catechol} + \text{Methane} \quad (3.1)$$

$$\text{Catechol} + H_2 \Leftrightarrow \text{Phenol} + H_2O \quad (3.2)$$

$$\text{Phenol} + H_2 \Leftrightarrow \text{Benzene} + H_2O \quad (3.3)$$

• *Materials*

The monoliths used in this study were: Inconel Metpore® EFCS (Exhaust Filtration/Catalyst Support) with a relative density of 4.3 % and 100 pores per inch; and cordierite with a honeycomb geometry obtained from Applied Ceramics Inc. with a diameter of 0.89 cm, length of 2.54 cm and 400 cells per squared inch. Catalyst metal precursors for nanofiber growth (Cu) and deoxygenation reactions (Cu, Ni, Re, Pt, Sn) were copper (II) nitrate pentahemihydrate 99% (Riedel-De-Haen), nickel (II) nitrate hexahydrate (Alfa Aesar), rhenium (VII) oxide (Alfa Aesar), dihydrogen hexachloroplatinate (IV) hexahydrate 99.9% (Alfa Aesar), and tin (II) chloride dihydrate reagent grade (Alfa Aesar), respectively. Guaiacol (2-methoxyphenol) and anisole (methoxybenzene) were 99 % from Sigma Aldrich. Standards for product identification were: benzene 99.9% (Sigma Aldrich), toluene 99.7 (Alfa Aesar), phenol 99% (Sigma Aldrich), and o-cresol 98% (Alfa Aesar). Gases were Ultra High Purity hydrogen, Ultra High Purity nitrogen, and Ultra High Purity ethylene, all from Airgas.

• *Catalyst synthesis*

- Inconel-supported catalysts. The Inconel material was shaped into cylinders of diameter equal to the reactor tube diameter and 1/2 inch length. The

resulting monoliths were treated with nitric acid solution in order to remove impurities from the surface and enhance the anchoring of the precursors. Following this treatment the monoliths were washed in DI water and dried overnight. These monoliths are referred to as Blank/Inconel in the text. Impregnation of single metals (copper for nanofiber growth and copper, nickel, rhenium, platinum and tin for reaction) was done by sonication during 3 h in a precursor aqueous solution that contained 3 wt.% of the active metal, followed by room temperature drying for 5 h and overnight drying at 110 °C. This procedure was performed twice. Then, calcination was carried out under flow of air for 2 h at 350 °C for rhenium catalysts, 400 °C for platinum and copper, 500 °C for nickel, and 600 °C for tin catalysts. Samples impregnated with copper, nickel, rhenium, platinum and tin are referred to as Cu/Inconel, Ni/Inconel, Re/Inconel, Pt/Inconel and Sn/Inconel, respectively. Platinum and tin co-impregnation was done following the same procedure used for the individual metals, but using a precursor solution containing 1.5 wt.% of each metal (3 wt.% total metal, Sn/Pt molar ratio of 1.6), and carrying out calcination at 450 °C. This catalyst is referred to as Pt-Sn/Inconel in the text. All catalysts were reduced in-situ for 2 h under 200 mL/min of hydrogen at 350 °C (Cu/Inconel and Re/Inconel), 450 °C (Ni/Inconel), 330 °C (Pt/Inconel), 600 °C (Sn/Inconel), and 400 °C (Pt-Sn/Inconel). Copper-impregnated Inconel (i.e., Cu/Inconel) was further treated in a continuous flow reactor for growing carbon-nanofibers on the monolith surface. In-situ reduction of Cu/Inconel monoliths was carried out

under hydrogen flow at 600 °C and subsequent treatment with ethylene took place at 700 °C for half an hour. These conditions have been shown to be successful in carbon nanofibers growth.[47] Monoliths resulting from this treatment were called CNF/Inconel. The carbon-nanofiber-coated monoliths were co-impregnated with platinum and tin using the procedure described before, calcined at 450 °C, and in-situ reduced at 400 °C. This catalyst was called Pt-Sn/CNF/Inconel.

- Cordierite-supported catalysts. Before synthesis, the cordierite monoliths were dried overnight at 110 °C. Afterwards, monoliths were dipped in an aqueous colloidal solution of alumina particles (0.05 μm diameter) with a solid content of 20 %. Drying was subsequently performed overnight and at room temperature while keeping the monoliths in a horizontal position and under continuous rotation. Next the monoliths were treated at 450°C for four hours under 100 ml/min air in order to strengthen the attachment of the alumina layer to the substrate. This catalyst was called Al_2O_3/Cordierite. An aqueous solution of nickel nitrate containing enough precursor to reach a 10 % nickel content with respect to the mass of alumina coating was used for impregnation of the cordierite monoliths. A monolith was dipped in the solution for about a minute and the solution remaining inside the channels was removed by pressurized air. Immediately following impregnation, the monoliths were dried by two different methods, i.e. freeze-drying and vacuum drying (200 °C). A second high temperature treatment (400 °C for 2h) was performed in order to decompose the nickel precursor on the surface

and the resulting catalyst was called Ni/Al_2O_3/Cordierite. In-situ reduction of these monoliths was carried out under hydrogen flow at 400 °C and subsequent treatment with ethylene took place at 600 °C for half 4 hours. Monoliths resulting from this treatment were called CNF/Cordierite. The carbon-nanofiber-coated monoliths were oxidized with a hydrogen peroxide solution for 2h hours and finally co-impregnated with platinum and tin. The impregnation solution was prepared with 200 ml of 0.5M HCl, 0.285g of hydrochloroplatinic acid and 0.205 g of tin chloride (total metal concentration is 0.1%wt.). This mixture gave a Sn/Pt molar ratio of 1.6. The monoliths were dipped in the precursor solution for 1 hour (sample A) and 24 hours (sample B), calcined at 450 °C, and in-situ reduced at 400 °C. This catalyst was called Pt-Sn/CNF/Cordierite.

• *Catalyst characterization*

BET surface area of the catalysts was measured on a Micromeritics ASAP 2000 physisorption apparatus, using N_2 as probe molecule. Carbon content of the CNF/Inconel sample was determined both by measuring the weight difference before and after treatment with ethylene, and by thermogravimetic analysis, using a Netzsch combined TGMS with STA 449 Jupiter TG and QMS 403 C Aeolos MS. The latter measurement was done under air atmosphere and with a temperature ramp of 10°C/min. The topography of the catalysts surface was imaged on a Zeiss DSM 960A Scanning Electron Microscope (SEM). Geometry of carbon-nanofibers and metal particle size were investigated with a JEOL 2000-FX Transmission Electron Microscope (TEM).

Metal loading of the catalysts was estimated in the following manner. In the case of Pt/Inconel and Sn/Inconel, it was assumed that after the impregnation and calcination steps, the active phase was only in the form of PtO_2 and SnO, respectively. Then the weight gained after calcination was used for the estimation of the total metal present in the monolith. The same procedure was followed for other metals. In the case of the bimetallic catalysts, the presence of the complex $(PtCl_2(SnCl_3)_2)^{-2}$ in a aqueous hydrochloric acid solution during impregnation with Pt-Sn has been reported before.[48] This complex has a Sn/Pt ratio of 2.0, which is higher than that of the precursor solution used for the synthesis of our catalysts (Sn/Pt=1.6). It can be assumed that all the tin present in solution is consumed for the formation of the complex, while some platinum precursor remains in solution without forming any complex. Therefore the fraction of complex ions in solution with respect to the fraction of non-complex $(PtCl_6)^{-2}$ chloroplatinate ions can be estimated. Using the weight gained after impregnation and assuming the fraction of complex ions and chloroplatinate ions on the monoliths is the same as that of the impregnation solution, the total metal content (Pt+Sn) was estimated.

Thermal Programmed Reduction (TPR) experiments were performed in a 1/4 inch OD quartz tube. After being ground to 250-425 μm particles, 30 mg of the monolithic catalyst were treated under 30 ml/min of 5% H_2 in argon, using a temperature ramp of 10°C/min. Hydrogen consumption was monitored with a Thermal Conductivity Detector (TCD), using argon as the reference gas.

• *Catalytic reaction*

Deoxygenation of anisole and guaiacol was carried out at atmospheric pressure and 400°C in a quartz tube 3/8 inches OD and 12.5 in length. In a typical experiment, the liquid reactant (guaiacol or anisole) was injected from a syringe pump (0.1 ml/h) into a heated stainless steel tube, where it was mixed with a gas stream (50 ml/min) of N_2 (83%) and H_2 (17%) and vaporized before entering the reactor. The H_2 to phenolic compound molar feed ratio was 30:1. Products were analyzed online using a Varian 3800 GC equipped with Rxi-5Sil MS column and FID detector. Liquid products were condensed in an acetone/ice trap. Identification of products in the collected liquid was done with a GCMS-QP2010S system equipped with HP-5 column and confirmed by injection of standards to the GC-FID.

3.4. Results and discussion

• *Thermodynamic calculations*

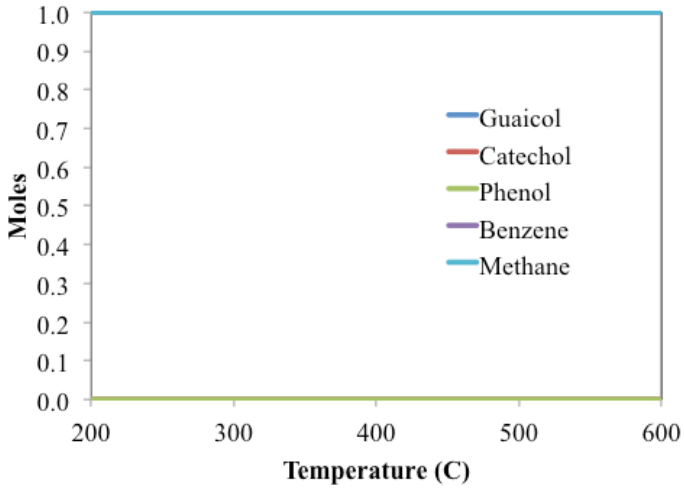

Figure 3.1. Concentrations at equilibrium for reactant and products of guaiacol hydrodeoxygenation at 1 atm

Figure 3.1 displays the concentrations at equilibrium of guaiacol and its hydrogenation products according to reactions 3.1 – 3.3. Throughout the whole temperature range, guaiacol can be fully hydrodeoxygenated to benzene, so there are not thermodynamic limitations for these hydrogenation reactions. Also, at the particular temperature of the experimental studies (400 °C) hydrogenation of the ring is not favored, and benzene would be the dominant product.

• *Inconel supported catalysts characterization*

Figure 3.2(a) shows the Inconel monolith used as catalyst support. The low magnification SEM picture in Figure 3.2(b) illustrates the geometry of the monolith openings. The random nature of the channels is favorable for the reaction since it provides improved contact between the gas and the catalyst surface. A closer look to the Blank/Inconel and CNF/Inconel in Figure 3.3 reveals the surface of the metal monolith before and after treatment with ethylene at high temperature.

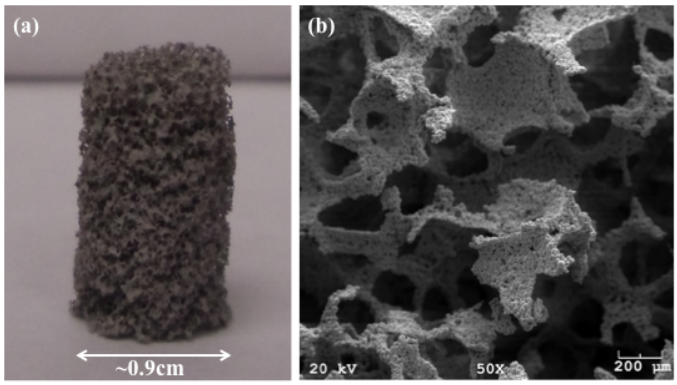

Figure 3.2. (a) Cylindrical shape Inconel monolith, (b) SEM picture showing monolith structure

The higher magnification images in Figure 3.3 (c and d) show more details of the morphology of the surface covered by carbon-nanofibers.

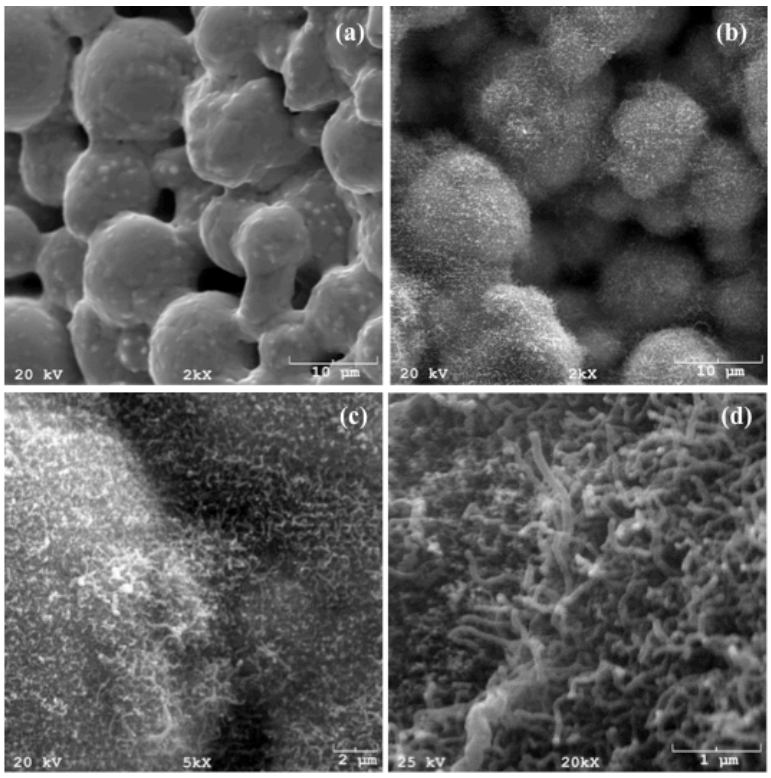

Figure 3.3. SEM pictures of monolithic catalysts: (a) Blank/Inconel, (b) and (c) CNF/Inconel (d) High magnification image to show the CNF

In addition to the images, energy dispersive X-ray spectroscopy (EDS) analysis, performed on the same SEM, gave evidence for the high carbon coverage of the surface. Figure 3.4 shows the surface composition of this sample, where some of the metals that are part of the Inconel alloy were observed.

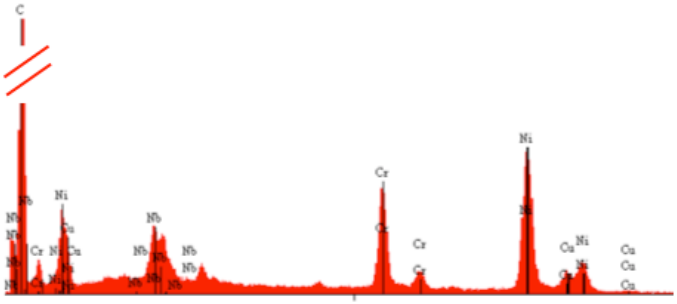

Figure 3.4. Energy dispersive X-ray spectroscopy (EDS) analysis of a Cu-Inconel sample covered with carbon nanofibers

However, copper was not observed on the surface, indicating the fibers fully covered the copper particles, preventing them from participating in catalytic reactions. Since the main purpose for growing carbon-nanofibers on the monolith was to increase the support surface area, the BET surface area of carbon-nanofiber-coated monolith was compared to that of the bare monolith. The results were 14 ± 1 m^2/(g monolith) for CNF/Inconel and less than 1 m^2/(g monolith) for Blank/Inconel sample. The carbon content of CNF/Inconel measured by weight difference was 17.0 wt.%.

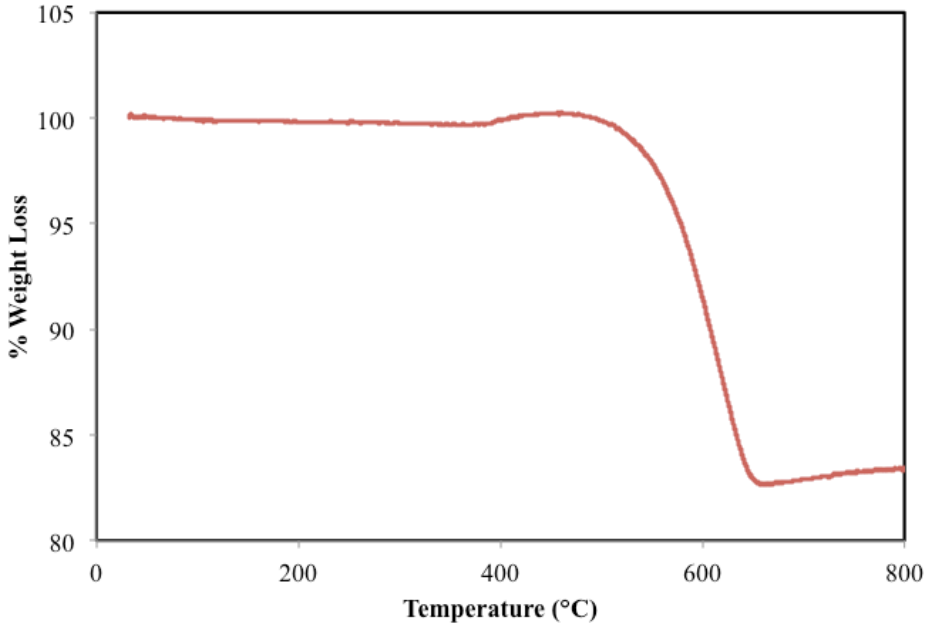

Figure 3.5. Carbon-nanofibers burn off profile in CNF/Inconel catalyst

At the same time, thermogravimetric analysis indicated that the weight loss of the sample when treated under air atmosphere from 30°C to 800°C was 16.7 wt.% (See Figure 3.5), which is in very good agreement with the previous result. Based on the carbon content and surface area measurements, the support surface area was

estimated to be 82 ± 1 m^2/g CNF. This value is in good agreement with previous reports for carbon-nanofibers surface area.[47] Sonication experiments of a CNF/Inconel sample were performed in order to evaluate the mechanical strength of the carbon coating during the incorporation of the active phase. One single monolith was dipped in a water/acetone solution and placed in a sonication bath under the same conditions used for the impregnation of the active phase. A total weight loss of 0.6 wt.% was observed, which suggests that the carbonaceous support is strongly bound to the Inconel surface.

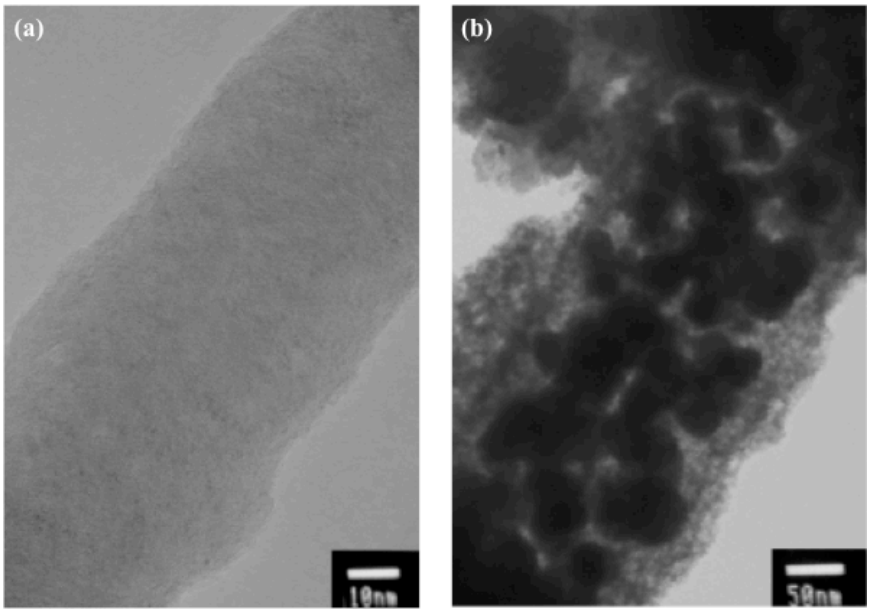

Figure 3.6. TEM pictures of carbon nanofibers: (a) Before impregnation with Pt-Sn (b) After impregnation with Pt-Sn and calcination

Figure 3.5 shows the weight loss (carbon burn off) of CNF/Inconel as a function of temperature. This analysis suggests that oxidation of carbon nanofibers might still take place, probably not to the point of combustion, but still generating oxidized groups that could even play a role in catalytic activity.

Observation of the carbon-nanofibers under the TEM shows that they can vary in diameter from 50nm to 200nm (see Figure 3.6). The fact that the fibers can be seen in the Pt-Sn/CNF/Inconel sample gives additional evidence about their stability after Pt-Sn impregnation/calcination. Figure 3.6(b) shows active phase particles anchored on the carbon-nanofiber with particle size around 50 nm. In the same sample particles with greater diameter (several hundreds of nanometers) were observed as well. TEM analysis of Pt-Sn/Inconel was also performed, however it was not possible to distinguish the Pt-Sn particles due to the metallic nature of the support (Inconel).

TPR experiments were carried out in order to investigate the presence of an alloy between platinum and tin. Figure 3.7 shows the TPR profiles for the supports (Blank/Inconel and CNF/Inconel), monometallic catalysts (Pt/Inconel and Sn/Inconel), and bimetallic catalysts (Pt-Sn/Inconel and Pt-Sn/CNF/Inconel). Blank/Inconel shows two small peaks for hydrogen consumption, one at 400°C and one at 510°C. It is possible that some of the components of the metal alloy Inconel are reduced at this temperature, but as it will be explained later, this reduction does not generate any activity for the reactions of interest in this study. CNF/Inconel does not show any consumption of hydrogen, which suggests the Inconel surface and the copper particles are fully covered by the fibers, so that the metal sites are not able to react with hydrogen. For Pt/Inconel two peaks for hydrogen consumption are observed, the first one at 300°C and one more at 400°C. The latter can be attributed to the partial reduction of the Inconel support, as it appears at the same temperature as one of the peaks identified in the Blank/Inconel sample. Therefore the peak at

300°C should correspond to the reduction of platinum. Sn/Inconel shows a main reduction peak at 450°C accompanied by a smaller peak at around 550°C. Previous TPR studies of Pt-Sn/Al_2O_3 catalysts have shown the existence of reduction peaks at 250°C for platinum and at 400°C for tin (including a shoulder at almost 500°C).[48] These results are in good agreement with our experiments, taking into account the difference in the support (Inconel vs. Al_2O_3) and the possibly different particle size (greater in our case). The reduction profile for Pt-Sn/Inconel appears as one single peak at 300°C, whereas Pt-Sn/CNF/Inconel presents multiple reduction peaks ranging from 160°C up to 600°C. The former does not show any hydrogen consumption in the region where tin would reduce. This would suggest that tin is not present as monometallic particles in this catalyst, but is rather combined with platinum, forming an alloy. As it was mentioned before, during the impregnation step it is possible that not all the platinum precursor is consumed for the formation of the Pt-Sn complex. Therefore unalloyed platinum may exist on the surface of the Pt-Sn/Inconel. However it is not possible to identify a hydrogen consumption peak for platinum because its reduction takes place at the same temperature that the Pt-Sn alloy does. The appearance of multiple peaks in the reduction of Pt-Sn/CNF/Inconel can be attributed to a wide distribution in the metal particle size, as it was observed with TEM, causing the reduction of the alloy to occur in several steps. Furthermore, there could be anchoring sites (carboxyl and carbonyl groups) present on the surface of CNF/Inconel, which provide a stronger interaction between the metal precursors and the supports. This interaction would end in lower mobility of the species on the surface and therefore the formation of a non-uniform alloy, which would show a

multi-staged reduction profile. Carboxyl and carbonyl groups are present on the support surface as a result of the oxidation of the fibers, which has been reported to take place even at room temperature.[49] In order to estimate the metal loading of the catalysts, a series of precursor solutions with known concentration was analyzed with UV-Vis spectroscopy, and one particular band of the spectra was chosen in order to follow up the concentration of platinum-tin complex in solution during impregnation.

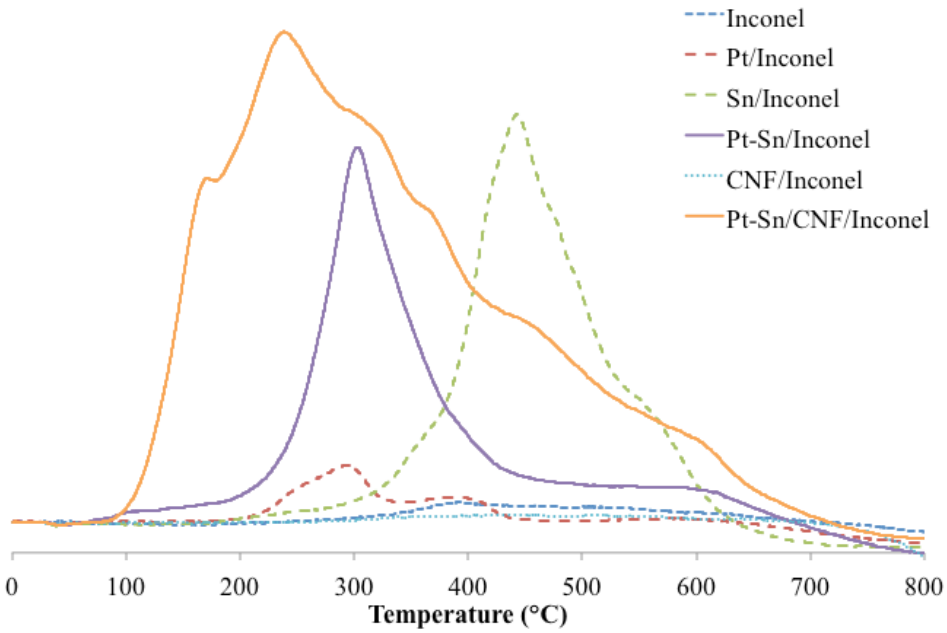

Figure 3.7. TPR profiles for catalyst supports, monometallic catalysts and bimetallic catalysts

This solution did not show significant changes in concentration after two consecutive impregnation steps, nevertheless a progressive weight gain was observed in the monoliths. From these observations it could be inferred that the incorporation of the active phase onto the support happened preferentially via a true impregnation process rather than adsorption of the precursor molecules from the

solution to the monolith surface. Most likely, the precursor solution first wets the surface of the monolith and as the solvent evaporates, the active species remain on the surface of the catalyst. Metal loading for mono and bimetallic catalysts is reported in Table 3.1.

• *Cordierite supported catalyst characterization*

As opposed to the random nature of the channels in the Inconel monolith, the cordierite monoliths have an array of squared straight channels, as it is shown in Figure 3.8 (a). The surface of the channel walls exhibited rugosity and some macropores (Figure 3.8 (b)), but still the surface area demonstrated to be quite low (below $1 m^2/g$). Because of this it was necessary to increase the surface area of the monolithic support before the incorporation of the active species.

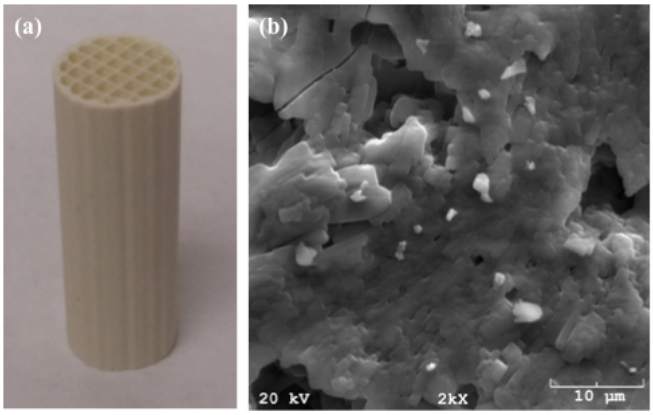

Figure 3.8. (a) Honeycomb geometry cordierite monolith, (b) SEM picture showing morphology of the channel wall's surface

As shown in the previous section, metals like copper or nickel serve as precursors for carbon nanofibers growth, which have high surface area and are a good inert substrate. In order to ensure a uniform distribution of the precursor for carbon fibers growth, in this case nickel, a washcoat of alumina was applied on the bare cordierite

monolith, creating a 7%wt. Al_2O_3/Cordierite. The surface area of this monolith was reported to be 21 m^2/g of monolith or 285 m^2/g of coating. A critical step on the synthesis of monolithic catalysts is drying because the precursor solutions would tend to accumulate at the mouth of the monolith channels, creating a gradient of active species along the catalyst support.

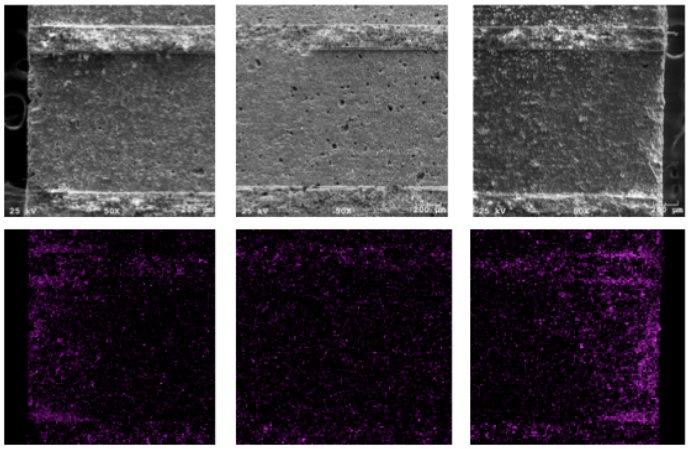

Figure 3.9. Nickel concentration along the walls of cordierite monolith synthesized with vacuum oven drying. Top: SEM photographs showing morphology of the wall. Bottom: EDS map for the element nickel (purple)

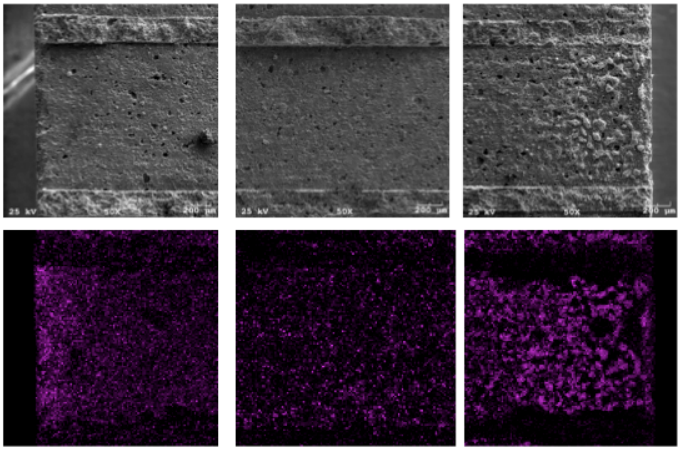

Figure 3.10. Nickel concentration along the walls of cordierite monolith synthesized with freeze-drying. Top: SEM photographs showing morphology of the wall. Bottom: EDS map for the element nickel (purple)

It has been suggested that freeze-drying is an optimal method because it quickly immobilizes the precursor solution before the gradient starts to form.[39] Al_2O_3/Cordierite monoliths impregnated with nickel and dried by two methods (vacuum oven drying and freeze-drying) were analyzed using energy dispersive X-ray spectroscopy (EDS) within a scanning electron microscopy. The concentration of nickel along the channels of the monolith was mapped in order to observe its uniformity (Figures 3.9 and 3.10). It was evident that a gradient was present in both samples, however it seemed that freeze-drying provided a higher uniformity, as predicted from the literature studies. Therefore the freeze-dried sample was used for the synthesis of Pt-Sn/CNF/Cordierite monoliths. Figure 3.11 shows the morphology of the monolithic catalyst before and after the alumina coating and after carbon nanofibers growth.

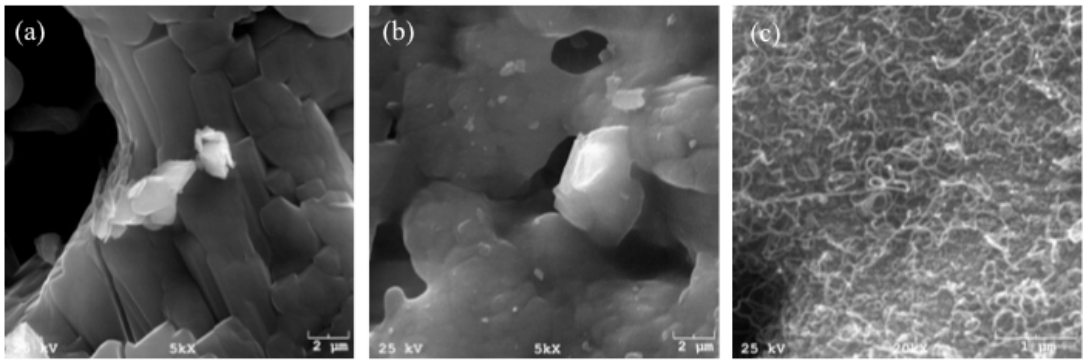

Figure 3.11. SEM pictures of monolithic catalysts: (a) Bare cordierite, (b) Al_2O_3/Cordierite (c) CNF/ Al_2O_3/Cordierite

- *Guaiacol deoxygenation on Inconel supported monometallic and bimetallic catalysts*

Figure 3.12 shows the conversion of guaiacol on different monometallic catalysts. Nickel, platinum and tin showed a higher activity than copper and rhenium,

however after about 1 hour of time on stream, all of them exhibited drastic deactivation, reaching a level of conversion around 5%, except tin which stayed at around 10% conversion. The main product over the non-noble metals was phenol, thus full deoxygenation of guaiacol was not observed. The only catalyst that produced fully deoxygenated compounds was the noble metal platinum (Table 3.1) and therefore it was used for further studies, together with tin, in bimetallic catalysts.

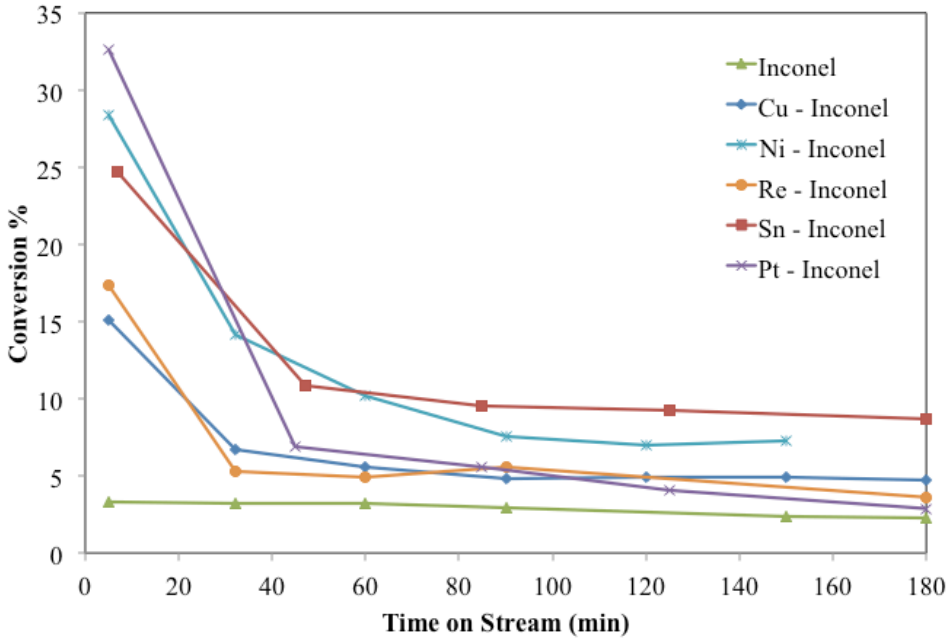

Figure 3.12. Guaiacol conversion over monometallic catalysts. Conditions: P=1atm, T=400°C, W/F=3.4 g catalyst/(g reactant/h), H_2/feed molar ratio=30

The variation of guaiacol conversion, at 1 atm and 400°C, as a function of time on stream is compared in Figure 3.13 for monometallic plantinum (Pt) and bimetallic platinum-tin (Pt-Sn) catalysts. Table 3.1 reports the initial activity (5 minutes time on stream) and initial benzene yield in a metal weight basis for mono and bimetallic catalysts. The Blank/Inconel monolith without any metal impregnation showed low

conversion, i.e., less than about 3% (not shown). Traces of phenol were observed as the main product.

Table 3.1. Catalysts metal loading and initial activity

Catalyst	Estimated Metal Loading wt.%	Initial Conversion (mol/h)/g metal	Initial Benzene Yield (mol/h)/g metal
Cu/Inconel	13.60	0.002	0
Sn/Inconel	8.01	0.008	0
Ni/Inconel	4.90	0.014	0
Pt/Inconel	3.38	0.024	0.001
Re/Inconel	1.50	0.027	0
Pt-Sn/Inconel	7.25	0.034	0.012
Pt-Sn/CNF/Inconel	16.12	-	0.020

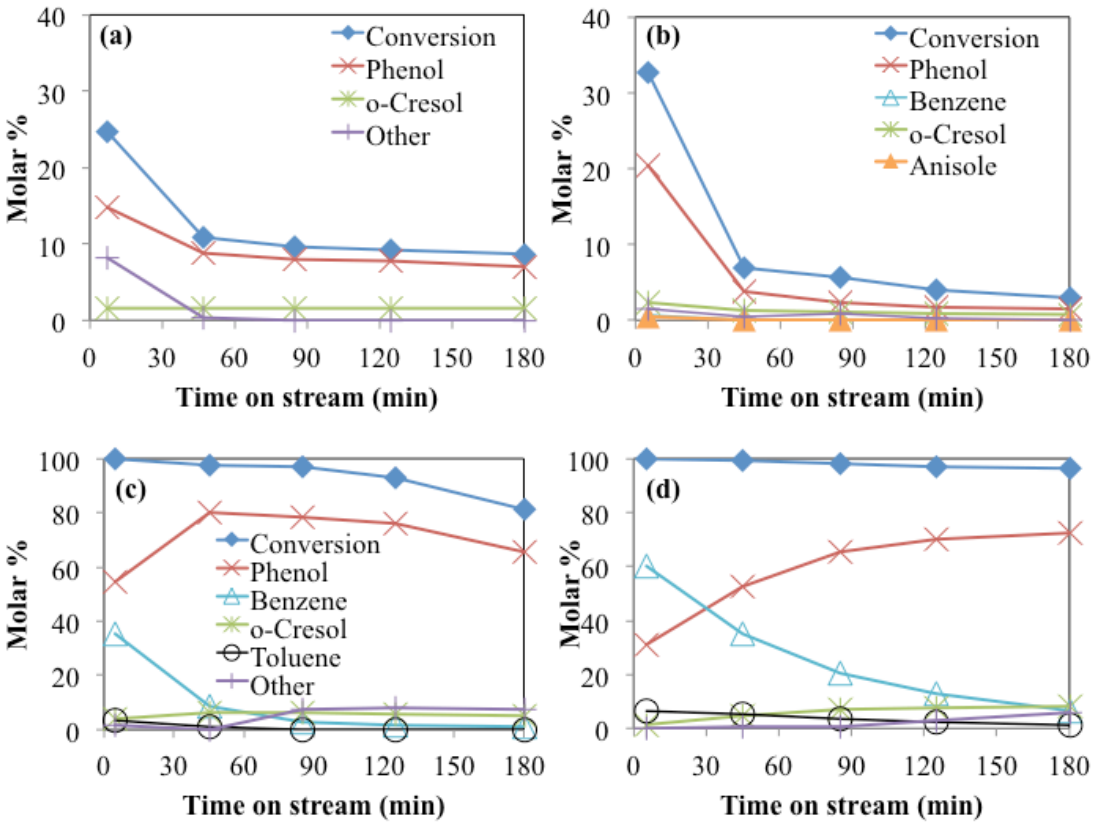

Figure 3.13. Guaiacol conversion and product yields over mono- and bimetallic catalysts: (a) Sn/Inconel, (b) Pt/Inconel, (c) Pt-Sn/Inconel, and (d) Pt-Sn/CNF/Inconel. Conditions: P=1atm, T=400°C, W/F=3.2 g catalyst/(g reactant/h), H_2/feed molar ratio=30

When either platinum or tin was incorporated onto the monoliths, the guaiacol conversion increased. The Pt/Inconel monolith had higher initial activity (see Table 3.1) but it rapidly deactivated (see Figure 3.13(b)); after 3 h on stream its activity was that of the Blank/Inconel monolith. While the initial activity of the Sn/Inconel was lower than that of the Pt/Inconel, the deactivation was less severe and after 3 h on stream it was able to maintain about half its initial activity. When platinum and tin were co-impregnated on the bare Inconel surface, the initial activity showed a significant improvement with respect to the Pt/Inconel monolith (see Table 3.1). Both Pt-Sn/Inconel and Pt-Sn/CNF/Inconel catalysts reached 100% conversion of guaiacol initially. The product distribution as a function of time on stream is also shown in Figure 3.13. Phenol is the main product for both Sn/Inconel and Pt/Inconel, accompanied by a smaller amount of o-cresol.

Several studies have reported phenol to be an important compound in guaiacol deoxygenation, either as a main product or as an intermediate to further deoxygenation.[50-53] Other products included di- and tri-methyl phenols, while only traces of anisole and catechol were observed. In the reaction on the Pt/Inconel, a small amount of benzene was observed at short time on stream, but after the catalyst deactivated benzene was no longer produced. Complete hydrodeoxygenation of guaiacol has been reported to take place on conventional hydrotreating metal catalysts at high pressures of hydrogen.[54] In the present study, we have found that bimetallic Pt-Sn monoliths were able to fully deoxygenate guaiacol at atmospheric pressure; on the monometallic monoliths full deoxygenation

was either not achieved or occurred to a very small extent, probably due to the faster deactivation that occurs in the absence of the second metal.

Not only the metallic composition, but also the nature of the substrate seems to have an important impact on the performance of the monolith. For instance, Figure 3.13(c) summarizes the product yields over the Pt-Sn/Inconel monolith as a function of time on stream. Phenol, o-cresol, toluene, and benzene were observed in the products. Initially, the C6 products (phenol and benzene) were obtained in about the same proportion while the C7 products were present in smaller amounts. At longer times on stream, the catalyst deactivates and the product distribution showed a lower concentration of fully deoxygenated products, which dropped to almost zero after 3 h on stream, with the concomitant increase in the yield of mono-oxygenated phenol and cresols.

For comparison, Figure 3.13(d) shows that the Pt-Sn bimetallic catalysts supported on CNF-coated monolith displayed a much-improved performance (see Table 3.1, initial benzene yield). In this case, at the beginning of the run the yield of benzene was higher than that of phenol, and, while the product distribution still changed as a function of time on stream, the yield of fully deoxygenated products was still significant after 2 h on stream. It is evident that the complete deoxygenation of guaiacol is a sequential reaction that has the mono-oxygenated compounds as intermediate products. Therefore, while the feed conversion is close to 100% in all cases, when the catalyst is less active or deactivates faster, the selectivity to fully deoxygenated products decreases.

In this comparison, a relatively low initial activity is observed with the Sn/Inconel and Pt/Inconel monoliths (Figure 3.13). When platinum and tin were co-impregnated on the monolith surface, the initial activity of the catalyst significantly increased (100% conversion), as it is observed in Table 3.1. This difference is a good indication of superior properties of the bimetallic catalyst, most likely due to the formation of a Pt-Sn alloy, as suggested by the TPR profile for this sample. In fact, Pt-Sn alloys are widely recognized as stable and selective catalysts for a number of reactions,[55] including some related to biofuel upgrading.[56] Finally, when carbon-nanofibers were grown onto the Inconel monolith surface, the performance was even better. While the initial guaiacol conversion was already 100% on the Pt-Sn/Inconel monolith, the CNF/Inconel monolith not only had a 100% conversion but also a higher benzene yield (see Table 3.1). The enhanced surface area generated by the carbon-nanofibers can clearly improve the uptake of metal (as shown in Table 3.1), and possibly increases the metal surface that is available for the reaction to take place. A similar positive effect has been reported with other carbon-nanofiber catalysts.[40]

- *Comparison of guaiacol and anisole deoxygenation on Inconel supported bimetallic catalyst*

Based on the superior performance displayed by the Pt-Sn/CNF/Inconel monolith, the rest of the studies were conducted on this catalytic material. For instance, a comparison was made on this monolith for the deoxygenation reactions of guaiacol and anisole. The overall feed conversion at different contact times and space times (W/F) is compared in Figure 3.14. It is obvious that guaiacol is much more reactive

than anisole; only at the lowest W/F investigated the reactant disappearance was less than 100 %. However, despite a higher reactivity, guaiacol shows a higher rate of catalyst deactivation that is only apparent in the distribution of products.

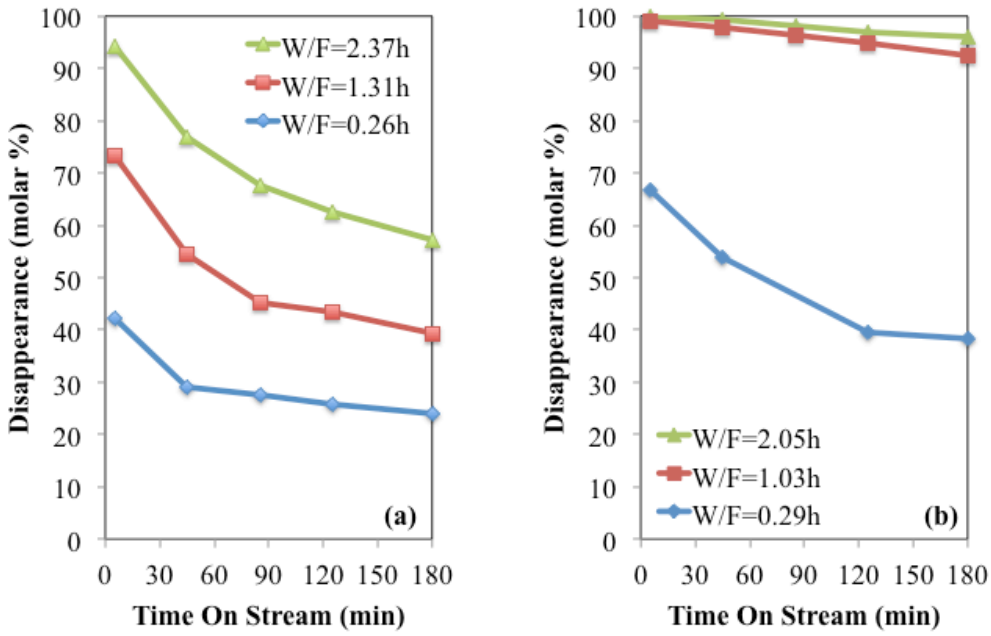

Figure 3.14. Pt-Sn/CNF/Inconel catalyst deactivation for two different reactants: (a) Anisole, and (b) Guaiacol. W/F is g catalyst/(g reactant/h). Conditions: P=1atm, T=400°C, H_2/feed molar ratio=30

As illustrated in Figures 3.15(a)-(d), the difference in reactivity and degree of deactivation causes some important differences in the distribution of products obtained from anisole and from guaiacol as a function of space-time at different times on stream. For instance, the conversion of anisole yields benzene as the main end product, with phenol as the major intermediate, while o-cresol and toluene appear as minor products. Other products, such as methylanisole, were observed only in traces. A comparison between Figures 3.15(a) and (b) shows that, with anisole feed, benzene remains as the main product, even after 125 min on stream.

That is, while some degree of catalyst deactivation is apparent, full deoxygenation is still possible. In the case of the guaiacol feed, after the same times on stream as those used for anisole (45 and 125 min), phenol dominates over benzene at almost every W/F investigated, with the latter becoming more important only at the highest W/F.

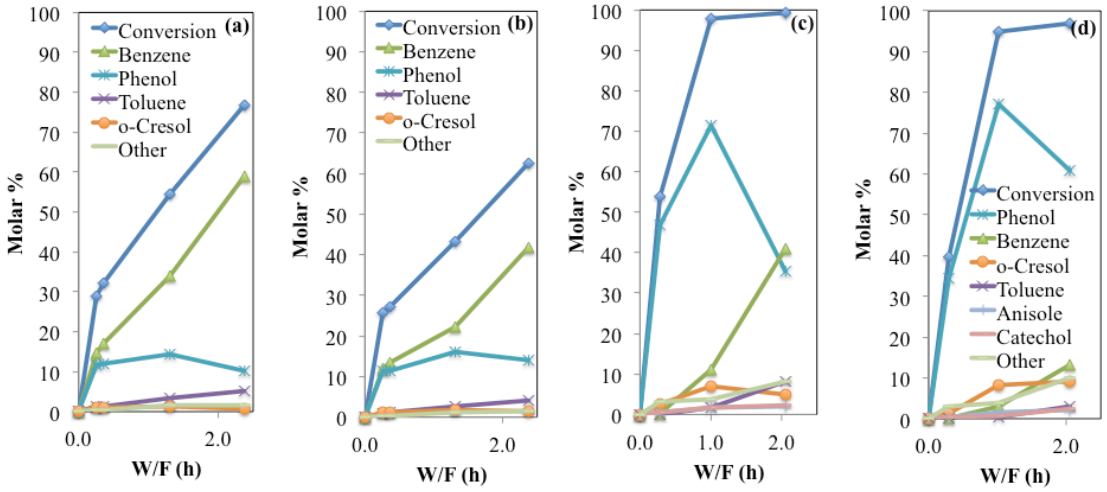

Figure 3.15. Product yields over Pt-Sn/CNF/Inconel catalyst for different reactants: (a) Anisole TOS 45 min, (b) Anisole TOS 125 min, (c) Guaiacol TOS 45 min, (d) Guaiacol TOS 125 min. W/F is g catalyst/(g reactant/h). Conditions: T=400°C, and P=1atm, H_2/feed molar ratio=30

As in the case of anisole, toluene and o-cresol are observed only as minor products. Catechol (obviously not observed from anisole) appears as a minor product from guaiacol. Dimethoxybenzene and poly-methyl phenols are also observed in low concentrations (Figures 3.15(c) and (d)). Analysis of non-condensable gases from the reaction of guaiacol and anisole showed the presence of methane (Figure 3.16), which can be expected from the hydrogenolysis of the methoxy group. As explained before, there is a marked difference between the product distribution of anisole and guaiacol.

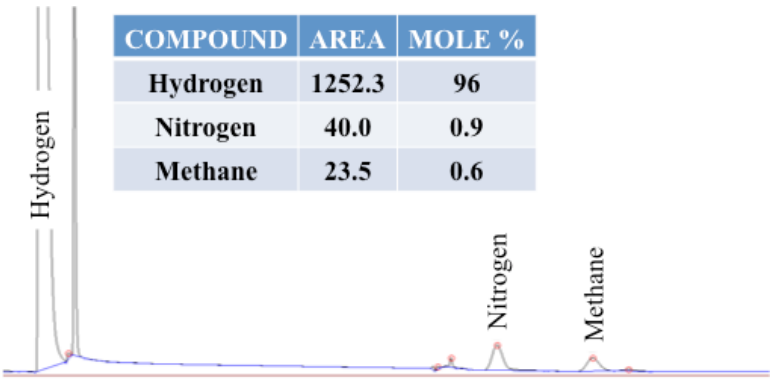

COMPOUND	AREA	MOLE %
Hydrogen	1252.3	96
Nitrogen	40.0	0.9
Methane	23.5	0.6

Figure 3.16. Gas chromatography analysis of non-condensable gases from anisole hydrodeoxygenation

A series of pulse experiments were performed in order to gain more understanding about the interaction of these molecules with the catalyst surface. In a single experiment, 61 mg of the catalyst were heated up to 400°C and subsequently two pulses of 9.5×10^{-8} moles of reactant (every 5 minutes) were carried through the catalyst bed by means of a carrier flow of 100 ml/min (carrier gas was helium). When anisole was fed, 74% of the first pulse and 39% of the second pulse were retained on the catalyst surface. The percentage of material retained by the catalyst was measured by the difference in the GC area of a pulse without catalyst versus a pulse with catalyst. With guaiacol as the feed, 90% of the pulse was retained on the catalyst for both of the pulses. These results can be interpreted as follows. Anisole preferentially adsorbs and reacts on the most active sites during the first pulse; when the second pulse comes, a fraction of the most active sites have been already deactivated and less adsorption of the reactant is observed. On the other hand, guaiacol adsorbs on both highly and non-highly active sites. As a consequence, the amount of guaiacol retained by the catalyst is the same during both pulses (higher than anisole), and it would continue to do so until the surface is fully populated.

The retention of the pulse is not 100%, probably due to the short contact time between the reactant and the catalyst bed. The observed stronger adsorption of guaiacol compared to anisole would be in agreement with the observations of both a higher reactivity, but at the same time, a more severe deactivation for guaiacol compared to anisole.

The different extent of catalyst deactivation caused by the two different feeds can be best evaluated by analyzing the yield of fully deoxygenated products as a function of time on stream. For instance, while benzene remains as the most abundant product from the deoxygenation of anisole for at least the first two hours, it is only most abundant at the very beginning of the run in the case of guaiacol feed (see Figure 3.15). Clearly, the catalyst is more severely deactivated by guaiacol and its products than by anisole and its products. As mentioned above, guaiacol first produces catechol, followed by deoxygenation to phenol and finally benzene. In turn, anisole first produces phenol, which is then deoxygenated to benzene. Some studies currently taking place in our group showed that catechol adsorbs more strongly to catalyst surfaces than phenol does; the same way guaiacol adsorption was proved stronger than that of anisole with the pulse experiments. Therefore, guaiacol and catechol are likely to remain on the surface, more effectively inhibiting the deoxygenation of phenol to benzene.

The observed variation of products with W/F and time on stream in the conversion of guaiacol and anisole is consistent with simplified reaction pathways previously proposed by us and others.[57,58] These reaction steps are shown in Figures 3.17 and 3.18. The deoxygenation path starts with decomposition of the methoxy group.

Both metals and acids can catalyze this reaction. In this case, the metal function dominates and it is expected that this step occurs via hydrogenolysis of the C-O bond, producing methane as the gaseous product, experimentally observed. At the same time, the decomposition of the methoxy group results in catechol and phenol, from guaiacol and anisole respectively. Thermodynamically, this C-O bond is weaker than the C-O bond connecting the methoxyl to the aromatic ring and weaker than the C-O bond of the hydroxyl group.[57] Therefore, producing catechol from guaiacol is more favorable than directly producing anisole or phenol.

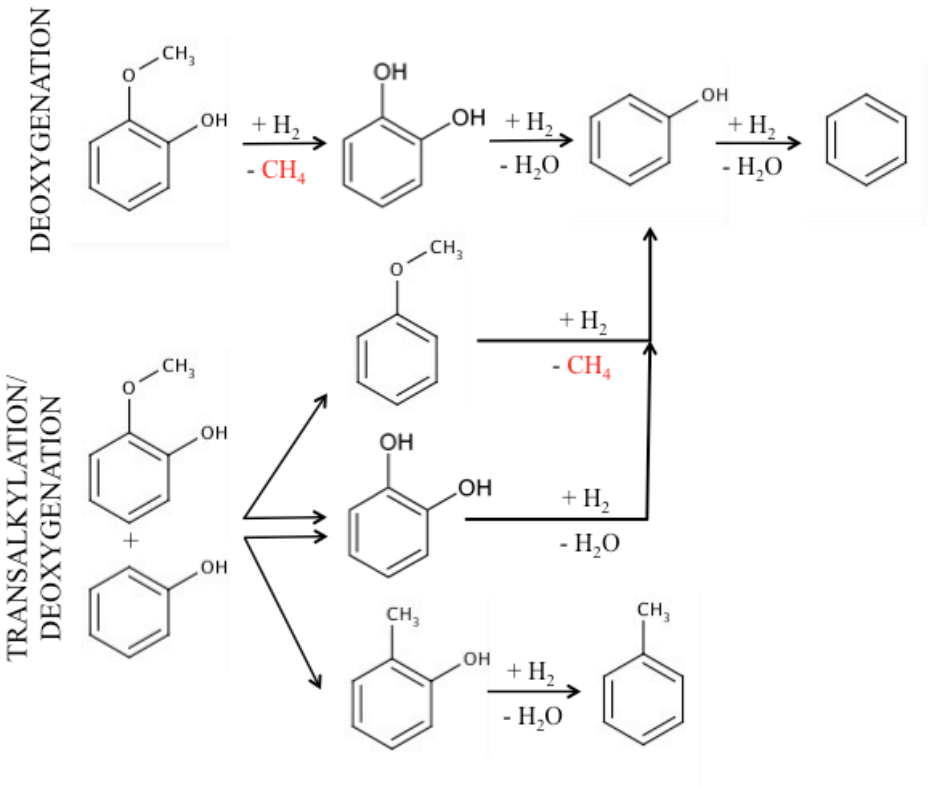

Figure 3.17. Reaction scheme for guaiacol deoxygenation on Pt-Sn/CNF/Inconel catalyst.

However, only traces of catechol are observed in the product from guaiacol, which suggests that catechol is rapidly converted to phenol, perhaps before it desorbs from

the metal surface. By contrast, on acid catalysts,[57] catechol is a major product since it is much less reactive. We have also recently shown that another route for the conversion of phenolics is transalkylation, in which the methyl group from the methoxyl is transferred to another aromatic molecule. Through this transalkylation path, catalyzed by acid sites, [57,58] two anisole molecules can form phenol and methylanisole, and later cresol. The subsequent metal-catalyzed deoxygenation of these compounds will produce benzene, phenol, and toluene, respectively. In a similar way, guaiacol can undergo transalkylation and deoxygenation to produce benzene and toluene. The very low yields of toluene and mono-oxygenated alkylated phenolics (cresol, methylanisole, etc.), together with the significant amounts of methane observed in this case are consistent with the low acidity of the substrate used in these monoliths, Inconel alloy (support) and carbon nanofibers (coating) and show that the main catalytic function for the methoxyl decomposition on these monoliths is metallic. However, the mechanism for hydrodeoxygenation of catechol and phenol may involve some weak acid sites. From this study it was not clear whether deoxygenation occurred through direct C-O cleavage or by (partial) hydrogenation of the aromatic ring followed by dehydration.[57,59] Although several authors have proposed the presence of unidentified partially hydrogenated intermediates, recent studies in our group have shown the possibility of a direct cleavage through a tautomerization reaction pathway. The former appears less plausible when taking into consideration the high concentration of hydrogen as well as the fast rate of ring hydrogenation once the first carbon in the ring is hydrogenated.

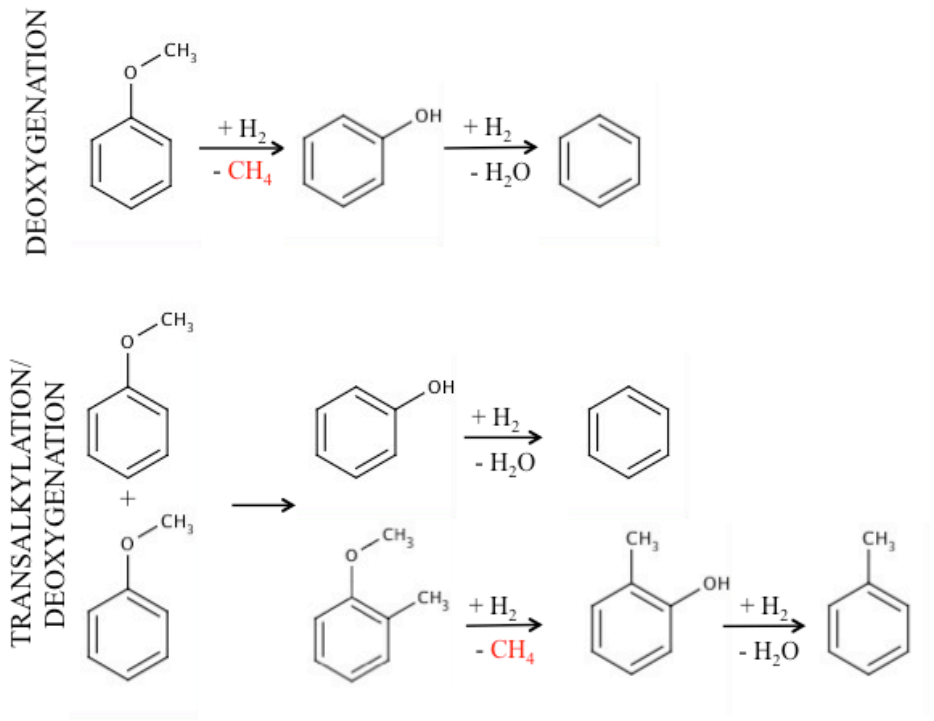

Figure 3.18. Reaction scheme for anisole deoxygenation on Pt-Sn/CNF/Inconel catalyst

• *Inconel supported catalyst regeneration.*

As it was observed, even with the bimetallic catalysts deactivation appears to be a challenge. It was not clear what the source of deactivation was, whether strongly adsorbed guaiacol molecules or excessive coke formation. An attempt to regenerate the catalyst without burning up the carbonaceous support was done using high temperature and hydrogen. A sample of Pt-Sn/CNF/Inconel was used in a reaction with guaiacol as described before; after 3 hours on stream, the flow of guaiacol was suspended, the temperature of the catalyst bed increased to 500°C and hydrogen was passed through the catalyst at a rate of 200ml/min for two hours. Subsequently the guaiacol flow was restarted and the conversion was measured again. Figure 3.19

shows that activity was slightly recovered, however the aromatics production could not be restored to its original level. This result indicates that coke removal by oxidation might be required, however the temperature should be carefully controlled in order not to decompose the support (see Figure 3.5). Further investigation is required in this aspect of the system.

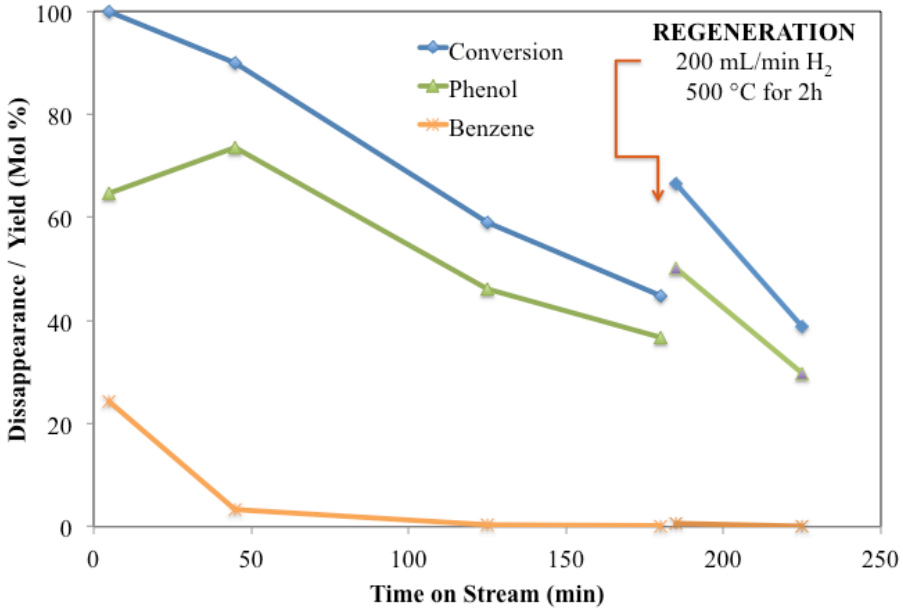

Figure 3.19. Regeneration of a Pt-Sn/CNF/Inconel catalyst using hydrogen flow at high temperature. Reaction conditions: Conditions: P=1atm, T=400°C, W/F=0.39 g catalyst/(g reactant/h), H_2/feed molar ratio=30

• *Cordierite supported catalysts activity tests.*

The CNF/Cordierite as well as Pt-Sn/CNF/Cordierite monoliths were tested for the hydrodeoxygenation of guaiacol under the same conditions as the Inconel supported monoliths. Figure 3.20 depicts the activity and product yield for each of these catalysts. Both CNF/Cordierite monoliths (with and without oxidation) showed significant activity for the production of catechol. This is an indication of the easy decomposition of the methoxy group yielding methane and the corresponding

phenolic. However, phenol was not observed under these conditions. On the other hand, Pt-Sn catalysts exhibited a higher activity and phenol was obtained as a deoxygenation product, however no fully deoxygenated products were detected.

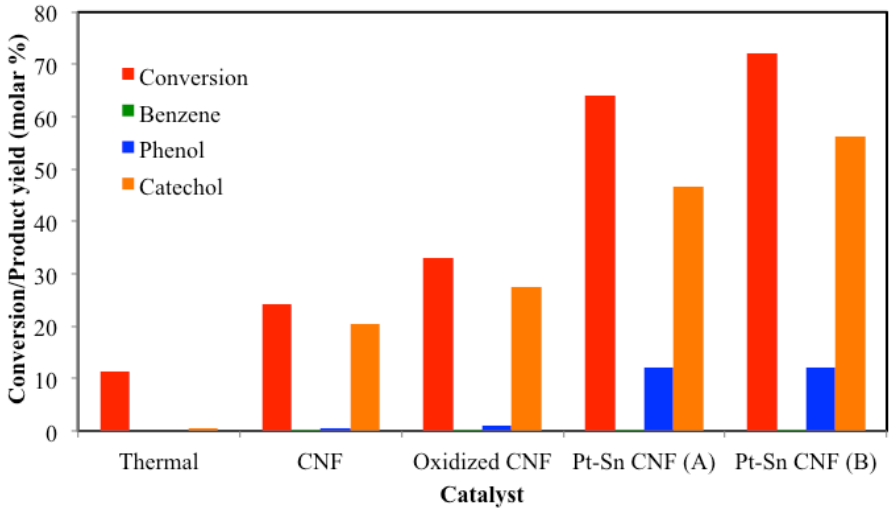

Figure 3.20. Activity and product yields for cordierite supported catalysts. Conditions: P=1atm, T=400°C, W/F=1.1 g catalyst/(g reactant/h), H_2/feed molar ratio=30, time on stream=85min

The metal content of the impregnation solution used with Inconel monoliths was 3%wt., whereas for cordierite monoliths it was 0.1%wt. As a consequence, it was reported in Table 3.1 that the metal loading of Inconel catalysts was very high (even higher than 10% in some cases). When using the cordierite monoliths it was desired to lower the metal loading and therefore the particle size, thus increasing the dispersion of the metal phase. As compared to the Inconel supported monoliths, during synthesis of Pt-Sn/CNF/Cordierte, the uptake of Pt-Sn was not detected by the weight difference before and after incorporation of the precursor solution. Therefore it is reasonable to expect that the active metal content of this catalyst was much lower and therefore no full deoxygenation of guaiacol was observed. Notice

as well that when the impregnation time was increased from 1 hour to 24 hours (Figure 3.20, Pt-Sn/CNF (A) vs. Pt-Sn/CNF (B) respectively), the increase in activity was minimal. This indicates that the method for incorporation of Pt-Sn must be modified in order to increase the metal content in the catalyst.

3.5. Conclusions

Monometallic and bimetallic (Pt-Sn alloy) monoliths were synthetized and tested for the deoxygenation of guaiacol and anisole. Both Pt-Sn/Inconel and Pt-Sn/CNF/Inconel were able to fully deoxygenate guaiacol and anisole. Coating with carbon nanofibers increased the surface area of the monoliths more than ten times, allowing for a higher metal uptake during the active phase incorporation, when compared to monoliths without coating. Deactivation of the catalyst still needs to be improved, however Pt-Sn/CNF/Inconel monolith is a promising catalyst for the upgrading of pyrolysis bio-oil.

3.6. Remarks for future work

- *Catalyst deactivation and regeneration*

Since a monolithic catalyst is a structured catalyst bed, the replacement of the catalyst in a reactor of this type is a more difficult task than in the case of pelletized catalysts. Therefore an important aspect for the utilization of this catalyst is that it possesses a long lifetime or that in-situ regeneration be easily performed. In either case, it will be necessary to perform further studies in order to determine the cause for deactivation and the best strategy for regeneration.

• *Synthesis of monolithic catalysts*

It was observed that catalysts supported in CNF/Inconel had a high active metal content, mainly due to the high concentration of the precursor solution during synthesis. When synthesizing catalyst with cordierite, this concentration was much lower and in turn the metal uptake appeared to be much lower. A study of this step in the synthesis procedure would be helpful in optimizing the conditions in order to obtain a reasonable metal content that can provide the desired activity. Other aspects worth of study during synthesis are the uniform distribution of the active species along the channels of the monoliths and controlling the amount of carbon nanofibers grown on the catalyst support.

• *Catalyst characterization*

The rates reported in this study are on a metal weight basis, however it is likely that each catalyst has a different metal dispersion. It would be important to characterize the dispersion of the catalysts in order to have a better comparison of activity between different catalysts.

• *Other metals for the active phase*

From the results of this study platinum appeared to have a high activity compared to other metals and coupled with tin offered a superior activity. At the same time, rhenium also reported a high activity on metal weight basis. Platinum-rhenium bimetallic catalysts have shown to improve stability of monometallic platinum catalysts and therefore further exploration in that area would be of interest for phenolics upgrading, where deactivation demonstrated to be a major challenge.

4. Liquid phase upgrading: Phenolics alkylation with short oxygenates

4.1. Introduction

Small oxygenates can undergo ketonization and produce longer chain ketones,[21,60] which upon hydrogenation produce secondary alcohols. By this methodology isopropanol can be easily derived from acetone, which is a product of acetic acid ketonization. Isopropanol is an excellent alkylating agent that can be combined with the phenolics fraction from the bio-oil to generate alkylphenols in the C10-C13 range.[61] These compounds not only fall in the desirable carbon-chain fuel range, but are also widely used as chemical intermediates in the synthesis of antioxidants, fragrances, agrochemicals and fuel additives.[62-64] In bio-oil upgrading, once the products from thermal treatment have been condensed, it is desirable to conduct the reactions in the liquid phase since re-heating the whole bio-oil or its fractions leads to an increase in the rate of degradation. However, the high water content of bio-oil could present a challenge for catalyst stability in liquid phase systems. In a recent study,[61] it was shown that alkylation of phenolic compounds with isopropanol in a biphasic system (aqueous and oil phases) could be successfully achieved using a hydrophobic HY zeolite with minimum zeolite degradation. This remarkable result is worth further studies such as kinetic modeling, seeking to gain insight about reaction pathways and mechanisms. With this in mind, and with the objective of gaining fundamental understanding about this reaction, the present work is a simplified study of the liquid phase alkylation in a

single organic solvent, with no water present, and with a regular HY zeolite, without hydrophobization.

Alkylation of phenolic compounds has been widely studied during the last decades. Products like cresols, xylenols, isopropylphenols, and *tert*-butylphenols are of high value in the chemical industry and it is important to understand the processes and mechanisms by which they are obtained. It is well known that alkylation of phenolics can lead to either ring-alkylated products (C-alkylation) or ether products (O-alkylation). This is dependent on whether the alkylating agent preferentially attacks the ring or the oxygen atom in the hydroxyl group, respectively. Selectivity towards a particular product has been attributed to a number of factors, including the type of catalytic site (acidic or basic, strong or weak), reaction temperature and residence time, among others.[65-70] There have been numerous studies aiming to understand the mechanistic aspects of this reaction and even though it has not been yet clarified, there are some points of general agreement according to both experimental observations and theoretical calculations. O-alkylation appears to occur at milder conditions as compared to C-alkylation, i.e. lower temperatures,[67-74] short residence times, and weaker acid sites.[66,73] Experimentally, a change in selectivity towards C-alkylation products has been observed with an increase in temperature or residence time. The mechanism for this transformation is still a point of discussion, but it is believed that an alkylaryl ether can undergo intramolecular rearrangement to produce the respective alkylphenol.[75,76] This has led to the conclusion that O-alkylation products are favored kinetically and are further converted into the more thermodynamically stables C-alkylation products.[77]

Some kinetics studies have favored an Eley-Rideal type mechanism for these alkylation reactions, in which the alkylating agent is adsorbed on the catalyst surface and reacts with a phenolic molecule from the bulk phase.[78-80]

In light of the potential application of this type of reactions in biomass utilization, a detailed kinetic study for the alkylation of m-cresol with isopropanol is presented here. Previous investigations have been limited to the use of simplified first and second order kinetics and have not considered surface coverage of reactants and products. In this study, the aim is to understand the reaction pathways in this system and bring clarity to some of the mechanistic aspects discussed above. This was done with the help of a Langmuir-Hinshelwood kinetic model with inputs from independent measurements that enhance the robustness of the model. Additionally, a comparison of this model with an Eley-Rideal type model was done, as this has previously been suggested to be the preferred mechanism for this reaction.

4.2. Objectives

- *General*
    - To study the reaction pathways and mechanisms involved in alkylation of m-cresol with isopropanol in liquid phase.
- *Specific*
    - To identify, quantify and distinguish C-alkylation products from O-alkylation products.
    - To determine the stability and reactivity of O-alkylation products in the reaction medium.

- To determine the role of different alkylating agents (i.e. isopropanol and propylene) in the reaction mechanism.
- To estimate rate constants for different alkylation steps using Langmuir-Hinshelwood and Eley-Rideal models.
- To estimate adsorption constants for all species involved in the reaction scheme and determine which species are dominant on the catalyst surface.
- To identify preferred pathways under the reaction conditions, based on the estimated rate constants.

4.3. Experimental methods

• *Thermodynamic calculations*

The concentration of each species at equilibrium was calculated using ASPEN software, with Peng-Robinson as the preferred model for estimation of thermodynamic properties. A simulation was setup with a stream of reactants (isopropanol and m-cresol in a molar ratio 4:1) going into an equilibrium reactor held at 47.6 atm and 200 °C (this value was varied to study the equilibrium at different temperatures). The two effluents from this reactor (vapor and liquid phase) were combined in a mixer and the molar flows of each species at the exit of the mixer were reported. The following reactions were allowed to take place inside the equilibrium reactor:

$$\text{Isopropanol} \Leftrightarrow \text{Propylene} + H_2O \qquad (4.1)$$

$$\text{m-Cresol} + \text{Isopropanol} \Leftrightarrow \text{Thymol} + H_2O \qquad (4.2)$$

$$\text{m-Cresol} + \text{Propylene} \Leftrightarrow \text{Thymol} \qquad (4.3)$$

$$\text{m-Cresol} + \text{Isopropanol} \Leftrightarrow \text{Methyl-isopropoxybenzene} + H_2O \qquad (4.4)$$

m-Cresol + Propylene ⇔ Methyl-Isopropoxybenzene (4.5)

• *Materials*

The reactants used in this study were m-cresol (99%), 2-propanol (anhydrous, 99.5%), thymol (≥99.5%), all from Sigma-Aldrich, and isopropoxybenzene (97%) from Oakwood Chemical. Propylene and helium (Ultra High Purity) gases were obtained from Airgas. All reactants were used as received, without further purification. Decahydronaphthalene, a mixture of cis+trans from Sigma-Aldrich (reagent grade, 98%) was used as the solvent. The catalyst used in the kinetics study was a HY zeolite from Zeolyst International (CBV 760) with a Si/Al ratio of 30, unit cell size of 2.424 nm, and surface area of 720 m^2/g.

• *Catalytic reaction*

Experiments were carried out in the liquid phase on a bench-top 0.3 liter Parr pressure reactor (model 4561), equipped with a 4843 Parr controller for temperature, pressure and stirring. In a typical experiment, 20-50 mg of the catalyst and 60 ml of the solvent were combined in a glass liner. Then, the solid was dispersed with the help of a horn sonicator (15 min. at 25% amplitude). The liner was placed in the stainless steel reactor vessel and the system was purged and pressurized with He to 2.7 MPa. A separate solution containing m-cresol or thymol (0.0434 moles), isopropanol (0.0434 – 0.173 moles) and additional solvent (enough to complete a total reaction volume of 85 ml) was prepared. For reactions with isopropoxybenzene (0.0434 moles) no isopropanol was added. The temperature in the reactor was adjusted to the desired value. Then, the solution containing the feed was introduced in the reaction vessel by pressure difference from a separate vessel.

When using propylene as the alkylating agent, the corresponding moles of gas where introduced at the same time as the liquid feed in the reactor. After injecting the feed the pressure was adjusted to 4.8 MPa by adding helium. The reaction was then performed in the batch mode for a given time in the closed vessel. Conversion data as a function of time were obtained with individual runs for each selected reaction time. At the end of each run, the liquid mixture was analyzed with a Shimadzu GCMS-QP2010S gas chromatograph/mass spectrometer in order to identify the products and a Varian 3800 gas chromatograph equipped with a FID detector for quantification. Both GC's were equipped with a Zebron ZB-1701 column with dimensions of 60 m x 0.25 mm x 0.25 μm.

• *Transport limitations test*

The Koros-Nowak / Madon-Boudart test [36] was employed to determine whether the measured reaction rates were affected by the rate of mass transfer. For this test, the HY zeolite was Na exchanged to a varying extent to generate samples with the same crystallite size, but with different acid site concentrations. In particular, 1 g of zeolite powder, with a theoretical acid density of 538 μmol/g, was exchanged with 50 ml of a Na(OH) solution containing enough base to neutralize 12% and 19% of the theoretical acid sites. The solution was stirred for 24 h at room temperature and then the solids were separated by centrifugation and dried overnight at 100°C. The acid site density of the original zeolite and the resulting residual acidity of the exchanged samples were measured using TPD of isopropylamine, as described elsewhere.[81] Briefly, the TPD system consisted of a ¼" quartz tube inside a tubular furnace and a MKS Cirrus MS. During each run, the MS scanned the

following fractions (m/z) at a rate of 1 scan/s: 4, 16, 17, 18, 28, 32, 41, 44, and 58. The system had the capability for injecting liquids through a rubber septum and gases through a 6-port valve into a stream of pre-heated He carrier gas. The system was calibrated using 10 pulses of propylene through an empty quartz tube. For the TPD run, a constant flow of helium was kept at 20 ml/min; 50 mg of the zeolite were placed in the quartz tube and pretreated for 2 h at 673 K, and then overnight at 373 K. Adsorption of isopropylamine at 373 K was accomplished by multiple 2 μl injections, until saturation of the catalyst was confirmed in the MS. Following the injections, the samples were purged in He at the same temperature for 4 h in order to remove weakly adsorbed isopropylamine. Finally, the desorption was measured under a heating ramp of 10°C/min in the 373-873 K range. The moles of propylene evolved during TPD were correlated to the concentration of Brønsted acid sites in the catalyst, following Gorte's method.[82]

4.4. Results and discussion

- *Thermodynamic calculations*

Figure 4.1 shows the concentrations at equilibrium for alkylation of m-cresol with isopropanol at different temperatures. Dehydration of isopropanol is preferred at higher temperatures, but at the reaction temperature there is a limitation in how much isopropanol can be dehydrated. At the same, production of thymol (C-alkylation product) is completely favored over methyl-isopropoxybenzene (O-alkylation product). As a matter of fact, the latter is not thermodynamically favored at any of the temperatures in the range studied. At higher temperatures cracking of

thymol is favorable resulting in m-cresol and propylene as the most stable compounds.

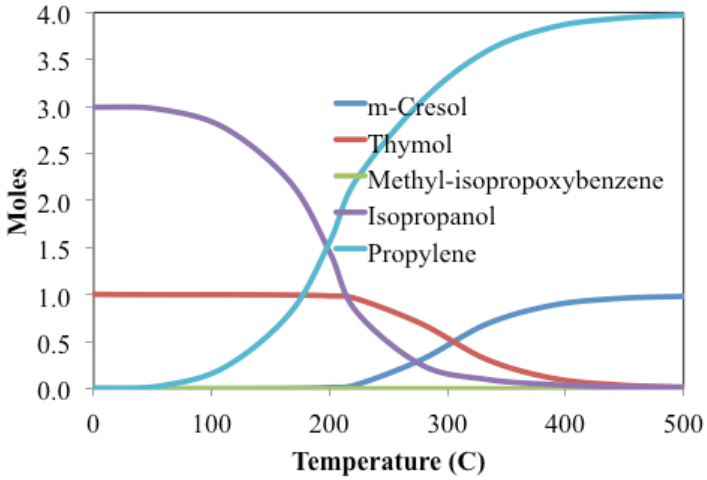

Figure 4.1. Concentrations at equilibrium for reactant and products of m-cresol alkylation at 47.6 atm

• *Product distribution from alkylation of m-cresol with isopropanol*

The reaction between m-cresol and isopropanol was monitored as a function of time. As shown in Figure 4.2a, isopropanol rapidly converts, forming the dehydration products diisopropyl ether and propylene. While direct dehydration to propylene seemed to be a significant path, it was clear that diisopropyl ether also formed as a primary product and then decomposed to produce propylene and water. From the thermodynamic calculations it was observed that the dehydration of isopropanol was limited at 200 °C, however the experimental results show a rather quick conversion of isopropanol, beyond the equilibrium concentration. It should be noted that the thermodynamic calculation did not include secondary and tertiary alkylations, which would also consume isopropanol. Furthermore, the thermodynamic calculations did not have the ether as a significant product, however

this product was observed experimentally and abundantly at early time of reactions. The formation of ether products would also required consumption of isopropanol and could cause the observed rapid decrease in concentration. Subsequently, propylene underwent oligomerization to form higher olefins, although in this case only methylpentenes were observed. Higher olefins are likely to stay on the surface and participate in the formation of coke.

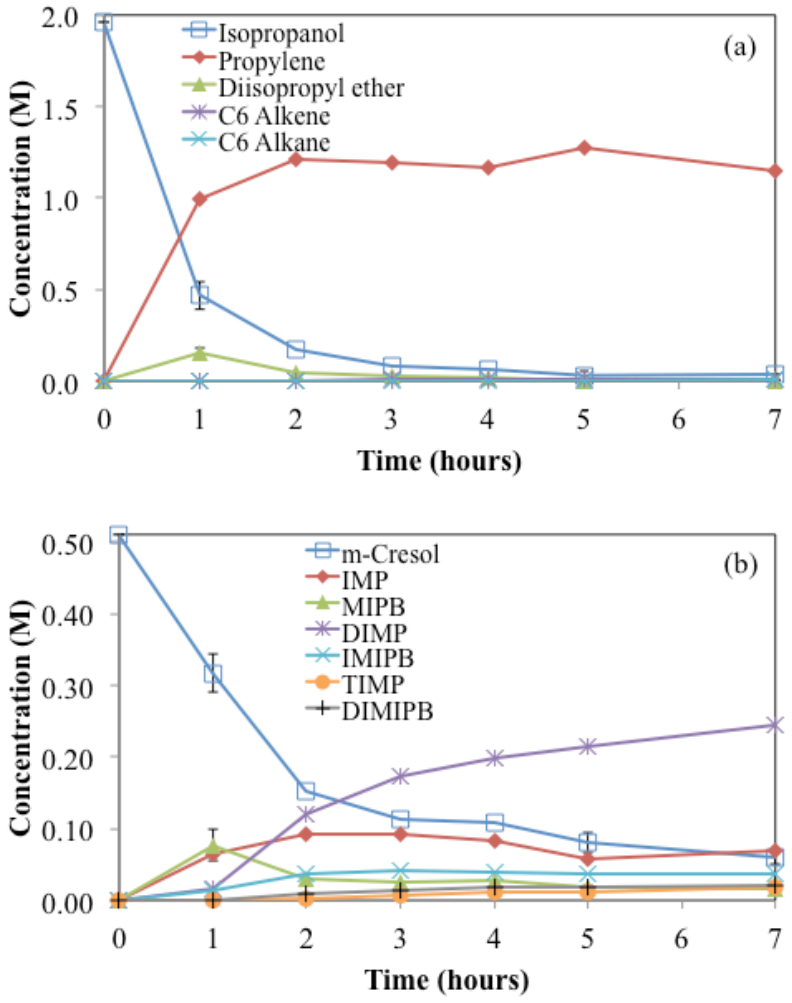

Figure 4.2. Product distribution from alkylation of m-cresol with isopropanol. (a) Dehydration/oligomerization products. (b) Alkylation products. Conditions: isopropanol/m-cresol=3.8, T=473K, P=4.8MPa, catalyst mass=50mg HY

Multiple alkylation products were identified by GC-MS. As summarized in Figure 4.3, both C-alkylation (IMP, DIMP, TIMP) and O-alkylation (MIPB, IMIPB, DIMIPB) products were formed under the reaction conditions investigated. Only IMP and DIMP could be directly matched to a registry in the mass spectrometer library. Therefore, the other products were identified by analyzing the observed fragmentation patterns. In general, ethers tend to cleave at the oxygen-carbon bond, in this case releasing an isopropyl fragment with m/z of 42. For example, methyl-isopropoxybenzene (MIPB) has a molecular mass of 150 and would produce as a main fragment an isomer of cresol, with m/z of 108 (Figure 4.4). Likewise, it could be anticipated that the main fragmentation observed in the ring-alkylated products should result from C-C cleavage and release a methyl fragments with m/z of 15. Figure 4.5 shows the fragmentation for isopropylmethylphenol (IMP), where the main fragment corresponds to an isopropylphenyl ion with m/z=135.

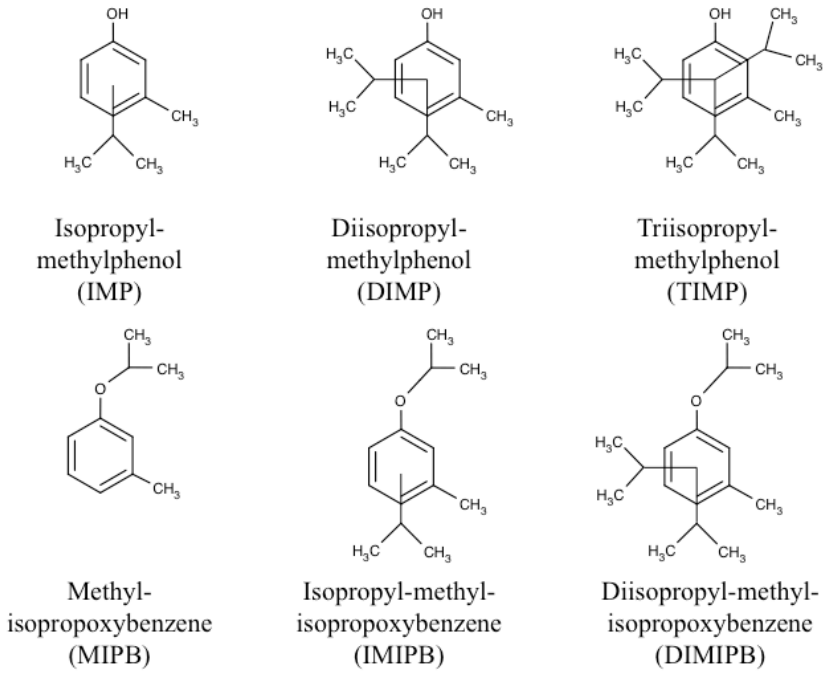

Figure 4.3. Products from alkylation of m-cresol with isopropanol.

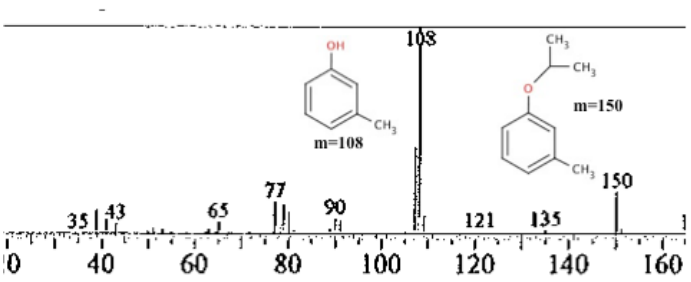

Figure 4.4. MS fragmentation pattern for methyl-isopropoxybenzene from the reaction mixture

These simple fragmentation rules were sufficient for distinguishing ethers from ring-alkylated products. Notice that this analysis does not differentiate among the specific isomers that, as depicted in Figure 4.6, number from one to seven depending on the structure. Therefore, they were lumped together, with the acknowledgment that isomerization and transalkylation of the ring-alkylated products is likely to occur under these conditions.[11,83] Figure 4.2 (b) shows the evolution of the alkylation products as a function of reaction time. Initially, the two primary alkylation products, IMP and MIPB, were formed at similar rates, but soon they were consumed to make secondary products. It is important to note that the O-alkylated products (MIPB) undergo a much faster decay compared to the ring-alkylated products. This observation is in agreement with previous reports indicating that selectivity to ethers decreases with reaction time (or space time in flow systems).[63,84] Even though ethers are not thermodynamically favored, they are kinetic products because the oxygen in the hydroxyl group is a stronger nucleophile when compared to the ring, and can therefore be alkylated easier.

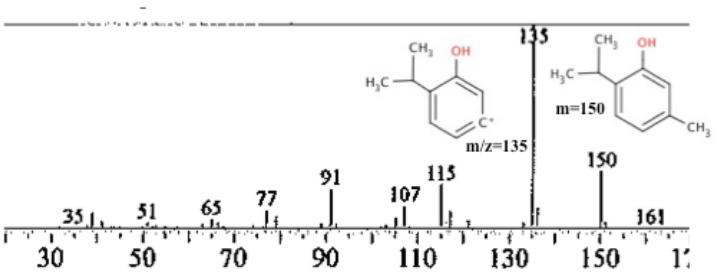

Figure 4.5. MS fragmentation pattern for isopropylmethylphenol from the reaction mixture

As discussed below, this is due to the fast ether decomposition rate in the presence of an acid catalyst. As a result, it is observed that after 2 h of reaction, DIMP became the dominant product, with a smaller concentration of IMIPB. The concentration of TIMP and DIMIPB was always minor as compared to the other products.

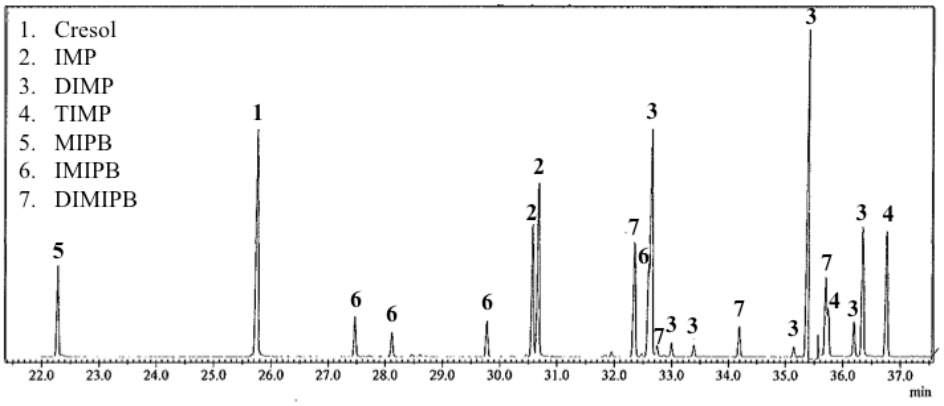

Figure 4.6. GC-MS chromatogram with products from alkylation of m-cresol with isopropanol over a HY zeolite. Column was Rtx-1701 with mid-polarity

It is also worth noting the change in the conversion rate of m-cresol, which reached a plateau with reaction time, even before the reactant was consumed, or reaching equilibrium. Therefore, in a batch reactor, this is an indication of catalyst

deactivation, and as presented below, catalyst deactivation needs to be incorporated in the analysis when developing the kinetic model.

• *Verification of the absence of mass transport limitations*

Before further experimentation or data analysis, it was important to probe the system and rule out mass or heat transfer limitations. The Koros-Nowak criterion states that the rate of reaction is directly proportional to the concentration of active sites in a catalyst. However, when the reaction is influenced by external or internal mass transfer or heat transfer limitations the rate will not be directly proportional to the concentration of active sites. Koros and Nowak[85] used their test by mixing two powders, one inert and the other catalytic, at varying ratios, thus creating a series of samples with different active sites concentration. If the reaction rate, after being normalized to the concentration of active sites, does not change for the different catalysts then the system is exempt from transport limitations. In a similar test, Madon and Boudart[36] compared a series of supported metal catalysts with varying metal loading. This test, proposed more than 30 years ago, has been used successfully in many studies on supported metal catalysts. However, the criterion has been much less common in studies of acidic zeolites.[86] In this work, we varied the concentration of acid sites of a HY Zeolite (Si/Al=30) by ion exchange with sodium hydroxide and used the resulting catalysts to determine whether the alkylation reaction was transport-limited. Three zeolites were obtained and their Brønsted acidity is reported in Table 4.1. As observed, about 50% of the target acid sites were exchanged and a significant difference in acid site concentration between the samples was obtained.

Table 4.1. Acid site density of zeolites used for mass transport limitations test. Original zeolite was an HY with Si/Al=30 (first row)

Sodium used for exchange (µmol/g zeolite)	Theoretical Brønsted acid site density (µmol/g zeolite)	Measured Brønsted acid site density (µmol/g zeolite)
0	538	248
67	538	218
100	438	190

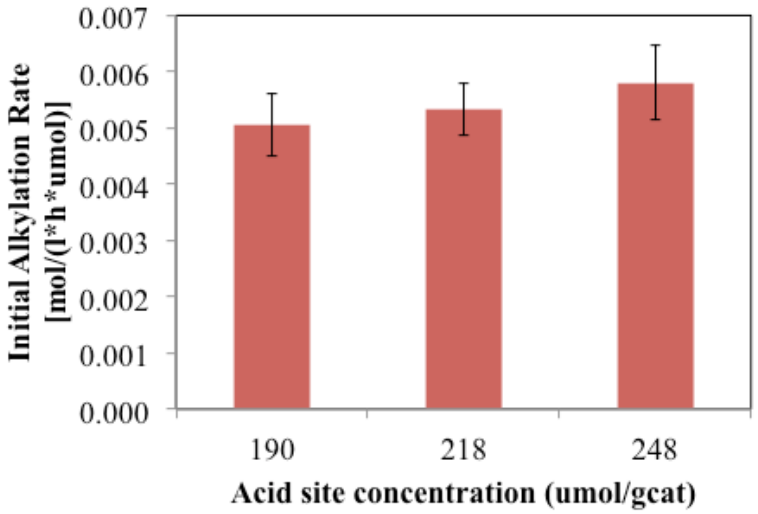

Figure 4.7. Initial alkylation rates for catalysts with different acid site concentration. Conditions: IPA/m-cresol=3.8, T=473K, P=4.8MPa, reaction: 1h

Figure 4.7 shows the specific reaction rate (TOF) for the alkylation of m-cresol on a per site basis with the various exchanged zeolites. The values are equivalent within the experimental error and certainly do not decrease as a function of acid site density, which would be expected if mass transfer limitations were present. In order to avoid the effects of any catalyst deactivation, the values reported correspond to short reaction times, since deactivation could depend on density of acid sites and mask the true TOF.

• *Conversion of isopropyl-methylphenol (thymol) and isopropoxybenzene*

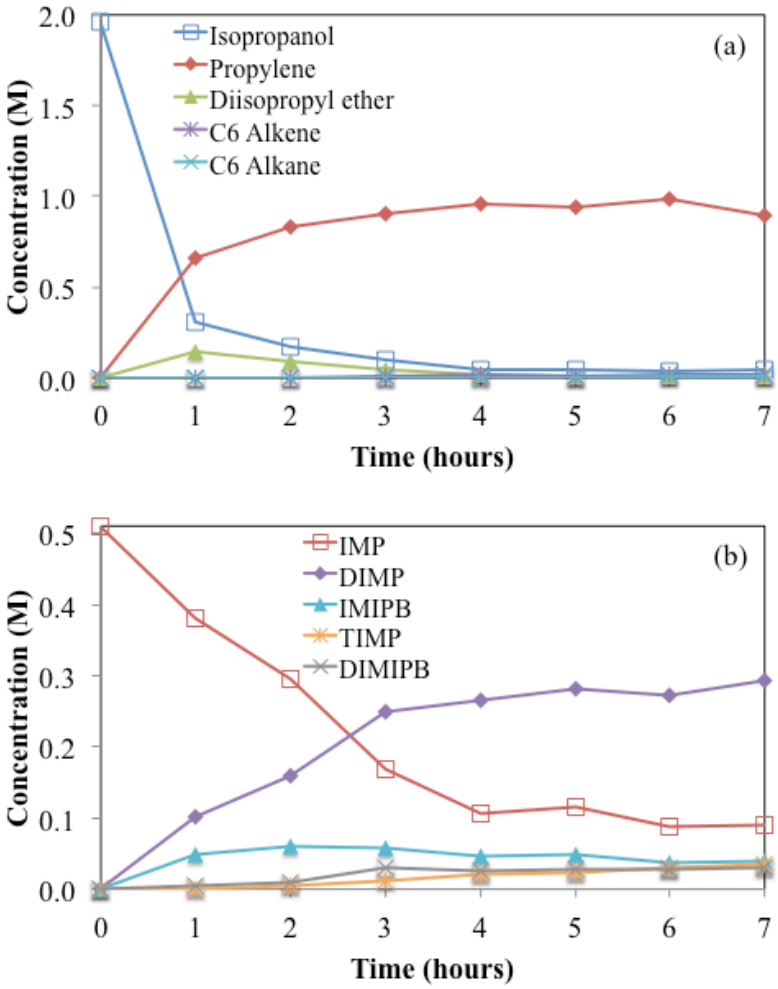

Figure 4.8. Product distribution from alkylation of thymol (IMP) with isopropanol. (a) Dehydration/oligomerization products. (b) Alkylation products. Conditions: isopropanol/thymol=3.8, T=473K, P=4.8MPa, catalyst mass=50mg HY

The observed product distribution revealed the complexity of the alkylation reaction system in terms of the number of different steps that possibly take place. It is clear that to get a better understanding of the reaction pathways and generate a reliable kinetic model additional experimental data are required. Accordingly, the alkylation of one of the isomers of IMP, thymol, with isopropanol was carried out under the

same conditions as those used for m-cresol alkylation. As shown in Figure 4.8, dehydration of isopropanol to diisopropyl ether and propylene readily occurred, as in the case of m-cresol alkylation. On the other hand, DIMP was the dominant alkylation product, while MIPB and trialkylated products (TIMP and DIMIPB) only appeared in low concentrations. A similar deactivation pattern to that observed during m-cresol alkylation was evident as the rate of IMP (thymol) consumption leveled off after 4 h of reaction, despite the presence of a significant amount of unconverted IMP.

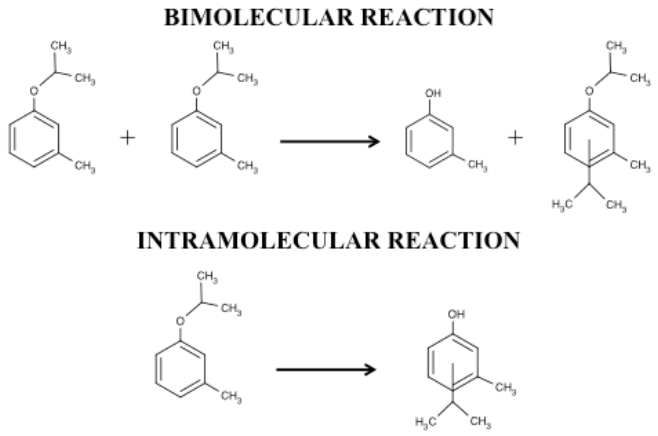

Figure 4.9. Possible routes of conversion for methyl-isopropoxybenzene

In order to study the reactivity of the ether products, a series of experiments with aryl-alkylethers was performed. Methyl-isopropoxybenzene, or MIPB (Figure 4.3), was not available commercially; therefore the reactivity of the ether was studied with methoxybenzene (MB) and isopropoxybenzene (IPB). These molecules provided valid information regarding the reactivity of the ether functionality, which has been a subject of interest in previous studies reported in the literature. For example, in a study on the alkylation of phenol with methanol,[83] it was proposed

that anisole (i.e., the ether product) reacts with phenol to give cresol and phenol, suggesting a bimolecular mechanism for interconversion of ether- to ring-alkylated products. Alternatively, computational studies about alkylation of phenol with tert-butanol indicate that the ether product undergoes an intramolecular rearrangement, leading to a direct transformation into a ring-alkylated product. [87]

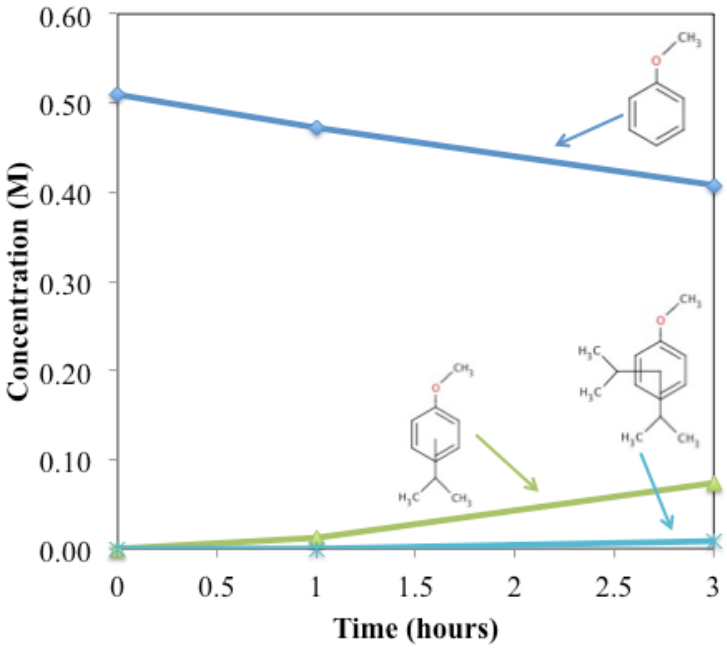

Figure 4.10. Alkylation of methoxybenzene with isopropanol as a function of time. Conditions: isopropanol/methoxybenzene=4:1, temperature=200°C, pressure=700psi

If the conversion of ethers takes place through a bimolecular mechanism, methyl-isopropoxybenzene should yield cresol and isopropyl-methyl-isopropoxybenzene as the primary products. On the other hand, shall intramolecular rearrangement be the correct route of conversion, isopropyl-methylphenol would be the primary product (Figure 4.9). Alkylation of methoxybenzene was studied under the same conditions as those of m-cresol (Figure 4.10). Products from two consecutive ring alkylation

steps where detected. This indicates the ability of methoxybenzene to undergo alkylation while preserving the ether group. However, neither phenol nor cresols were observed as products, suggesting that the methoxy group is not subject to cleavage under these reaction conditions. On the other hand, it is possible that the stability of the methoxy group is higher than the isopropoxy group, and thus it was necessary to consider the reactivity of isopropoxybenzene before drawing a conclusion.

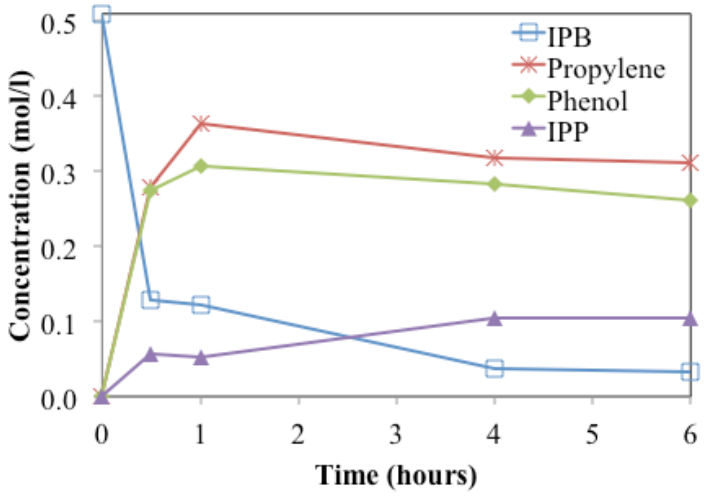

Figure 4.11. Product distribution from decomposition of isopropoxybenzene. Conditions: initial concentration=0.51M, T=473K, P=4.8MPa, catalyst mass=50mg

Figure 4.11 shows the product distribution from IPB decomposition as a function of reaction time. In this case no isopropanol was added in order to distinguish how susceptible to cleavage was the isopropoxy group. It was clear that phenol and propylene were the primary products from a fast cleavage of the ether bond. Thus, the proposed intramolecular rearrangement mechanism was not supported by our experiments. Rather, as depicted in Figure 4.12, the ring-alkylated product

isopropylphenol, IPP was a secondary product that arises from the alkylation of phenol with propylene, both resulting from the initial ether decomposition.

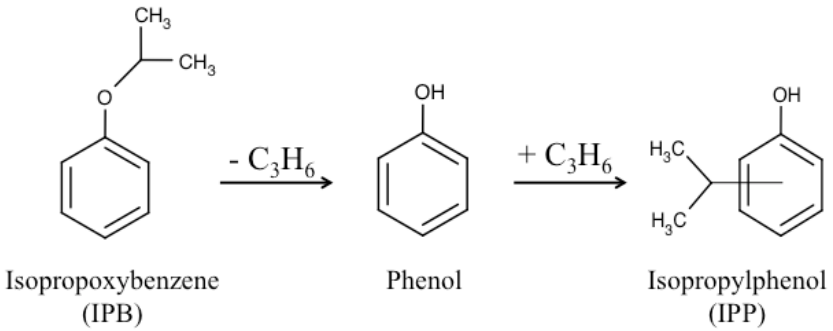

Figure 4.12. Isopropoxybenzene decomposition and subsequent alkylation

• *Effect of alkylating agent*

Alkylation of phenolic compounds is an electrophilic substitution reaction, in which an electrophile attacks an electron-enriched group in the phenolic molecule. There are two possibilities for an electrophilic attack in m-cresol: the aromatic ring and the oxygen atom in the hydroxyl group. They are able to yield C-alkylation products and O-alkylation products, respectively. The oxygen atom in the hydroxyl group has a higher electron density in the highest occupied molecular orbital as compared to the carbon atoms in *ortho* and *para* positions, making O-alkylation favored over C-alkylation, at least initially.[87] Regarding the electrophile (alkylating agent), there are also two possibilities. In the presence of an acid, isopropanol can undergo protonation and generate an oxonium species.

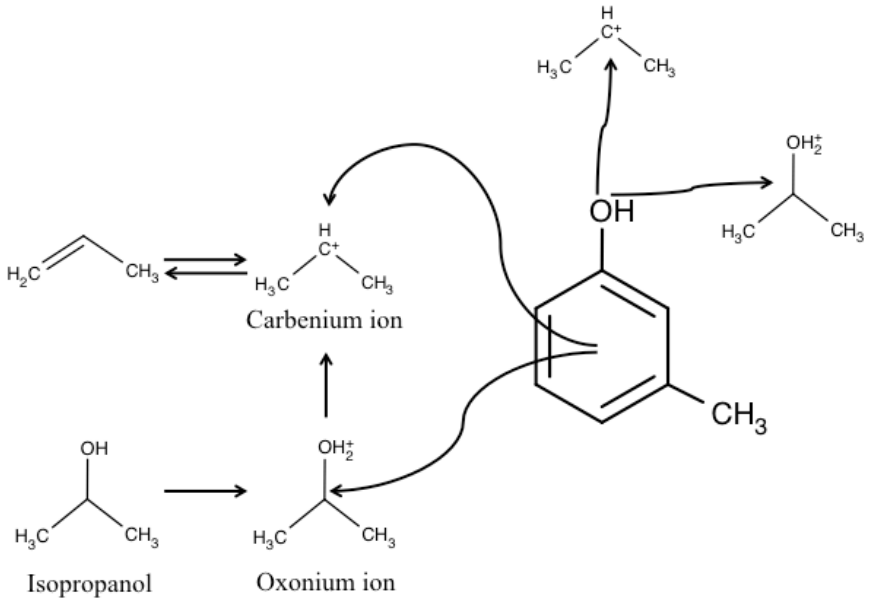

Figure 4.13. Electrophilic substitution of m-cresol with isopropanol and propylene

Also, upon dehydration of this oxonium ion, a carbenium ion is formed on the surface, which after desorption produces an olefin. At the same time an olefin from the bulk phase can re-adsorb and form again a carbenium ion. Due to the high concentration of propylene observed in the reactor, it can be assumed that the main source of carbenium ion formation is the protonation of propylene rather than the dehydration of an oxonium ion. Both of these ionic species (oxonium and carbenium ions) would be able to perform an electrophilic attack (Figure 4.13). From our initial experiments it is not clear whether isopropanol or propylene is the alkylating agent for C- and O-alkylation, or if the two of them play a similar role in both alkylation reactions.

To clarify the role of the alkylating agent, a series of experiments was performed with different concentrations of isopropanol and propylene and the selectivity

towards C-alkylated (IMP, DIMP, TIMP) and O-alkylated (MIPB, IMIPB, DIMIPB) products was compared.

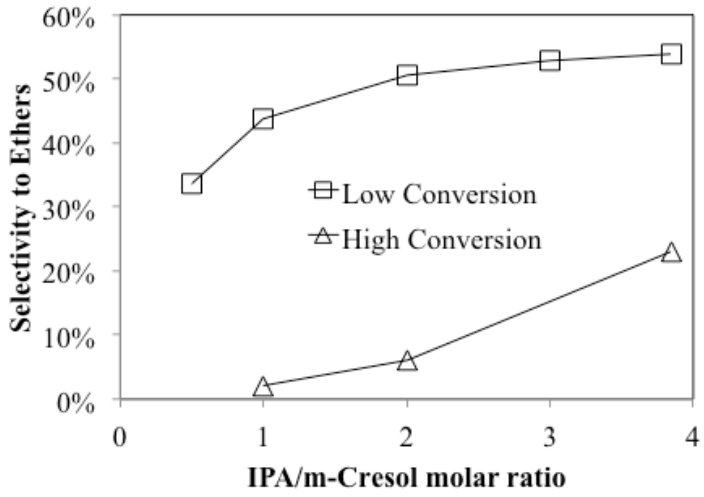

Figure 4.14. Effect of isopropanol/m-cresol molar ratio and conversion on the selectivity to etherification products. Conditions: T=473K, P=4.8MPa

Figure 4.14 shows the variation of selectivity towards ethers with the isopropanol/m-cresol molar ratio in the feed. The comparison was done at two levels of conversion, low (11-17%) and high (56-62%). It was clear that the selectivity to ethers is significantly higher at lower conversion. The drastic decrease in the overall ether selectivity at high conversion is most likely due to the fast ether decomposition mentioned above. However, for a given conversion level, this selectivity increased with the isopropanol/m-cresol ratio, in agreement with the trends reported for the alkylation of m-cresol and o-cresol with isopropanol[63,88] and tert-butanol.[84] As shown in Figure 4.15, using propylene as alkylating agent instead of isopropanol, at the same C3/m-cresol ratio and same level of conversion, resulted in a much lower selectivity towards ethers. Therefore, while the carbenium ion forming from the olefin was able to alkylate both the oxygen and the carbon

atoms in m-cresol, the use of isopropanol as alkylating agent favored the formation of the ether as primary product.

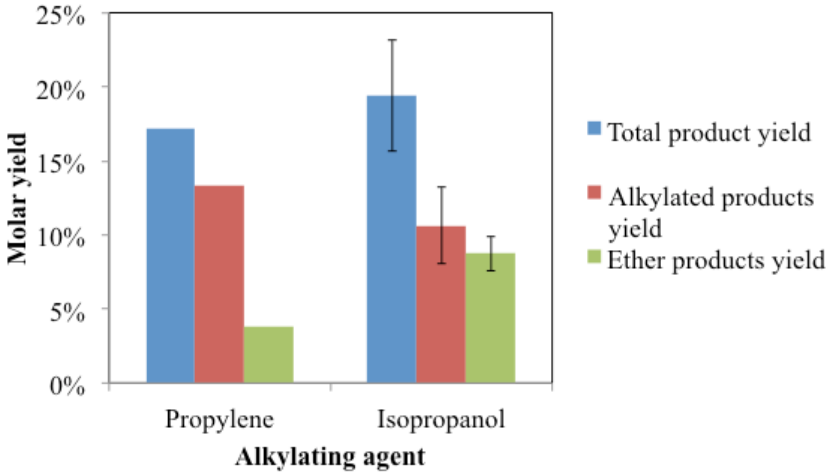

Figure 4.15. Alkylated and ether product yields for alkylation of m-cresol with propylene and isopropanol. Conditions: isopropanol or propylene/m-cresol=3.8, T=473K, P=4.8MPa, catalyst mass=20mg HY, reaction time=1h

From previous studies conducted in the vapor phase,[11] one would have not predicted this difference. In fact, it was shown that isopropanol dehydration was much faster than the m-cresol alkylation reaction and as a result, propylene would be the alkylating agent, essentially erasing any differences in the subsequent alkylation. Likewise, as shown in Figure 4.16, dehydration was also faster than alkylation in the liquid phase, enhancing the possibility that the oxonium ion quickly dehydrates and forms an olefin on the surface before it can start the alkylation step. In that case, the protonated olefin would be responsible for both O- and C-alkylation, while isopropanol would only be the precursor for the alkylating agent. In order to shed light to this conundrum, alkylation of m-cresol was performed with n-propanol. Protonation of this alcohol should form a primary oxonium ion, which upon dehydration would form a secondary carbenium ion,

because of its higher stability over a primary carbenium ion. Alkylation from a secondary carbenium ion would in turn lead to isopropyl-alkylated phenols. However, if the primary oxonium ion serves as the alkylating agent, then n-propyl-alkylated phenols should be observed (Figure 4.16).

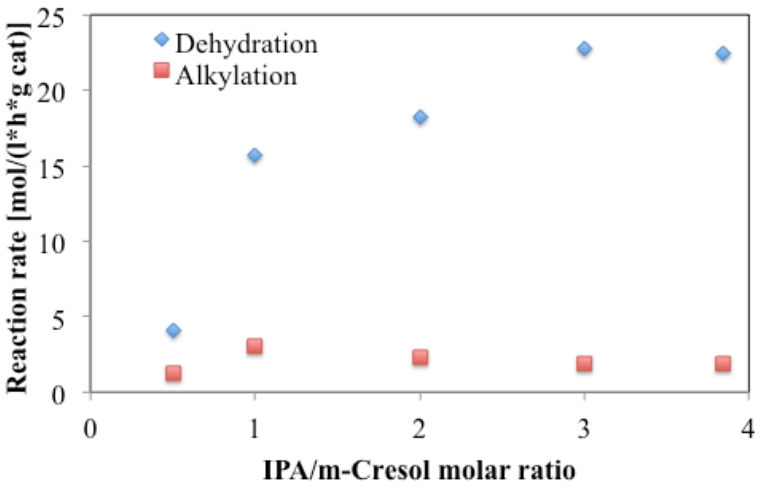

Figure 4.16. Rate of dehydration and alkylation during reaction of isopropanol with m-cresol over a HY zeolite. Conditions: T=473K, P=4.8MPa

In fact, as shown in Figure 4.18, both n-propyl-alkylated ring and n-propyl ethers are the main reaction products of the alkylation with n-propanol, leading to the conclusion that the oxonium ion formed by protonation of the alcohol was able to attack both the aromatic ring and the oxygen of the hydroxyl group in m-cresol. However, it should be noted that n-propanol dehydration was significantly slower than dehydration of isopropanol. This was evident by the significantly lower yield of alkylation products obtained with the former (i.e., comparing Figure 4.15 and Figure 4.18). One could argue that, due to the slower dehydration of n-propanol, the oxonium ion had more time to act as direct alkylating agent, whereas in the case of isopropanol dehydration was fast and the presence of oxonium ions was limited.

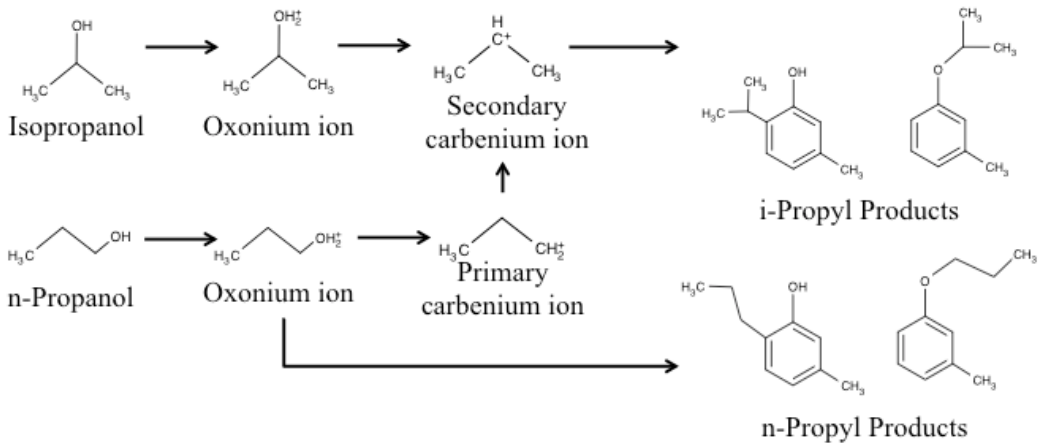

Figure 4.17. Alkylation via an oxonium and a carbenium ion

Nevertheless, taking all the results together, it was concluded that, even if it is less important than the carbenium ion, the oxonium ion was also a direct alkylating agent. Also, both O- and C-alkylation could take place with both ionic species, oxonium and carbenium.

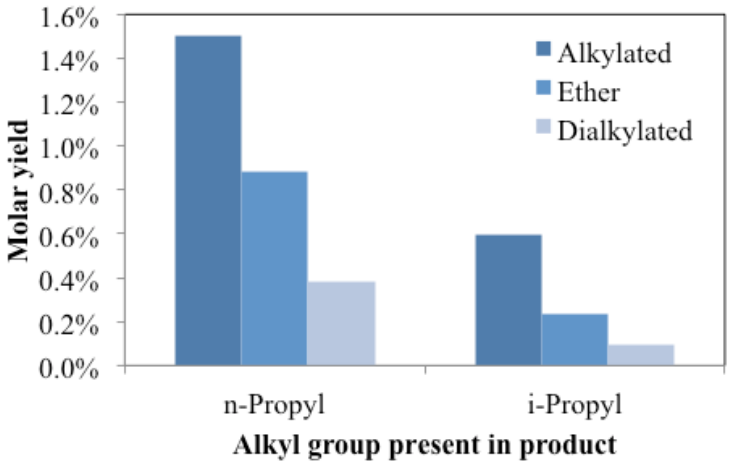

Figure 4.18. Product yields for alkylation of m-cresol with n-propanol. Conditions: n-propanol/m-cresol=3.7, T=473K, P=4.8MPa, catalyst mass=50mg HY, reaction time=1h

This conclusion is in agreement with recent computational studies of alkylation of phenolics with tert-butanol, which show that the energy barriers for alkylation with the alcohol and the respective olefin are not significantly different.[*89*]

• *Reaction pathways and kinetic model*

Based on this qualitative analysis of the experimental results, we have proposed a reaction scheme for alkylation of m-cresol with isopropanol in a HY zeolite (Figure 4.19) that forms the basis of a more quantitative kinetic model. Accordingly, the first step is the dehydration of the alcohol. From this work as well as previous studies it was observed that dehydration of isopropanol could occur via two parallel paths, one was the direct dehydration and the other via formation of diisopropyl ether, which could further decompose to propylene and water.[88]

$$\text{Isopropanol} \rightarrow \text{Propylene} + \text{Water} \qquad (4.6)$$

$$2\ \text{Isopropanol} \rightarrow \text{Diisopropyl ether} + \text{Water} \qquad (4.7)$$

$$\text{Diisopropyl ether} \rightarrow 2\ \text{Propylene} + \text{Water} \qquad (4.8)$$

In order to reduce the number of parameters in the model, and taking into account the fast rate of diisopropyl ether decomposition, these three reactions were simplified into equation (4.6). To consider the potential role of the reverse reaction, the equilibrium constant at 200°C was calculated (K_{EQ} = 2508) and used to relate the forward reaction with the reverse reaction.

$$k_{d\text{-}1}=k_{d1}/K_{EQ} \qquad (4.9)$$

According to the previous discussion, the alkylation of m-cresol was considered to occur by the O- and C-alkylation routes, involving both, isopropanol and propylene as alkylating agents. The ether products could undergo decomposition to form propylene and the correspondent phenolic or subsequent C-alkylation with either isopropanol of propylene. In parallel, ring-alkylated products participated in the same type of reactions as m-cresol. It is important to note that, based on the

experimental results above, intramolecular arrangement (isomerization) of ethers was not considered. Additionally, a zero-order polymerization reaction leading to insoluble products was included in the model. This path showed a low rate compared to other relevant reactions, since the mole balance for most reactions was above 90%. However, it is required to completely close the mass balance and account for all the species formed during reaction.

The two conventional Langmuir-Hinshelwood and Eley-Rideal models were used to analyze the reaction scheme. In both cases, the participation of reactants, products, and solvent in competitive adsorption on the catalyst surface was considered. For Langmuir-Hinshelwood, the rate-limiting step was the reaction between two adsorbed species (phenolic and alkylating agent), except in the case of ether decomposition and alcohol dehydration, where the rate was only proportional to the surface concentration of a single reactant. As an example, the coverage and mole balance for isopropanol are shown below.

$$\theta_{IPA} = [K_{IPA}C_{IPA}] / [1+K_{IPA}C_{IPA}+K_PC_P+K_{H2O}C_{H2O}+K_CC_C+K_{PHEN}(C_{IMP}+C_{DIMP}+C_{TIMP})+ K_{ETHER}(C_{MIPB}+C_{IMIPB}+C_{DIMIPB})] \quad (4.10)$$

$$dC_{IPA}/dt = [-k_{d1}\theta_{IPA} + k_{d-1}\theta_P\theta_{H2O} - k_{o1}\theta_{IPA}\theta_C - k_{o2}\theta_{IPA}\theta_{IMP} - k_{o3}\theta_{IPA}\theta_{DIMP} - k_{c1}\theta_{IPA}\theta_C - k_{c2}\theta_{IPA}\theta_{IMP} - k_{c3}\theta_{IPA}\theta_{DIMP} - k''_{c2}\theta_{IPA}\theta_{MIPB} - k''_{c3}\theta_{IPA}\theta_{IMIPB}] \quad (4.11)$$

(θ_i's are the surface coverages of each species, k_i's are the rate constants, C_i's are the species concentrations in the liquid phase, and K_i's are the adsorption constants). For simplicity, a general adsorption constant K_{PHEN} was defined for ring-alkylated products (IMP, DIMP, TIMP) and K_{ETHER} for ether products (MIPB, IMIPB, DIMIPB).

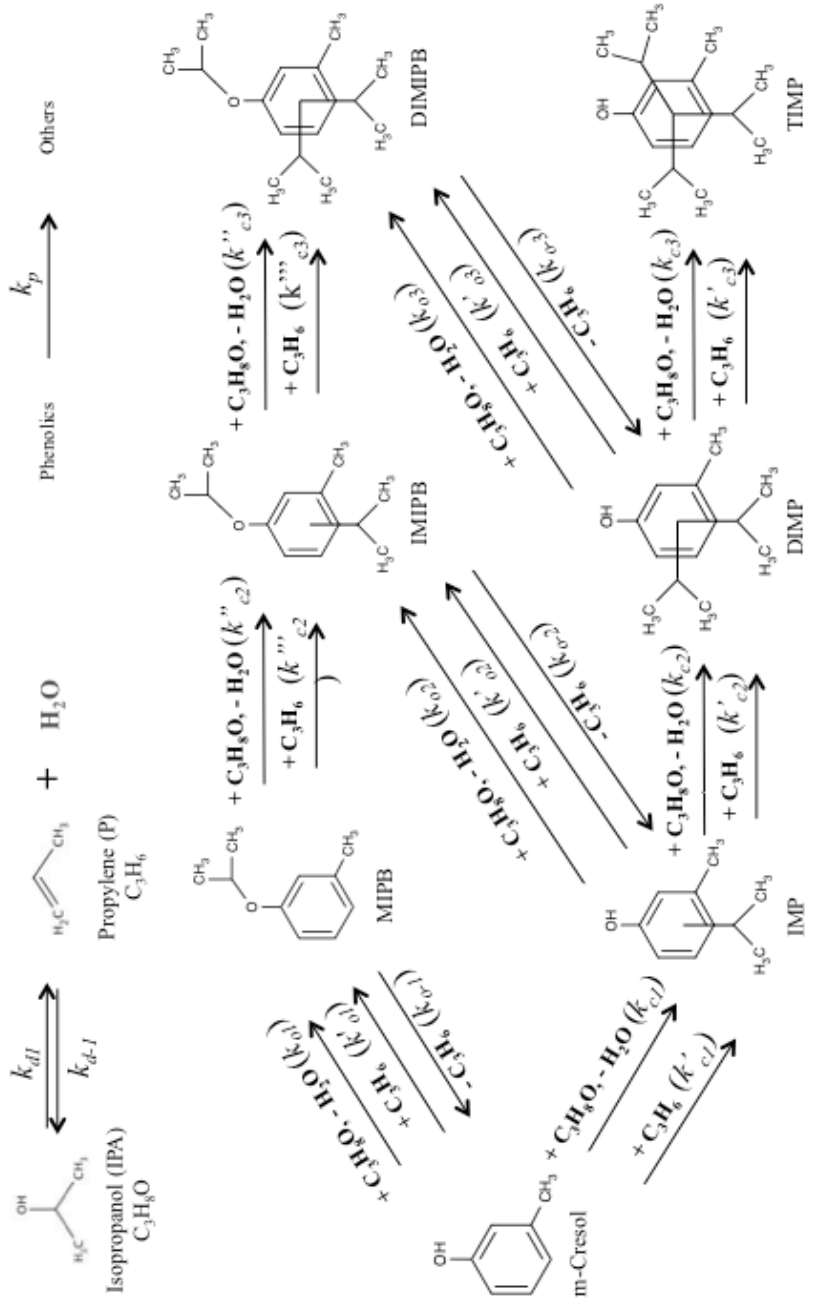

Figure 4.19. Reaction scheme for the reaction of m-cresol with isopropanol in the presence of HY zeolite. C_3H_8O: isopropanol. C_3H_6: propylene

On the other hand, for the Eley-Rideal model, the rate-limiting step for alkylation was the reaction between an adsorbed molecule of alkylating agent and a non-adsorbed phenolic molecule (m-cresol, ring-alkylated or ether). Again, an example of the mole balance for isopropanol is shown below (k_i's are the rate constants, C_i's are the species concentrations in the liquid phase, and θ_i's are the surface coverages).

$$dC_{IPA}/dt=[-k_{d1}\theta_{IPA}+k_{d-1}\theta_P\theta_{H2O}-k_{o1}\theta_{IPA}C_C-k_{o2}\theta_{IPA}C_{IMP}-k_{o3}\theta_{IPA}C_{DIMP}-k_{c1}\theta_{IPA}C_C-$$

$$k_{c2}\theta_{IPA}C_{IMP}-k_{c3}\theta_{IPA}C_{DIMP}-k''_{c2}\theta_{IPA}C_{MIPB}-k''_{c3}\theta_{IPA}C_{IMIPB}] \quad (4.12)$$

The concentration of propylene was modeled using an estimate of the Henry's constant under the reaction conditions.[90] Propylene partial pressure was estimated from the moles of propylene in the system and the ideal gas equation. Since Henry's constant relates the partial pressure to the liquid composition, the liquid concentration of propylene was calculated from the following equation.

$$C_P=(p_P*\rho_{Solv})/H_P^{200°C} \qquad (4.13)$$

Here p_P is the partial pressure, ρ_{Solv} the density of the solvent and $H_P^{200°C}$ the Henry's constant at 200 °C. Finally, as mentioned above, the catalyst underwent significant deactivation under the reaction conditions. Decay in activity could be due to oligomerization of propylene that promotes coke formation,[91] strong adsorption of phenolic compounds,[64] or zeolite degradation due to the presence of liquid water.[10,61] Previous studies have described the deactivation of zeolites in terms of an activity function, defined in terms of the deactivation mechanism, either pore plugging or active sites fouling.[92,93] This deactivation function has two adjustable parameters (A and B) and it was coupled with our kinetic model by

combining it with each mole balance. Also for isopropanol, the resultant equation is shown below. As expected, the rate of reaction decreases as a function of time when this function is used.

$$dC_{IPA}/dt=[-k_{d1}\theta_{IPA}+k_{d-1}\theta_P\theta_{H2O}-k_{o1}\theta_{IPA}\theta_C-k_{o2}\theta_{IPA}\theta_{IMP}-k_{o3}\theta_{IPA}\theta_{DIMP}-k_{c1}\theta_{IPA}\theta_C-$$

$$k_{c2}\theta_{IPA}\theta_{IMP}-k_{c3}\theta_{IPA}\theta_{DIMP}-k''_{c2}\theta_{IPA}\theta_{MIPB}-k''_{c3}\theta_{IPA}\theta_{IMIPB}][(B+1)/(B+e^{At})] \quad (4.14)$$

• *Validating model by independent rate measurements and added constrains*

Due to the complexity of the several phenomena involved, the resulting reaction scheme generated a large number of adjustable variables (rate constants, adsorption constants and deactivation parameters) for the kinetic model. Therefore, in order to provide independent measurements, reduce the level of uncertainty, and improve the precision of the fitting results two additional sets of experiments with individual reactants were performed: dehydration of isopropanol and decomposition of isopropoxybenzene. Both reactions are simpler than the alkylation reaction, require only one reactant, and play a crucial role in the overall reaction scheme. They were performed individually to estimate rate constants for dehydration and ether decomposition that were then used as initial guesses and to define limits for these variables in the kinetic model.

Next, reaction measurements were conducted in differential mode (low conversion) to eliminate the influence of products in the rate expression and thus obtain kinetic constants with fewer adjustable parameters. That is, the rate of reaction for dehydration of isopropanol as stated in equation (4.6) can be written based on a Langmuir-Hinshelwood mechanism as follows:

$$r_{d1}=[k_{d1}K_{IPA}C_{IPA}]/[1+K_{IPA}C_{IPA}+K_PC_P+K_{H2O}C_{H2O}] \quad (4.15)$$

At low conversion, this expression can be simplified as:

$$r_{d1}=[k_{d1}K_{IPA}C_{IPA}]/[1+K_{IPA}C_{IPA}] \quad (4.16)$$

Equation (4.16) was used to fit the data in Figure 4.20 for isopropanol dehydration at low conversions. The resulting rate of dehydration was 1040 [mol l^{-1} h^{-1} $gcat^{-1}$] and the adsorption constant 0.34 (l mol^{-1}).

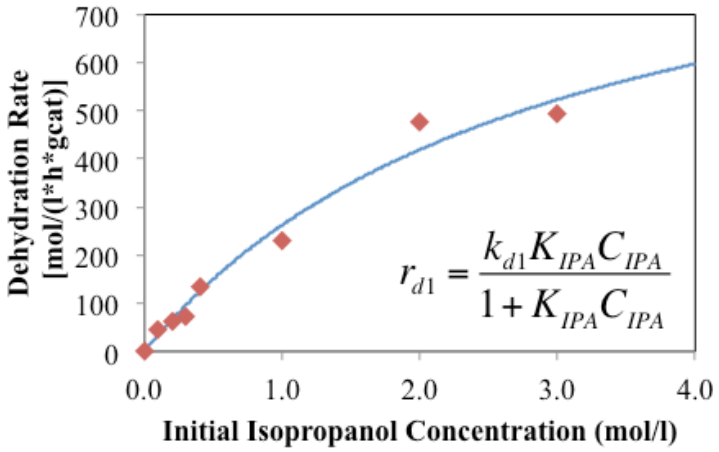

Figure 4.20. Rate of isopropanol dehydration measured at different isopropanol concentrations and short reaction time. Conditions: T=473K, P=4.8MPa, catalyst mass=10mg HY, reaction time=0.2h

In the same way, the rate of decomposition of isopropoxybenzene (an analog of methyl-isopropoxybenzene) at low conversions can be written based on a Langmuir-Hinshelwood mechanism:

$$r_{d1}=[k_{o\text{-}1}K_{IPB}C_{IPB}]/[1+K_{IPB}C_{IPB}] \quad (4.17)$$

Data from Figure 4.21 was fitted using equation (4.17). A rate constant of 5.9 [mol l^{-1} h^{-1} $gcat^{-1}$] and an adsorption constant of 26 (l mol^{-1}) were obtained.

Moreover, further constraints were set on the model based on general knowledge and experimental observations obtained from previous studies. The constraints used

for the kinetic fitting of both Langmuir-Hinshelwood and Eley-Rideal models are listed below.

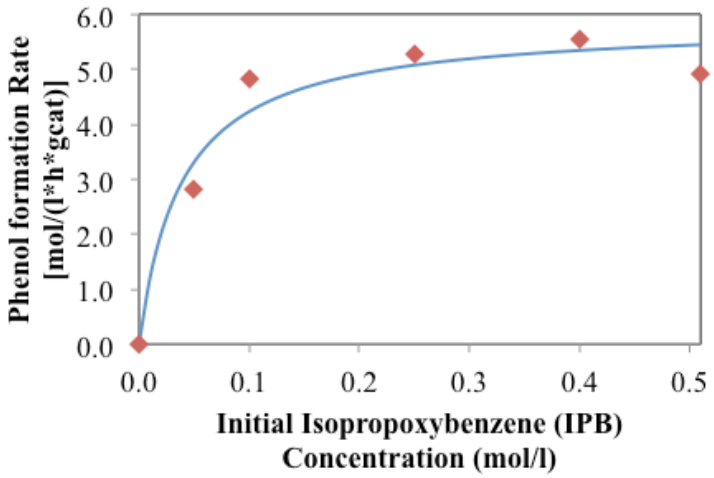

Figure 4.21. Rate of isopropoxybenzene decomposition measured at different isopropoxybenzene concentrations and short reaction time. Conditions: T=473K, P=4.8MPa, catalyst mass=20mg HY, reaction time=0.5h

- Isopropanol dehydration.
  - Rate constant initial guess (k_{d1}): 1040 [mol l^{-1} h^{-1} $gcat^{-1}$]. *From experiments (Figure 4.20).*
  - Rate constant limits: k_{d1}<1240 [mol l^{-1} h^{-1} $gcat^{-1}$]. *Allows k_{d1} to increase up to 20% of the initial guess.*
  - Adsorption constant initial guess (K_{IPA}): 0.34 (l mol^{-1}). *From experiments (Figure 4.20).*
  - Adsorption constant limits: K_{IPA}<1 (l mol^{-1}). *Allows K_{IPA} to increase without changing its order of magnitude.*
- Ether decomposition
  - Rate constant initial guess (k_{o-1}, k_{o-2}, k_{o-3}): 5.9 [mol l^{-1} h^{-1} $gcat^{-1}$]. *From experiments (Figure 4.21).*

- Rate constant limits: $4.7<k_{o-1}, k_{o-2}, k_{o-3}<7.1$ [mol l^{-1} h^{-1} $gcat^{-1}$]. *Allows k_o's to vary within ±20% of initial guess.*
- Adsorption constant initial guess (K_{ETH}): 26 (l mol^{-1}). *From experiments (Figure 4.21).*

- Deactivation parameters
  - Limits: $A,B<20$. *Limits parameters to the range reported in the literature.*[92,93]

- Adsorption constants
  - Ethers adsorption constant initial guess: 26 (l mol^{-1}). *From experiments (Figure 4.21).*
  - m-Cresol and phenolics adsorption constant limits: $(0.5*K_{ETH})<K_C, K_{PHEN}<(1.5*K_{ETH})$. *Limits K_C and K_{PHEN} to the same range of K_{ETH}.*
  - Propylene adsorption constant: $(0.5*K_C)<K_P<(1.5*K_C)$. *Limits K_P to the same range of K_C.*
  - Water adsorption constant: $K_{H2O} \geq K_P$. *Keeps K_{H2O} in the same range as that of hydrocarbons and phenolics.[94]*

- Alkylation.
  - Rate constants for O-alkylation with isopropanol were higher than the respective reaction with propylene. *From experiments (Figure 4.15).*
  - Rate constants for C-alkylation with propylene were higher than the respective reaction with isopropanol. *From experiments (Figure 4.15).*

• *Kinetic modeling results*

From the fitting of the experimental data with the constraints described above, it was possible to obtain thermodynamic and kinetic parameters with physical significance. For example, as shown in Table 4.2, adsorption constants were obtained for all the species present on the surface. Similarly, Tables 4.3, 4.4 and 4.5 summarize rate constants for all reactions, while Table 4.6 includes the resulting parameters for the deactivation function.

Table 4.2. Adsorption constants of reactants and products on HY zeolite in the reaction of m-cresol with isopropanol using two different kinetic models. Units are [l mol^{-1}]

Compound	Adsorption constant	
	Langmuir-Hinshelwood	Eley-Rideal
Isopropanol	1.0	1.0
Propylene	10	10
Water	10	10
Cresol	20	21
Ring-alkylated products	61	63
Ether products	41	42
Decalin	0	0

Table 4.2 shows the resultant adsorption constants for both Langmuir-Hinshelwood and Eley-Rideal models. No difference was observed in the values obtained from these models. Adsorption of propylene and water was significantly stronger than that of isopropanol, evident by an order of magnitude difference in adsorption constants. At the same time, the adsorption constant for m-cresol was an order of magnitude higher than isopropanol. Since dehydration and alkylation take place at the same time on the catalyst surface, it would be expected that the rate of dehydration be inhibited by the strong adsorption of m-cresol. This is actually what was observed when comparing dehydration in the absence and the presence of m-

cresol (Figure 4.22). The group adsorption constant for phenolic compounds K_{PHEN} was significantly higher than the adsorption constant for m-cresol. Phenolic compounds can take different configurations when adsorbing on acidic catalysts.[80,91,95] If the aromatic ring interacts in a parallel geometry with the surface, an increase in the number of alkyl-substituents could enhance the adsorbate-surface interaction.[96]

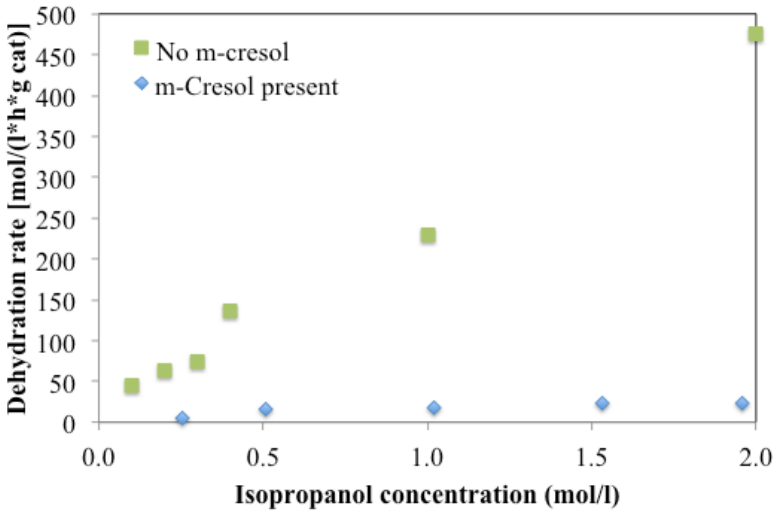

Figure 4.22. Effect of m-cresol on the rate of isopropanol dehydration. Conditions: T=473K, P=4.8MPa

Also, increasing the number of alkyl substituents can result in enhanced adsorption entropy with a corresponding increase in the observed adsorption constant for the ring-alkylated products compared to m-cresol. The adsorption constant for the ether lies somewhere between those of m-cresol and phenolics. Its interaction with the surface is likely to take place through the oxygen atom in the hydroxyl group, leading to the fast carbon-oxygen bond cleavage observed experimentally. Finally, decalin appeared to have a rather weak interaction with the surface, as compared to the reactants and products, as reflected by a low adsorption constant.

Rate constants for dehydration and polymerization are shown in Table 4.3. As in the previous case, there was not significant difference in the results from Langmuir-Hinshelwood and Eley-Rideal kinetic models. Table 4.4 shows the rate constants obtained from the Langmuir-Hinshelwood model for the multiple alkylation steps and both C- and O-alkylation. A clear trend was observed; the bulkier is the molecule being alkylated, the slower is the alkylation rate. For C-alkylation with isopropanol, the order in rate constant was as follows: $k_{c1} > k_{c2} > k_{c3}$ and $k''_{c2} > k''_{c3}$, and the same trend was true for C-alkylation with propylene and for O-alkylation.

Table 4.3. Rate constants for dehydration and polymerization in the reaction of m-cresol with isopropanol using two different kinetic models. Units are [mol l^{-1} h^{-1} $gcat^{-1}$]

Reaction	Rate constant	
	Langmuir-Hinshelwood	Eley-Rideal
Dehydration (forward) k_{d1}	1240	1240
Dehydration (reverse) k_{d-1}	16	16
Polymerization k_p	0.17	0.15

In principle, the addition of an alkyl group to the aromatic ring should increase its electron density, thus generating a higher probability for an electrophilic attack. However, steric constraints start to be important as the number of substituents in the phenolic molecule increases, leading to a limitation in the alkylation rate. These constraints could originate from the molecule itself, i.e. the high substitution of the ring could hinder the addition of an alkyl group, or from the porous character of the catalyst, i.e. the pores are not big enough to hold the product. The latter under the assumption that most active sites are inside the pores and the external surface does not play an important role in catalytic activity. As a matter of fact, it has been suggested that the pore size of zeolites could limit consecutive alkylation due to

geometric constraints,[11] and even some authors have used this limitation as a tool for controlling product selectivity in alkylation reactions.[83]

C-alkylation and O-alkylation happened at similar rates for m-cresol and IMP, whereas they showed a more pronounced difference for DIMP. A comparison of the C-alkylation of IMP vs. MIPB reveals a faster rate constant for the ether. MIPB has only two substituents in the ring, a methyl and an isopropoxy group, whereas IMP has three ring substituents. Electronically, IMP should be more active for ring alkylation than the ether, as suggested by previous results from alkylation of phenol with methanol.[64] However, a methyl group is not as bulky as an isopropyl group, and it is possible the latter could introduce important geometric constraints. Therefore one could expect for MIPB to undergo a faster alkylation due to lower steric limitations as compared to IMP. Another interesting result was found when comparing the rate constants for C-alkylation of m-cresol vs. MIPB. Even though these two compounds have the same number of substituents in the ring, alkylation took place faster in m-cresol. The presence of the bulky isopropyl group in the ether could indeed hinder alkylation at the ortho position, which would be the preferred substitution otherwise. As a consequence the overall rate of alkyation is lower for MIPB. Similar trends were observed for the Eley-Rideal kinetic model, although they were not as consistent with the expected trends as in the case of the Langmuir-Hinshelwood model.

Table 4.4. Rate constants for alkylation and ether decomposition in the reaction of m-cresol with isopropanol using a Langmuir-Hinshelwood kinetic model. Units are [mol l^{-1} h^{-1} $gcat^{-1}$]

Alkylating agent →	C-Alkylation		O-Alkylation		Ether decomposition
Phenolic →	Isopropanol	Propylene	Isopropanol	Propylene	None
m-Cresol	k_{c1}	k'_{c1}	k_{o1}	k'_{o1}	
	80	**80**	**88**	**44**	
IMP	k_{c2}	k'_{c2}	k_{o2}	k'_{o2}	
	20	**41**	**30**	**15**	
DIMP	k_{c3}	k'_{c3}	k_{o3}	k'_{o1}	
	4	**4**	**1**	**1**	
MIPB	k''_{c2}	k''_{c2}			k_{o-1}
	33	**66**			**7**
IMIPB	k''_{c3}	k''_{c3}			k_{o-2}
	22	**44**			**7**
DIMIPB					k_{o-3}
					7

Table 4.5. Rate constants for alkylation and ether decomposition in the reaction of m-cresol with isopropanol using an Eley-Rideal kinetic model. Units are [(h*g cat)$^{-1}$] for alkylation and [mol l^{-1} h^{-1} gcat^{-1}] for ether decomposition

Alkylating agent →	C-Alkylation		O-Alkylation		Ether decomposition
Phenolic →	Isopropanol	Propylene	Isopropanol	Propylene	None
m-Cresol	k_{c1}	k'_{c1}	k_{o1}	k'_{o1}	
	41	**41**	**37**	**19**	
IMP	k_{c2}	k'_{c2}	k_{o2}	k'_{o2}	
	27	**54**	**31**	**15**	
DIMP	k_{c3}	k'_{c3}	k_{o3}	k'_{o1}	
	4	**4**	**12**	**6**	
MIPB	k''_{c2}	k'''_{c2}			k_{o-1}
	27	**27**			**7**
IMIPB	k''_{c3}	k'''_{c3}			k_{o-2}
	3	**5**			**7**
DIMIPB					k_{o-3}
					7

As shown in Table 4.5, for this model the difference between alkylation of m-cresol and IMP was not as pronounced as predicted from the Langmuir-Hinshelwood model, but their rate constants were in roughly the same order. It is possible that phenolic molecules in the bulk phase have geometrically more freedom to interact with the alkylating agent than if they were adsorbed, therefore lifting some of the steric constraints implied by the Langmuir-Hinshelwood model. Overall, both models offered a good fitting as depicted in Figures 4.23 and 4.24.

Table 4.6. Deactivation parameters in the reaction of m-cresol with isopropanol

Deactivation Parameters	
A (h^{-1})	0.32
B	20

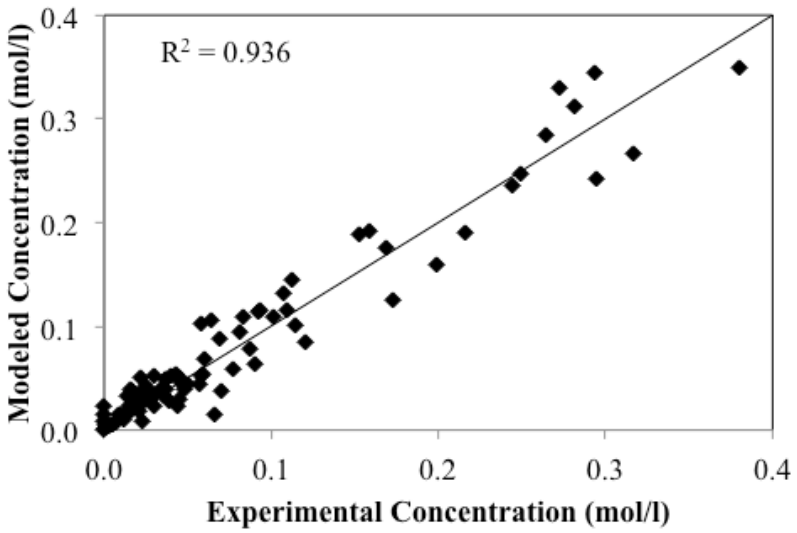

Figure 4.23. Langmuir-Hinshelwood kinetic model results

Water produced from dehydration was present in significant amounts, even to the point of creating a new phase in the reaction mixture. However, the role it played in activity is not clear yet. Some authors have highlighted the positive effects of water

in reaction rates when using zeolites, either by inhibiting olefin oligomerization or generating additional acid sites.[11,97] On the other hand, hot liquid water can significantly degrade the zeolite crystalline structure, and thus negatively impact activity.[10,61] In light of these observations, further studies are required in order to elucidate the role of water in zeolite deactivation during m-cresol alkylation.

The deactivation function provided a good representation of the variation of activity with time, but did not allow to establish a deactivation mechanism from the estimated deactivation parameters, mainly because there were many additional factors in play, as described above.

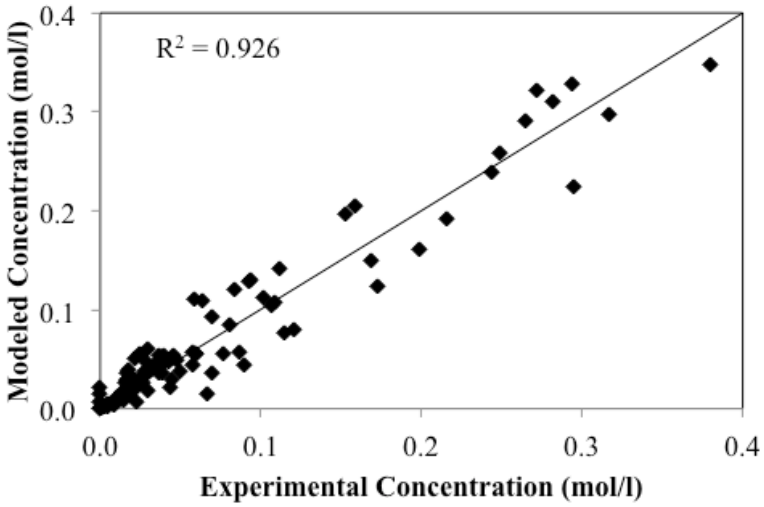

Figure 4.24. Eley-Rideal kinetic model results

4.5. Conclusions

Alkylation of m-cresol with short oxygenates in the liquid phase is an important reaction in the conversion of biomass for production of fuels and chemicals. The present study focused on the understanding of the alkylation of m-cresol with isopropanol reaction in the liquid phase on a HY zeolite. To gain insight about the

reaction pathways, experimental data was obtained and fitted using two kinetic models, Langmuir-Hinshelwood and Eley-Rideal. Products from C- and O-alkylation were observed followed by multiple alkylation products. C-alkylation was found to be favored in the presence of propylene, whereas O-alkylation was enhanced when isopropanol concentration increased. Propylene also alkylated phenolics via both, C- and O-alkylation. The O-alkylation product isopropoxybenzene rapidly decomposed into propylene and phenol, which could further undergo alkylation. This was contrary to the hypothesis of intramolecular arrangement (isomerization) of ethers into ring-alkylated products previously proposed in the literature. Fitting of the experimental data with the kinetic models allowed the estimation of adsorption and rate constants according to the proposed reaction pathway. Both models offered a similar quality in the fitting, and showed similar trends in the resultant kinetic and adsorption parameters. In general, the rate of alkylation decreased with the number of alkyl-substituents in the phenolic molecule, most likely due to steric constraints that limit the entrance of an additional alkyl group.

4.6. Remarks for the future

• *Extension of kinetic modeling to variable temperatures, solvents and catalysts*

Even though the modeling done in this work allowed understanding the reaction scheme for alkylation of m-cresol, it was not possible to estimate kinetic and adsorption parameters such as activation energies or heats and entropies of adsorption, since data at different temperatures is required for this purpose. These parameters are important to verify the thermodynamic consistency of the model, and

also provide insight into the reaction mechanism at a molecular level. Therefore it would be useful to extend the experimental data in order to obtain these quantities. At the same time, a kinetic study in the presence of water and with a hydrophobic zeolite would depict any change in reaction pathways and mechanism that the solvent or functionalization of the catalyst may cause in the reaction system.

• *Experimental setup*

Under the experimental setup used in this study, a long time would be needed to collect the amount of data required to expand the scenarios covered by the kinetic model. In order to speed up data collection, it would be useful to perform reactions in the liquid phase with higher reaction volumes (the maximum allowed in this reactor is 200ml) that would allow withdrawing samples during the course of reaction. In this way, instead of running 8 experiments to obtain 8 data points, 1 experiment could provide the same number of data points. This methodology would significantly decrease the time for collecting the required data. It should be noticed that the operation for sample withdrawing should be carefully performed in order to minimize catalyst and liquid losses.

5. Liquid phase upgrading: water effect on hydrophilic and hydrophobic zeolites for phenolics alkylation

5.1. Introduction

Previous research has shown that the presence of liquid water in catalytic systems containing zeolitic materials can drastically affect the activity of these catalysts. Ehrhardt et al. proposed that water molecules could cause acid hydrolysis of the Al-O-Si bonds as well as promoting the dissolution of the zeolite by an alkaline mechanism that starts at the surface of the crystal.[98] In a more detailed study, Ravenelle et al. investigated the stability of HY zeolite in hot liquid water at different temperatures (150 °C – 200 °C) in order to identify structural changes due to the presence of the aqueous phase.[99] As mentioned before, to use this type of catalysts in bio-oil upgrading, where water is an abundant component, it is necessary that they be hydrothermally stable. They found that HY zeolite with a Si/Al ratio higher than 14 would transform into an amorphous material under the treatment conditions, and the rate of this transformation increased together with the Si/Al ratio. They suggested as well that the mechanism for the zeolite degradation was hydrolysis of the siloxane bonds (Si-O-Si). A comparison with HZSM-5 zeolite was performed and the latter appeared to be more resistant to the water attack than HY zeolite. Zapata et al. studied the properties of an HY zeolite in the presence of hot liquid water and demonstrated the rapid deactivation the aqueous media caused during alkylation of m-cresol with isopropanol.[61] They monitored the structure of the zeolite through different characterization techniques and discovered that hot

liquid water provoked a dramatic loss in crystallinity, which was the major cause for catalyst deactivation. In order to clarify this point, it is important to notice that a transition from a crystalline to an amorphous material without a controlled environment can completely eliminate microporosity, and therefore most of the active sites initially present would be lost or not accessible. This in itself would cause the observed loss in catalytic activity. At the same time they proposed to use a modified zeolite with increased hydrophobicity that could prevent contact with the liquid water and therefore increase stability. An octadecylsilane-functionalized zeolite was synthesized and it showed outstanding stability under reaction conditions as compared with the regular zeolite. In a more recent study Zapata et al. also looked at the use of different organo-silanes as hydrophobic agents and the actual role water played on the zeolite degradation.[10] Figure 5.1 shows the decrease in cristallinity of regular zeolite as well as hydrophobized zeolites in the reaction environment (water and decalin were the solvents) as a function of time. OTS, HTS and ETS were the organosilanes used during synthesis and correspond to octadecyltrichlorosilane, hexyltrichlorosilane and ethyltrichlorsilane, respectively. It is evident that rate of degradation was significantly lower in the hydrophobic materials. As mentioned above, a loss in crystallinity while in the reaction environment would have to be accompanied by a loss in microporosity and consequently surface area. As a matter of fact, this is what was observed on the regular zeolite, which upon exposure to the reaction environment for 22 hours lost about 94% of microporosity and 83% of surface area (Table 5.1).

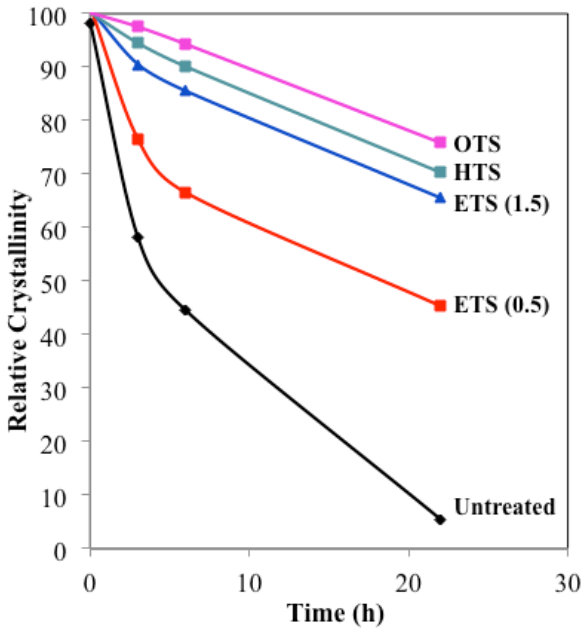

Figure 5.1. Evolution of zeolite crystallinity as a function of reaction time at 200°C and 700 psi in He in an emulsion system. Feed: isopropanol/m-cresol (3/1 molar ratio); total molar concentration: 2 M

In contrast, the hydrophobic zeolites showed a higher stability as indicated by their preserved microporosity and surface area. Notice that both the crystallinity and porosity studies indicate that the rate of degradation for the hydrophobic materials is lower, but not fully eliminated, i.e. these materials still degrade as a function of time.

Table 5.1. Specific Area (S_{BET}) and Micropore Volume (V_{micro}) of silane-functionalized H-USY zeolites compared to the untreated H-USY zeolite before and after reaction for 22 h at 200°C and 700 psi in He. Feed: isopropanol/m-cresol (3/1 molar ratio); total molar concentration: 2 M

Sample	Fresh		After Reaction	
	S_{BET} (m^2/g)	V_{micro} (cm^3/g)	S_{BET} (m^2/g)	V_{micro} (cm^3/g)
Untreated HY	692	0.32	116	0.02
OTS-HY	473	0.20	378	0.12
HTS-HY	572	0.26	397	0.14
ETS1.5-HY	550	0.26	416	0.16
ETS0.5-HY	630	0.29	323	0.13

Therefore under the reaction environment, much longer exposure times should cause these zeolites to completely degrade. Microscopy provided a visual illustration of the way in which zeolites degrade in the presence of hot liquid water. As it is shown in Figures 5.2 and 5.3, after 22 hours of reaction in the presence of water the regular zeolite crystallites were transformed into an amorphous material, while the morphology of the hydrophobic zeolite crystallites was pretty much preserved, confirming the results from other characterization techniques.

The study done by Zapata et al. was useful in understanding the transformation the catalyst undergoes during reactions in the presence of hot liquid water and provided insight on the mechanism by which this degradation takes place (not explained here). This knowledge is critical for bio-oil upgrading due to its high water content as well as the fact that many oxygen-eliminating reactions involve in-situ water production. Although Zapata et al. quantified the rate of degradation of the catalyst, no quantification of reaction rates when using regular and hydrophobic zeolites was performed. One way to relate catalyst degradation to activity is by using a deactivation function in the reaction rate expression. The parameters implicit in this function should provide quantitative information about the catalyst activity and allow for prediction of catalyst lifetime as well as productivity as a function of time.

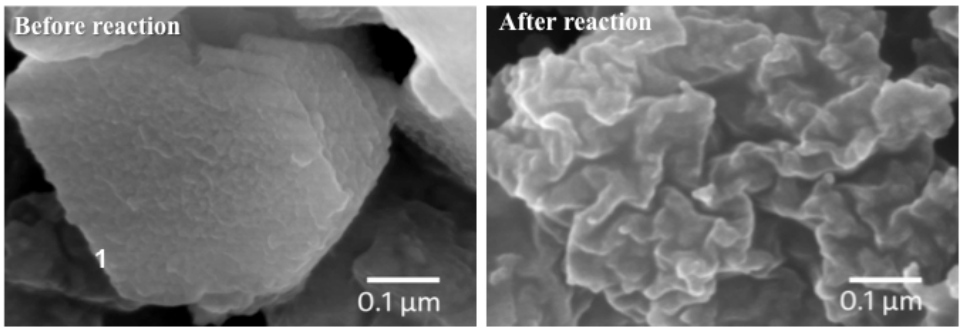

Figure 5.2. SEM images of the untreated H-USY zeolite (Si/Al = 30) after 22h reaction of m-cresol and isopropanol at 200°C and 700 psi of He in an emulsion system. Feed: isopropanol/m-cresol (3/1 molar ratio); total molar concentration: 2 M

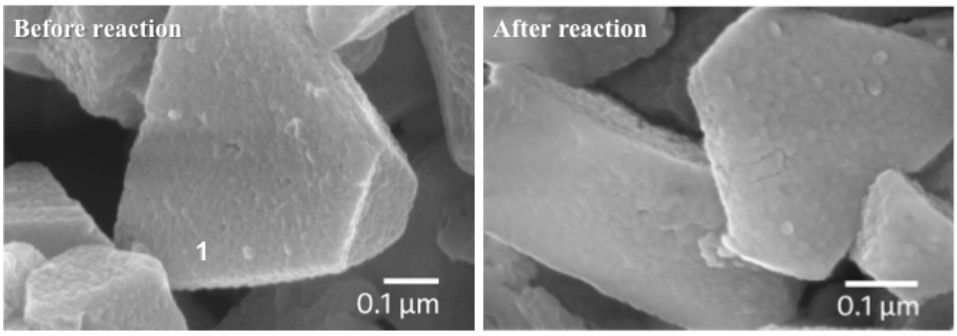

Figure 5.3. SEM images of the OTS-functionalized H-USY zeolite after 22 h reaction of m-cresol and isopropanol at 200°C and 700 psi of He in an emulsion system. Feed: isopropanol/m-cresol (3/1 molar ratio); total molar concentration: 2 M

In this work, the alkylation reaction that was studied in the single phase (Chapter 4) was also considered in a biphasic system containing liquid water and with the use of both regular and hydrophobic zeolites. A simplified kinetic model containing a deactivation function was utilized in order to compare the rate of deactivation of the different catalysts.

5.2. Objectives

- *General*
  - To quantitatively relate the degradation of a series of HY zeolites in aqueous media to its catalytic activity.

- *Specific*
    - To estimate deactivation parameters for a regular HY zeolite and a hydrophobic HY zeolite in two different reaction systems: organic solvent and organic/aqueous solvent.
    - To identify changes in selectivity due to the presence of an aqueous phase in addition to the organic phase.

5.3. Experimental methods

- *Hydrophobic zeolite synthesis*

The parent zeolite used in this study was a faujasite H-USY zeolite (Si/Al ratio: 30) supplied by Zeolyst International, product name CBV760. It has been reported that to reach this high Si/Al ratio, the initial Y zeolite is steamed (twice) and acid leached, which may be responsible for the observed mesoporosity present even in the sample called "untreated". The silylation of the zeolite's surface was performed by the same procedure as that described in previous works.[61] That is, 1g of the parent H-USY zeolite was dispersed in 20ml of toluene with a horn-sonicator (Fisher Scientific 600 W, 20kHz) operating at 25% amplitude for 1 h. The zeolite suspension was then added to a 50ml of organic solution containing the specific silane reagent OTS (purity 90%), at a silane/zeolite ratio of 0.5 mmol/g zeolite. The resulting suspension was stirred for 24 h at 500 rpm at 30°C in an IKA RCT B S1 lab hot plate/magnetic stirrer equipped with an ETS-D5 electronic contact thermometer. The zeolite was then filtered and washed thoroughly on a nylon filter (0.22 μm pore size) several times with ethanol, and finally dried at 100°C overnight.

The silane reagent, as well as m-cresol and isopropanol were purchased from Sigma Aldrich and used as received.

• *Catalytic reactions*

Catalytic tests for alkylation of m-cresol with isopropanol over the various zeolite samples were carried out in a 300 ml Parr 4843 batch reactor. The temperature and pressure inside the reactor were monitored with a CAL 9500P controller (CAL Controls Ltd.) and an Aschcroft transducer, respectively. In each reaction test run, a 0.5g catalyst sample was dispersed in a 60 ml mixture of equal volumes of deionized water and decalin, sonicating for 15 min at 25% of amplitude. The mixture was placed in the stainless steel reaction vessel and purged with a 200 ml/min flow of He. Pressure was increased to 300 psig, while stirring at 240 rpm, and the reactor was heated up to 200°C. At this point, 25 ml of a mixture of equal volumes of deionized water and decalin containing the reactants was injected from a pressurized feeding cylinder. Pressure of the reactor was adjusted to 700 psig with additional He, and finally the gas inlet was closed to let the reaction proceed in the batch mode. At the end of the reaction period, the reactor was cooled to room temperature and depressurized. The zeolite was separated from the reaction mixture by centrifugation at 5,000 rpm for 5 min. The aqueous and organic phases obtained after decantation of the zeolite were analyzed by gas chromatography (GC-FID and GCMS). At the end of each run, the liquid mixture was analyzed with a Shimadzu GCMS-QP2010S gas chromatograph/mass spectrometer in order to identify the products and a Varian 3800 gas chromatograph equipped with a FID detector for

quantification. Both GC's were equipped with a Zebron ZB-1701 column with dimensions of 60m x 0.25mm x 0.25µm.

5.4. Results and discussion

The evolution of catalyst activity, rate of deactivation, and distribution of products as a function of reaction time was investigated in a batch reactor operating in both, single organic phase and biphasic water/oil emulsions. To obtain each point at a given reaction time, a separate reaction run was conducted with m-cresol and isopropanol at 200 °C and 700 psi of He for four different cases:

- untreated H-USY in decalin single phase
- OTS-functionalized H-USY in decalin single phase
- untreated H-USY in water/decalin emulsion
- OTS-functionalized H-USY in water/decalin emulsion

Table 5.2. Kinetics analysis of the m-cresol and 2-propanol reaction with the proposed reaction pathway

Compound	Mole Balance
Isopropanol (IPA)	$dC_{IPA}/dt = -k_1C_{IPA}$
Propylene (P)	$dC_P/dt = k_1C_{IPA} - k_2C_CC_P - k_3C_{MONO}C_P - k_4C_{DI}C_P$
m-Cresol (C)	$dC_C/dt = -k_2C_CC_P$
Mono-alkylated products (MONO)	$dC_{MONO}/dt = k_2C_CC_P - k_3C_{MONO}C_P$
Di-alkylated products (DI)	$dC_{DI}/dt = k_3C_{MONO}C_P - k_4C_{DI}C_P$
Tri-alkylated products (TRI)	$dC_{TRI}/dt = k_4C_{DI}C_P$
Polymerization products (OTHERS)	$dC_{OTHERS}/dt = k_5$
Deactivation function: $k_i = k_i^0 e^{-\tau t}$ where τ is the deactivation parameter	

Figure 5.4 shows that, when the reaction was conducted in decalin solvent, in the absence of water, the reaction rate was relatively high, reaching about 80 % conversion in 8 h on both, the untreated and OTS-functionalized H-USY zeolites. In the presence of water, the initial activity was lower than in the absence of water

for both catalysts, showing that water competes with active sites on both, untreated and OTS-functionalized H-USY zeolites. However, the most important difference, in agreement with the discussion presented above, was the drastic rate of deactivation presented by the untreated zeolite, which became practically inactive after about 2 h in the reaction medium.

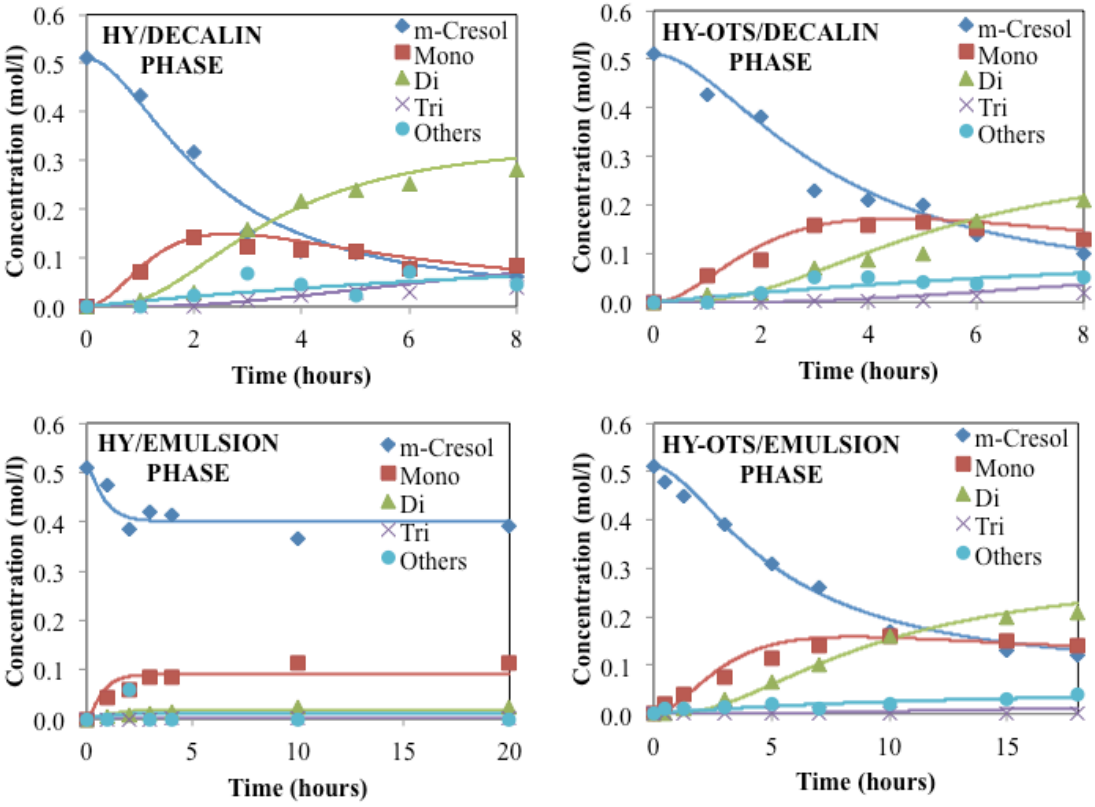

Figure 5.4. Kinetic fitting results for alkylation of m-cresol with isopropanol in 4 different systems (catalyst: untreated and OTS-functionalized H-USY; solvents: decalin single phase and water/decalin emulsion)

To better quantify these differences, a simplified kinetic analysis was performed based on the following reaction pathway (see Table 5.2):

- Dehydration of isopropanol to propylene
- Propylene alkylation of m-cresol to mono-alkylated cresol isomers
- Secondary alkylation of mono-alkylated to di-alkylated-cresol isomers

- Tertiary alkylation of di-alkylated to tri-alkylated-cresol isomers
- Polymerization of m-cresol and alkylated-cresols

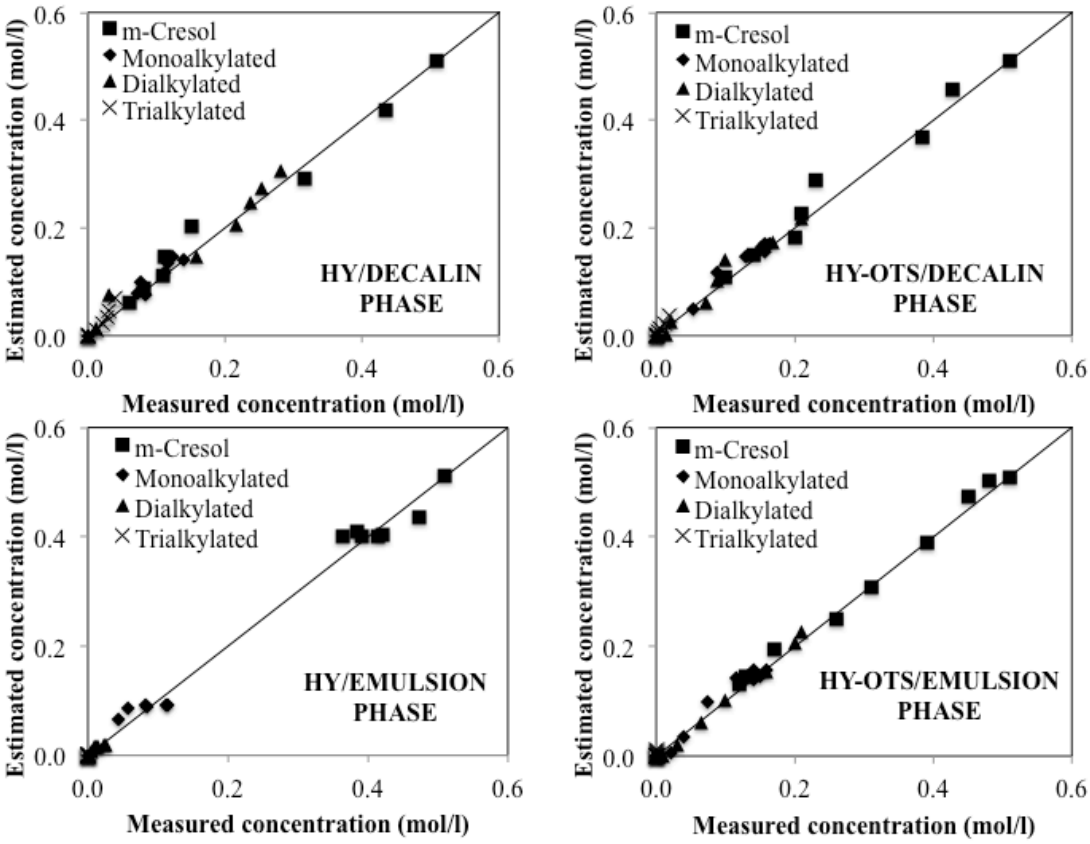

Figure 5.5. Comparison of measured product concentrations and calculated concentrations based on the fittings using the simplified kinetics model described in Table 5.2 for the four cases investigated (catalyst: untreated and OTS-functionalized H-USY; solvents: decalin single phase and water/decalin emulsion)

Notice that, as opposed to the reaction scheme presented in the last chapter, the alkylation products were lumped according to the number of isopropyl groups in the product (independent of whether they were C- or O-alkylation products), and alkylation was assumed to happen only through propylene, which is the dominant alkylating agent during most of the reaction time (see Figure 4.7a).

The individual fittings of the concentrations of each species as a function of reaction time are shown in Figure 5.4. Figure 5.5 illustrates the goodness of the overall fitting for all 4 cases. As seen in Table 5.3, in the decalin solvent, the OTS-functionalized zeolite had an intrinsic activity about 40-50 % lower than the untreated zeolite for both dehydration and alkylation steps, in good agreement with the observed BET surface area, which as mentioned above could be rationalized in terms of pore blockage.[61]

Moreover, interesting trends were observed when water was present in the system. First, both, the untreated and OTS-functionalized catalysts showed a similar drop in activity compared to the reaction in the absence of water. This result indicated that in both cases, water molecules did penetrate the zeolite structure and competed for adsorption sites with the reactants (isopropanol, propylene, cresols). This result was indeed expected, since regardless of the hydrophobicity of the external surface, the water coverage inside the zeolite crystal is given by the chemical potential of water, which in both cases is the same and in equilibrium with the partial pressure of water vapor above the liquid in the reactor, regardless of whether the zeolite is wetted or not by water.

Table 5.3. Reaction and deactivation constants obtained at 200°C and 700psi of He over untreated and functionalized HY zeolite (Si/Al molar ratio: 30). Feed: isopropanol/m-cresol moar ratio:4; total molar concentration: 2.5M

Rate constant/ Deactivation parameter	DECALIN PHASE		EMULSION PHASE	
	HY	OTS-HY	HY	OTS-HY
k_1 (g cat^{-1} h^{-1})	17.3	11.7	2.63	0.96
k_2 (l g cat^{-1} mol^{-1} h^{-1})	7.26	5.22	1.23	0.26
k_3 (l g cat^{-1} mol^{-1} h^{-1})	11.2	6.15	1.83	0.35
k_4 (l g cat^{-1} mol^{-1} h^{-1})	1.44	1.26	0.20	0.02
k_5 (l g cat^{-1} mol^{-1} h^{-1})	0.23	0.22	0.03	0.01
τ (h^{-1})	0.10	0.10	1.50	0.09

On the other hand, an enormous difference was observed in the rate of deactivation of the two zeolites in the presence of water. Figure 5.6 illustrates the deactivation functions predicted from the fitting for the four cases. It is clear that the untreated HY in the biphasic system was fully deactivated in about 2 h, while much lower deactivation was observed on the hydrophobized zeolite. This was the most important beneficial effect of the hydrophobic functionalization. By preventing the contact with liquid water, the silane groups have preserved the zeolitic structure and therefore its catalytic activity.

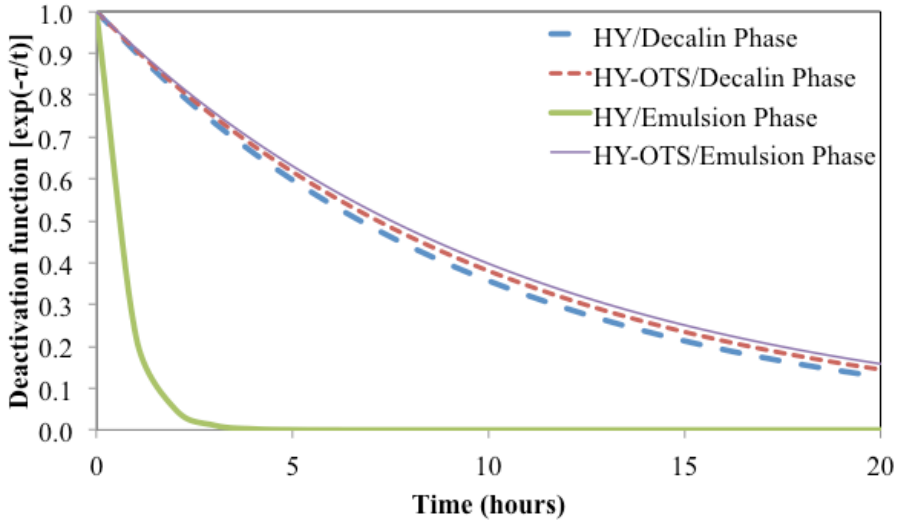

Figure 5.6. Deactivation function according to the expression $k_i = k_i^0 e^{-\tau t}$

Indeed, the fitting showed that the rate of deactivation of the functionalized zeolite was essentially the same in decalin as in the emulsion, while the same was certainly not true for the untreated zeolite.

• *Phase selectivity in alkylation of m-cresol with isopropanol*

One attractive aspect of performing reactions in a biphasic liquid system is the capability to favor the reaction in only one of the liquid phases, while suppressing it in the second liquid phase. Crossley et al. proposed this concept as the "phase-transfer selectivity" when working with hydrogenation of oxygenate compounds.[100] In their work, they observed that the single phase hydrogenation of a water soluble aldehyde (glutaraldehyde) was enhanced in a biphasic water/decalin system where the catalyst was amphiphilic in nature (hydrophobic and hydrophilic sections) and the metal particles where preferentially deposited on the hydrophilic side of the catalyst. At the same time, and using the same catalyst, they observed that the single-phase hydrogenation of a decalin soluble aldehyde (octanal) was suppressed in this biphasic system. This phenomenon was explained in terms of the rate of transport of the reactants through the bulk phases. In the case of octanal, its transport through the aqueous phase is limited due to its low solubility, and therefore the rate of reaction is dominated by the rate of mass transport. The possibility of phase selectivity in the alkylation of m-cresol with isopropanol was evaluated for two pairs of compounds: mono-alkylated vs. di-alkylated and ring-alkylated vs. ethers. The objective was to determine whether the use of a biphasic system could somehow modify the selectivity towards either final product as compared to the single-phase system. Figure 5.7 shows the product yield for single phase and biphasic systems and compares mono-alkylated and di-alkylated products. The red data points indicate the product yields in a biphasic system and when comparing at the same conversion with the single-phase system, no change in

product yield was observed. Moreover, it was also possible to conclude from this single data points that the ratio between ring-alkylated and ether products was not modified either.

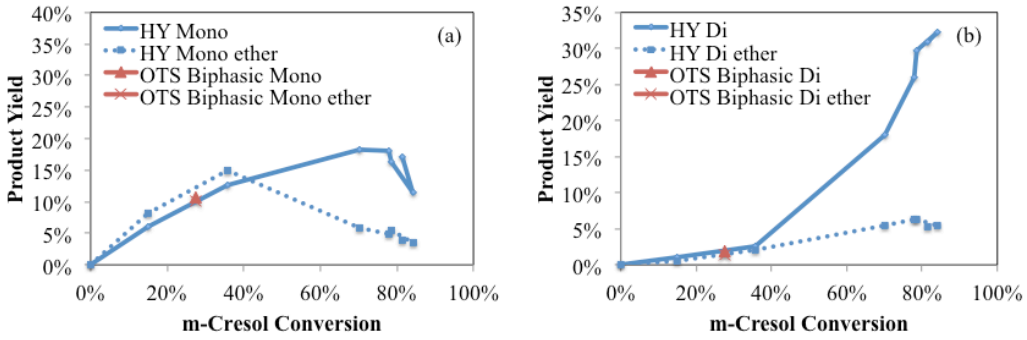

Figure 5.7. Product yield from alkylation of m-cresol with isopropanol in two different systems: HY indicates a hydrophilic zeolite in single decalin phase; OTS Biphasic indicates a hydrophobic zeolite in a biphasic water/decalin phase. (a) Mono-alkylated products. (b) Di-alkylated products

In order to further confirm this fact, the selectivity to these two products was plotted over the whole range of conversion and is shown in Figure 5.8. It was confirmed that overall, the selectivity of the reaction was not altered by the use of a biphasic system. During data analysis of the biphasic system most of the alkylation products were found to remain in the decalin phase and only isopropanol and small amounts of m-cresol were found in the aqueous phase. There was therefore a clear preference for the products towards the oil phase, however the active sites were equally distributed throughout the catalyst particles, being equally accessible from both liquid phases. This might be the reason why the use of a biphasic system did not alter the product selectivity. On the other hand, and taking into account that the presence of water is unavoidable when treating bio-oil, this could be an advantage. This result demonstrates that the hydrophobization of the zeolite did not cause

changes in the intrinsic properties of the active sites and therefore a similar product composition can be delivered with or without water in the system.

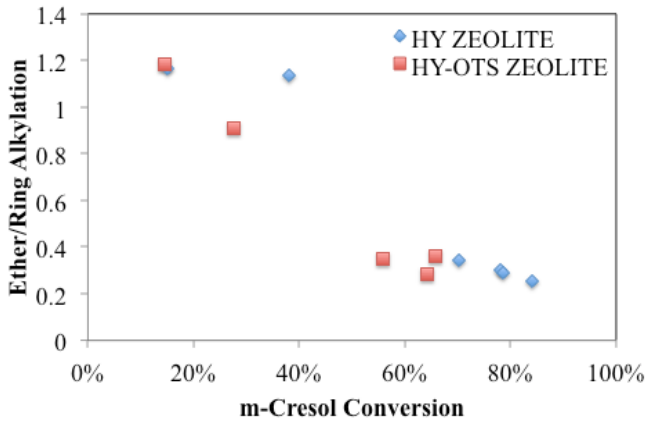

Figure 5.8. Ratio of ether to ring-alkylated products over two different systems: HY indicates a hydrophilic zeolite in single decalin phase; OTS Biphasic indicates a hydrophobic zeolite in a biphasic water/decalin phase

5.5. Conclusions

A first order kinetic model with a one-parameter deactivation function was successful to describe the alkylation of m-cresol with isopropanol in a single decalin phase system and a biphasic system using a regular (HY) and a hydrophobic zeolite (OTS-HY). According to the rate constants obtained from the model, the overall reaction rate over OTS-HY was lower than for the HY. This observation was attributed to a decreased accessibility of active sites in OTS-HY caused by organosilane chains that block some pores in the catalyst. At the same time, the rate constants for alkylation decreased when water was introduced in the reaction medium (both in HY and OTS-HY), presumably due to a competitive adsorption of water on the catalyst active sites. This indicated that water molecules could enter the zeolite pores even after hydrophobization. The rate of deactivation of the

hydrophobic zeolite was the same with and without water present, whereas for the regular zeolite the rate of deactivation was one order of magnitude higher in aqueous environment. The use of a biphasic system did not modify the product distribution when compared to a single-phase organic system.

5.6. Remarks for the future

- *Deactivation function*

In previous studies by Zapata et al. an extensive characterization of zeolite degradation was performed. Since the mechanism for deactivation was very well understood from this study, it would be good to derive a deactivation function which parameters are directly related to the properties of the zeolite, and therefore have a physical meaning. Crystallinity, for example, was quantified as a function of time, and in turn it could be related to the amount active sites remaining and available to the reactants. Therefore, the deactivation parameter could be a direct representation of the remaining crystallinity in the zeolite, and could be estimated independently from the characterization data.

6. Liquid phase upgrading: water effect on hydrogenation of furfural

6.1. Introduction

• *Water effect on hydrogenation reactions*

Extensive investigation in recent years has shown the potential for the utilization of biomass as a source of fuels and chemicals [101]. It has been proposed that biomass can be separated into its main components, i.e. cellulose, hemicellulose and lignin, each of which could be transformed into higher value products [12]. Hemicellulose is especially interesting because it can undergo dehydration under relatively mild conditions yielding furfural as the main product [102]. It has been stated that furfural is a potential platform molecule for the production of fuel additives as well as important chemicals [103], and it is therefore relevant to explore new routes for its synthesis, in particular those that make use of renewable sources.

A common factor in the sequential steps required to go from biomass to furfural is the presence of water. This water comes from biomass itself (20-30%wt. moist content) and from its use as a solvent for hydrolysis and dehydration reactions that yield furfural as a product. Therefore conversion of furfural in aqueous solution would be desirable because it would eliminate an additional separation step. It is then critical to understand the role that water might play as a solvent in this type of system. Among the different possibilities for furfural upgrading, hydrogenation is an important route because it can give a variety of partially and fully deoxygenated products as well as ring opening products [104]. Previous studies showed that water could have a significant effect in hydrogenation reactions, especially when carried

out in the liquid phase. It has been reported that water could both inhibit or promote rates of hydrogenation, depending on the catalyst active phase [105-108]. Additionally, and when the reactant has multiple functional groups that are suitable for hydrogenation, the presence of water introduced dramatic changes in product selectivity [109-111]. In light of the intriguing effects of water on this type of reaction and the potential of furfural as a platform molecule for chemicals and fuels production, this preliminary study provides evidence and insight about the influence water has on the liquid phase hydrogenation of furfural.

• *Solvent effects in liquid phase reactions*

Reactions carried out in the vapor phase commonly use a carrier gas in order to transport the reactants through the catalytic bed. This carrier is usually an inert gas, which does not interact with reactants in any significant way. In contrast, when reactions are carried out in the liquid phase, it is common to find interactions between the solvent, used to disperse the catalyst particles, and the species involved in the reaction. Singh and Vannice have reviewed the topic of solvent effects in catalytic reactions and some comments regarding the most relevant effects are discussed below.[112]

- Competitive adsorption. Solvents used in liquid phase reactions are usually organic in nature. In some cases they may have affinity for the catalyst surface and tend to adsorb on the active sites. As a result, the reactants need to compete for active sites with the solvent and the reaction rate may be significantly affected.

- Mass transport limitations. When a reaction in liquid phase is influenced by transport limitations, the rate of reaction is a function of a rate constant, a mass transfer coefficient and an effectiveness factor. Mass transfer coefficients depend on the diffusivity of the reactants through the liquid phase. It is expected that a given molecule would have different diffusivities in different solvents. Therefore, in a reaction that is controlled by external mass transfer, the choice of solvent may affect the measured reaction rate.
- Solvation of kinetically relevant species. This effect is probably the one of more importance for this research, and it rises from the interaction between the solvent and any species that are involved in the rate-limiting step of the reaction. Recall from transition state theory that the rate constant for a chemical reaction depends on the activation energy and on the change in entropy between adsorbed reactants and the activated complex. If the solvent interacts with adsorbed species or with the activated complex in such a way that the energy barrier or the change in entropy is affected, then the solvent would have a direct effect on the rate of reaction.

• *Furfural polymerization*

Under a variety of environments furfural is prone to the formation of polymers and humins, and therefore it is important to consider this side reaction while working in liquid phase systems.[113] A brand new bottle of furfural with a purity of 98% contains a dark brown liquid that is far from the transparent appearance of purified furfural. This is an indication of the instability of furfural under storage conditions and the drastic effect that a small percentage of impurities can cause on its physical

properties. The dark color of furfural is usually attributed to polymerization products, which in some cases can even reach resin like compounds. Aqueous and acidic environments can promote polymerization of furanic compounds, however even when stored under vacuum and absence of light, furfural can undergo condensation reactions (although the mechanism for condensation under these conditions is not clear yet). Some of the mechanisms that have been proposed in order to explain furfural polymerization in different media are mentioned below.

- In an aqueous acidic medium, furfural and its derivatives can undergo ring opening between the ring oxygen and the carbon at the position 5 leading to the formation of a di-ketone aldehyde compound. The latter is the precursor for condensation reactions.[114]
- The hydrogen attached to the carbon at the position 5 in the furanic ring can be removed upon attack from another protonated furfural molecule and form a dimer, which can further undergo multiple condensation steps and yield a linear polymerization product. This mechanism is plausible in acidic media, since protonation of the furfural molecule is required.[115]
- A molecule of the di-ketone aldehyde compound mentioned before can undergo condensation with a furfural molecule through the aldehyde group, followed by dehydration in order to produce an unsaturated dimer. As long as there are carbonyl groups present, condensation can happen multiple times. As in the previous case, this mechanism takes place in an acidic medium preferentially. [116]

6.2. Objectives

- *General*
    - To study the influence of the solvent on the reaction mechanism of furfural hydrogenation in liquid phase.
- *Specific*
    - To determine the influence of transport phenomena (mass and heat transport) on the reaction system.
    - To collect kinetic data that allows for calculation of true activation energies and entropies, heat and entropies of adsorption.
    - To compare the estimated kinetic and thermodynamic parameters and propose explanations for the effect exerted by the solvent on the reaction system.

6.3. Experimental methods

- *Thermodynamic calculations*

The concentration of each species at equilibrium was calculated using ASPEN software, with Peng-Robinson as the preferred model for estimation of thermodynamic properties. Two simulations were setup with a stream of reactants (H_2/furfural, and H_2/furfuryl alcohol, both with a molar ratio of 20:1) going into an equilibrium reactor held at 20.4 atm and 50 °C (this value was varied to study the equilibrium at different temperatures). The two effluents from this reactor (vapor and liquid phase) were combined in a mixer and the molar flows of each species at the exit of the mixer were reported. The following reactions were allowed to take place inside the equilibrium reactor:

Simulation 1: Furfural + H_2 ⇔ Furfuryl alcohol (6.1)

Simulation 2: Furfuryl alcohol + $2H_2$ ⇔ Tetrahydrofurfuryl alcohol (6.2)

• *Materials*

Decahydronaphthalene (decalin), mixture of cis+trans from Sigma-Aldrich (reagent grade, 98%), ethyl alcohol from Pharmco-AAPER (200 Proof) and furfuryl alcohol from Aldrich (98%) were used without further purification. Water was purified by consecutive reverse osmosis, ion exchange and microfiltration. Furfural from Sigma-Aldrich (99%) was distilled in order to remove polymerization impurities. Hydrogen gas (Ultra High Purity) was obtained from Airgas. The commercial catalyst was palladium on activated charcoal, 5 % Pd basis, and the palladium precursor was palladium (II) nitrate hydrate, both from Aldrich. Activated Charcoal Norit ® from Sigma Aldrich was used as the catalyst support.

• *Catalyst synthesis and characterization*

A series of carbon supported platinum catalysts with different metal loading was synthesized with the purpose of studying the influence of transport effects (mass and heat) on the reaction system. The metal loadings were 0.5%, 1.0%, 2.5%, and 5.0%, all on a weight basis, in addition to a commercial 5%wt. catalyst. A conventional incipient wetness impregnation method was used, where a precursor solution containing enough palladium to reach the desired loading and with a volume equal to the pore volume of the support was added drop wise to the later. Following impregnation the powder was dried at room temperature for 6 hours and then overnight at 100°C. Finally the precursor was decomposed under continuous flow of air (100ml/min) at 300°C. Reduction of the catalyst took place as explained in the

following section. Galbraith Laboratories Inc. performed quantification of the metal content of the catalysts (Table 6.1). Dispersion of the catalyst was measured by two separate methods. The particle size distribution was determined from Transmission Electron Microscopy and the dispersion was calculated from a weighted average particle size, as reported previously.[117] For this purpose, particle size was measured with a JEOL 2000-FX Scanning Transmission Electron Microscope. At the same time, the dispersion of these catalysts was also measured by carbon monoxide chemisorption using a Micromeritics ASAP 2020 sorption equipment.

• *Catalytic reaction*

Experiments were carried out in a bench top 0.3 liters Parr pressure reactor (model 4561), equipped with a 4843 Parr controller for temperature, pressure and stirring control. In a typical experiment, 20 mg of catalyst and 90 ml of solvent were combined in the stainless steel reactor vessel and the system was purged and pressurized with hydrogen to a pressure of 0.69 MPa. Then the catalyst was reduced for 1 hour at 373 K. A separate solution containing 0.012 moles of furfural or furfuryl alcohol and additional solvent (enough to complete a total reaction volume of 120ml) was prepared. After reducing the catalyst, the temperature in the reactor was adjusted to the reaction temperature and then the solution with the feed was introduced inside the reaction vessel through a pressure difference mechanism. Afterwards the pressure was adjusted to 2.1 MPa by introducing additional hydrogen. Reposition of consumed hydrogen during the reaction was allowed in order to maintain a constant hydrogen pressure. At the end of the reaction time the liquid mixture was analyzed with a Shimadzu GCMS-QP2010S gas

chromatograph/mass spectrometer in order to identify the products and a 7890B Agilent gas chromatograph equipped with a FID detector for quantification. The GC's were equipped with Zebron ZB-1701 and Zebron ZB-WAXplus columns respectively, both with dimensions of 60m x 0.25mm x 0.25µm.

6.4. Results and discussion

• *Thermodynamic calculations*

Figure 6.1 shows the concentrations at equilibrium for hydrogenation of furfural and furfuryl alcohol. In both cases hydrogenation is favored at low temperatures and therefore, at the reaction conditions used in the experiments, there should not be a thermodynamic limitation for either hydrogenation reaction.

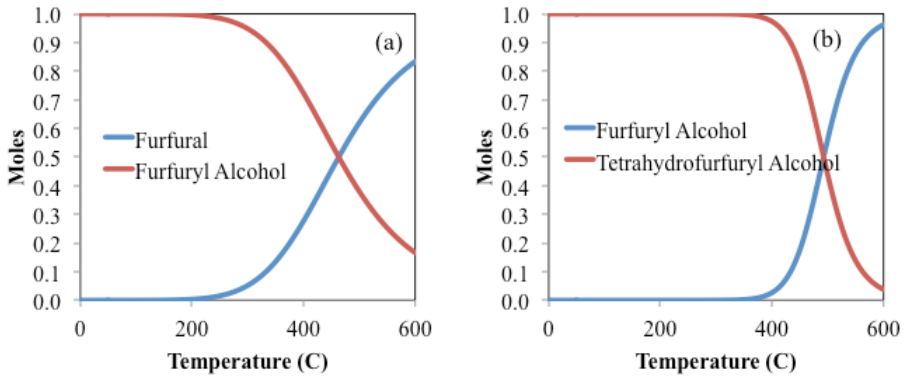

Figure 6.1. Concentrations at equilibrium of reactant and products of hydrogenation of furfural and furfuryl alcohol at 20.4 atm

• *Thermal stability of furfural in water*

Since the objective of this study was to understand the effect of water in the hydrogenation of furfural, it was desired to minimize polymerization reactions. During hydrogenation, the atmosphere is oxygen free and therefore reactions involving oxidation could be ruled out. On the other hand, water and high

temperatures could accelerate polymerization, even under vacuum. [114] At the same time temperature plays an important role in product selectivity during hydrogenation of furfural, as mentioned before. The thermal stability of furfural under typical reaction conditions was evaluated at three different temperatures (Figure 6.2) and using water as a solvent.

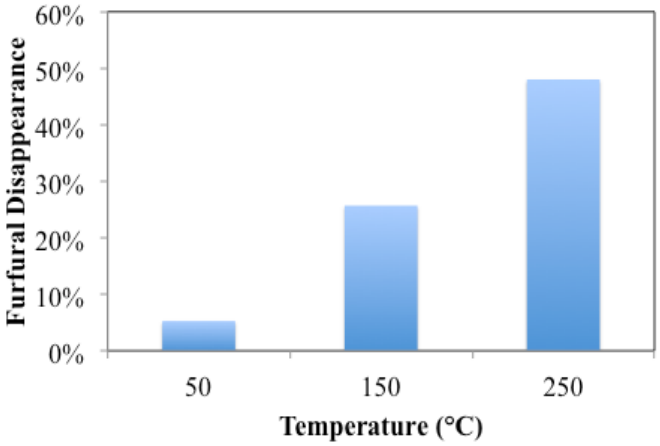

Figure 6.2. Furfural disappearance at different temperatures in an aqueous environment under pressurized hydrogen (500psi). Test time: 3h.

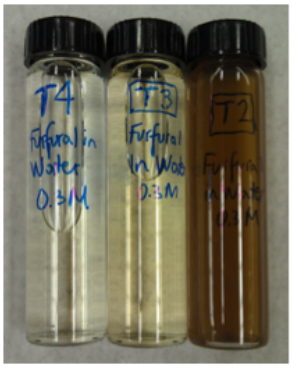

Figure 6.3. Products from furfural thermal stability test. Temperature of the test, from left to right, was: 50°C, 150°C and 250°C.

As expected, at higher temperatures the conversion of furfural increased and the change of color in the reaction medium indicated the formation of polymers (Figure

6.3). Unfortunately these polymerization products could not be identified by conventional gas chromatography. Based on these experiments, the temperature of 50°C was selected for the subsequent studies; it was low enough to prevent polymerization and high enough to allow for a good temperature control inside the reactor.

• *Catalysts dispersion*

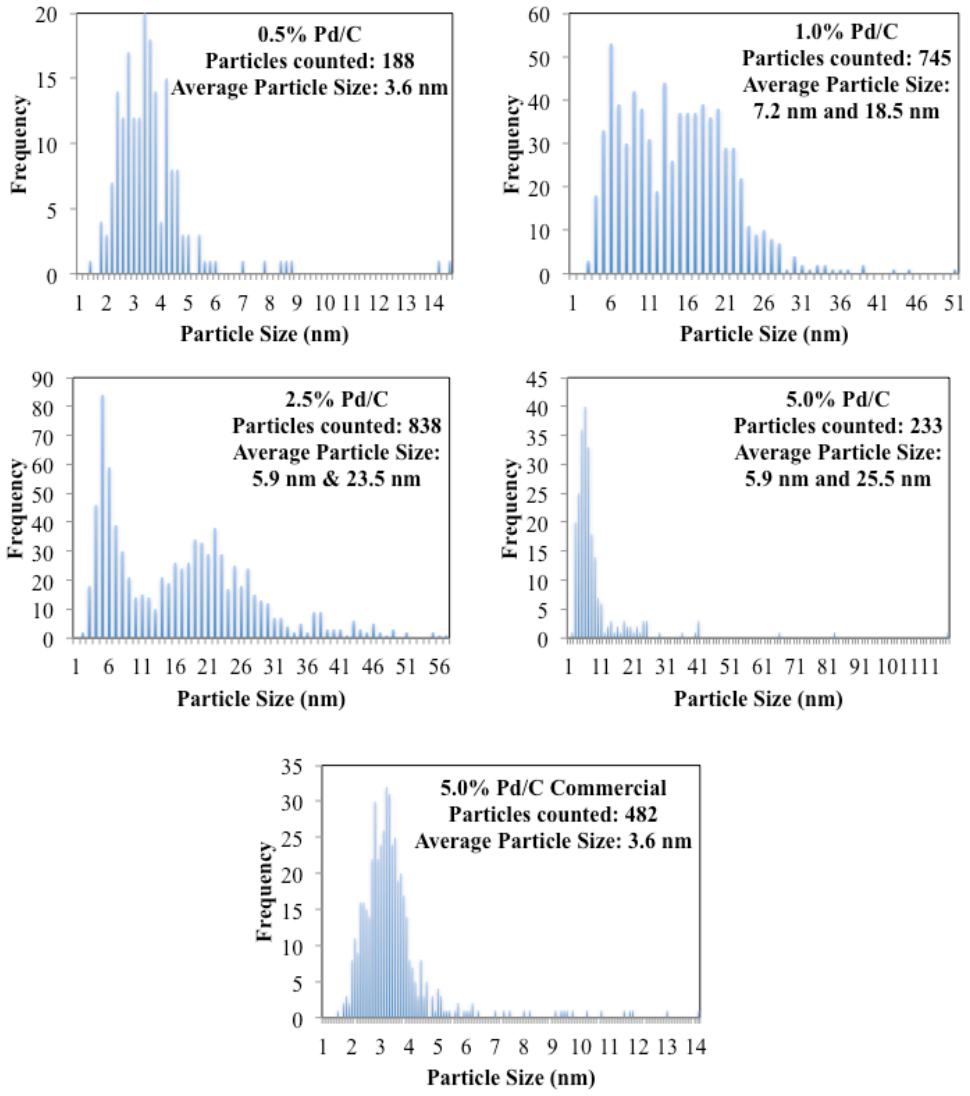

Figure 6.4. Particle size distribution for a series of Pd/C catalysts, measured by TEM

Significant differences were found when estimating the catalyst dispersion by TEM and CO chemisorption. Figure 6.4 shows the particle size distribution (measured by TEM) for a series of catalysts with different palladium loading, along with the number of particles that were measured for the calculation. With the exception of 0.5%wt. Pd/C, all the synthesized catalysts exhibited a bimodal distribution of particle diameters, centered at around 6 and 20 nm. This result is an indication of the non-uniformity of the metal distribution throughout the catalyst, and exposes the need for a more controlled synthesis procedure in order to improve uniformity. On the contrary, 0.5% Pd/C and the commercial catalyst showed a unimodal particle size distribution centered at 4 nm in both cases. Dispersion values estimated from the TEM measurements displayed a high variation in the synthesized catalyst, up to an order of magnitude. On the contrary, the chemisorption estimates did not support this result, indicating that all catalysts, including the commercial one, possess a dispersion in the same order of magnitude (Table 6.1).

Table 6.1. Dispersion of a series of Pd/C catalysts measured by two different methods

Catalyst	Actual metal loading (wt.%)	Dispersion from TEM (%)	Dispersion from CO chemisorption (%)
0.5%Pd/C	0.41	18.9	45.4
1.0% Pd/C	0.78	4.9	25.8
2.5% Pd/C	2.09	3.6	13.1
5.0% Pd/C	3.57	1.6	19.5
5.0% Pd/C (Commercial)	4.30	20.1	30.9

When looking at catalyst particles under the microscope it is often hard to select a sample that is highly representative of the bulk. This issue becomes more critical when the uniformity of the sample is low, as is the case of the synthesized catalysts,

where bimodal particle size distributions were observed. Because of this, CO chemisorption appeared to be a more reliable method for dispersion measurement in this case, since it samples a much higher mass of catalyst and therefore provides information more representative of the bulk.

• *Reactivity and product selectivity in different solvents*

The first interesting result was found on the activity for hydrogenation when different solvents were used. Figure 6.5 shows the conversion of furfural from hydrogenation reactions at the same conditions in different solvents. It is clear that ethanol and water increased the rate of furfural conversion as compared to decalin. As a starting point for discussion, the differences in the nature of these solvents should be pointed out; ethanol and water are both polar and able to form hydrogen bonds whereas decalin is apolar and does not have the capacity to form hydrogen bonds. These characteristics make ethanol or water likely to participate in kinetically relevant steps for hydrogenation, thus increasing rates of reaction. Such a role is due to their ability to interact with the polarized aldehyde group in furfural as well as hydrogen atoms participating in hydrogenation. On the other hand, decalin has a rather weak interaction with these species because of its low polarity, and it could be suggested that when compared to water and ethanol, decalin resembles more a vapor phase scenario where there is little or no interaction with the bulk phase surrounding the catalyst particles. Akpa et al. studied this type of effect in hydrogenation of 2-butanone [107]. They observed an increase on hydrogenation rate in the liquid phase as the concentration of water in the solvent (a mixture of isopropanol and water) increased. Using DFT they studied the formation of the

activated complex for the first hydrogenation step (hydroxybutyl intermediate) both in vacuum and in the presence of liquid isopropanol and water. In vacuum the activation energy for the formation of the complex was found to be 64 kJ/mol, whereas in isopropanol it was 32 kJ/mol and 20 kJ/mol when water was present. Lower activation barriers were observed for isopropanol and water because the activated complex was able to form hydrogen bonds with these solvents, thus being stabilized as compared to the vacuum case.

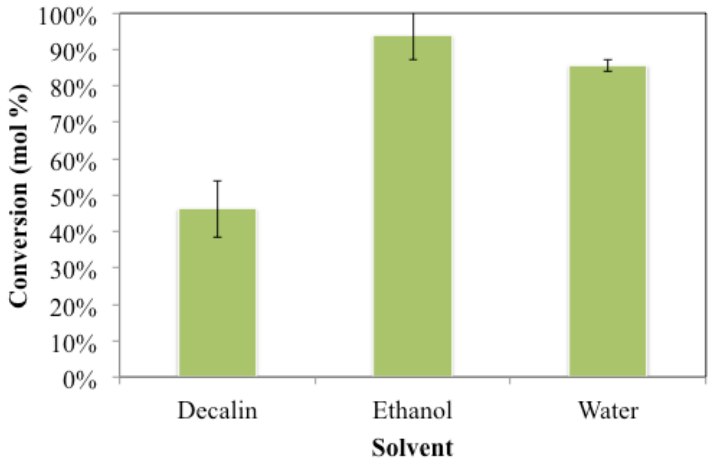

Figure 6.5. Furfural conversion in different solvents. Conditions: initial concentration=0.1M, T=323K, P=2.1MPa, catalyst mass=20mg 5%Pd/C (commercial), reaction time=1h

Hibbitts et al. have also described the role of water as being a stabilization agent through hydrogen bonding in the so-called hydrogen shuttling effect during Fischer-Tropsch synthesis [108]. Carbon monoxide dissociation was shown to be the rate-limiting step in this process, as well as the fact that the assistance of hydrogen in this dissociation significantly lowered the energy barrier for this process. Furthermore, it was experimentally observed that in-situ or externally added water provided an additional increase in rates of CO dissociation. With the help of DFT

calculations the authors proposed that, through hydrogen bonding, the surrounding water molecules could shuttle hydrogen atoms adsorbed on the surface towards the oxygen atom in carbon monoxide. This water-assisted process lowered the energy barrier for the overall CO dissociation step and increased the reaction rate. More recently, Wan et al. studied the hydrogenation of different oxygenate molecules, i.e. 2-butanone, 2-pentanone and phenol in the presence of different solvents [118]. They found that the activity for hydrogenation correlated very well with the hydrogen bonding donor (HBD) capability of the solvent, where the solvents with higher HBD capability resulted in higher activity. The observations from these studies are in agreement with the results presented here, strongly suggesting that water or ethanol could stabilize relevant activated complexes during hydrogenation of furfural and causing a significant increase in the rate of reaction.

In addition to increasing furfural conversion, ethanol and water caused important changes in the hydrogenation product distribution. These products and their proposed reaction pathways are shown in Figure 6.6.

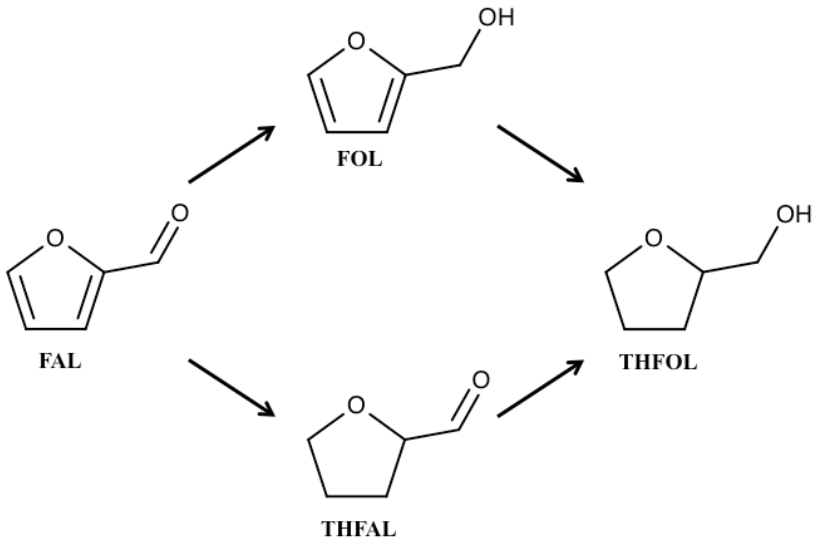

Figure 6.6. Furfural hydrogenation products at mild conditions

On one hand, the aldehyde group in furfural (FAL) can be hydrogenated to produce furfuryl alcohol (FOL), which upon hydrogenation of the ring yields tetrahydrofurfuryl alcohol (THFOL). At the same time, furfural can first undergo ring hydrogenation to give tetrahydrofurfural (THFAL) followed by hydrogenation of the aldehyde group to make tetrahydrofurfuryl alcohol (THFOL). Based on this reaction scheme it is possible to group the reaction products as ring hydrogenation products, i.e. THFAL and THFOL, and aldehyde hydrogenation products, i.e. FOL and THFOL. Figure 6.7 shows the product yields in different solvents according to this classification under the same reaction conditions. As compared to decalin, it was observed that ethanol enhanced both ring and aldehyde hydrogenation to a similar extent. On the other hand, water did not enhance ring hydrogenation but solely aldehyde hydrogenation.

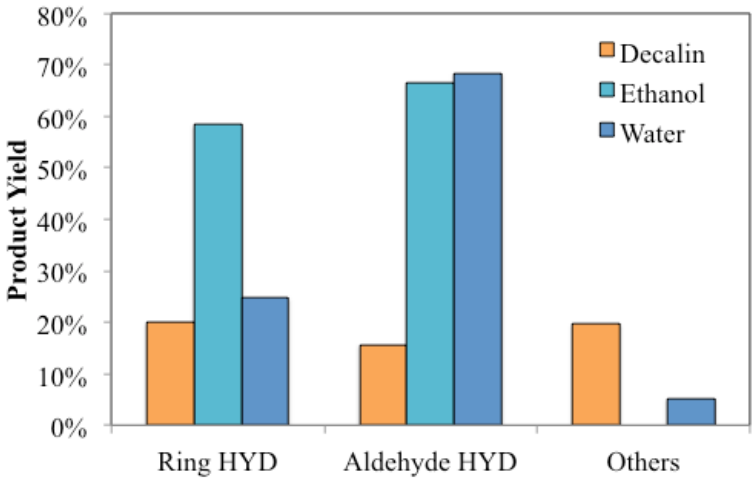

Figure 6.7. Product yield for furfural ring hydrogenation (Ring HYD), aldehyde hydrogenation (Aldehyde HYD) and other products in different solvents. Conditions: initial concentration=0.1M, T=323K, P=2.1MPa, catalyst mass=20mg 5% Pd/C (commercial), reaction time=1h

Therefore it appears that water not only increases the rate of furfural conversion but also is very selective towards the production of furfuryl alcohol. Figure 6.7 also depicts the yield of "Other" products. These were unaccounted moles of material not found in solution after reaction. It is well known that furfural can undergo oligomerization reactions even in the absence of oxygen and at mild temperatures.[114] It is then reasonable to think that there is a competition between oligomerization and hydrogenation reactions. Therefore, if ethanol and water enhance the hydrogenation route it is natural to expect that the oligomerization route be suppressed, in agreement with the lower yield of "other" products in these solvents shown in Figure 6.7. In order to have more clarity about the changes in product selectivity a comparison among the solvents was done at the same conversion level and the results are depicted in Figure 6.8.

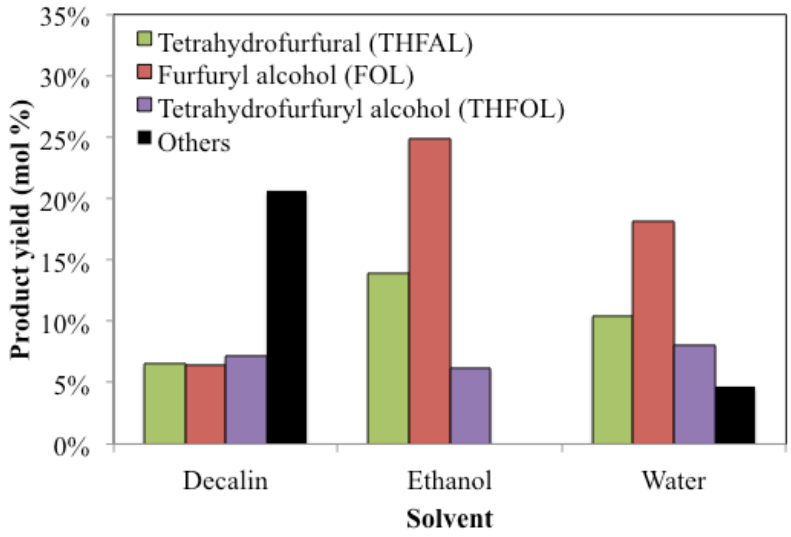

Figure 6.8. Product yield in different solvents at the same level of furfural conversion (41%). Conditions: initial concentration=0.1M, T=323K, P=2.1MPa, catalyst mass=20mg 5%Pd/C (commercial)

It is evident that the rate of aldehyde hydrogenation was higher in ethanol and water as compared to decalin, and that the rate of oligomerization was higher in the apolar solvent than the polar solvents. This drastic change in selectivity, especially between the two hydrogenation routes, was an important observation and is worth further analysis. First, consider how the adsorption of furfural on a metal surface can influence product selectivity. Sitthisa et al. studied the vapor phase hydrogenation/hydrodeoxygenation of furfural over Cu/SiO_2 and Pd/SiO_2 catalysts.[26] On the copper catalyst, furfural adsorbed on a η^1 configuration where the interaction between the molecule and the surface occurred mainly through the oxygen of the carbonyl group. In this case furfuryl alcohol was obtained with selectivity up to 98%. On the contrary, adsorption of furfural on palladium was suggested to occur preferentially in a η^2 configuration with both carbon and oxygen in the carbonyl group interacting with the surface. This configuration served as a precursor for the formation of acyl species, which are precursors for decarbonylation. Furthermore, the furanic ring had a parallel configuration with respect to the palladium surface, making ring hydrogenation readily possible. As described above, in the liquid phase and using decalin as the solvent, ring hydrogenation was the dominant path, in agreement with the rather flat adsorption mode observed in the vapor phase. Notice also that decarbonylation was not observed in our study due to the low reaction temperature. It could be suggested that in aqueous phase the change in selectivity towards furfuryl alcohol is due to a modification of the adsorption mode of furfural, similar to that observed on copper. This change in adsorption could be caused by a high surface coverage of water that

limits the available sites for furfural adsorption. Since furfural requires several adsorption sites in order to adsorb parallel to surface, in a surface with high concentration of water molecules and limited adsorption sites, furfural would be forced to adsorb on a more perpendicular mode (η^1 configuration) leading to a higher selectivity towards aldehyde hydrogenation. As a matter of fact, Masson et al. suggested this effect took place on the hydrogenation of acetophenone over Raney nickel catalysts in liquid phase [110]. A study of this reaction in a series of solvents, i.e. cyclohexane, 2-propanol and water, revealed not only an increase in activity in aqueous media but also a dramatic change in selectivity in the presence of water. It was proposed that adsorption of water on the metal surface prevented the adsorption of the aromatic ring and favored the interaction of the surface with the carbonyl group, leading to a higher 1-phenylethanol selectivity. However, studies for Fischer-Tropsch synthesis have shown that even in the presence of water the metal surface coverage is dominated by carbon monoxide [108], suggesting that furfural would dominate the surface concentration even in the presence of excess water. If this is the case then it is unlikely that water could modify the adsorption mode of furfural and affect selectivity in such a way. Another plausible explanation for the change in selectivity could be based on the transition state complex stabilization proposed by Akpa et al.[107] Such stabilization through hydrogen bonding would be more effective, although not exclusive, at the aldehyde group, leading to a higher increase in aldehyde hydrogenation as compared to ring hydrogenation even under a flat adsorption mode. At the aldehyde group water can

interact through hydrogen bonding both with the carbonyl oxygen and with the incoming hydrogen atoms, whereas at the ring only hydrogen interaction is possible. Figure 6.9 depicts the conversion of furfuryl alcohol in different solvents. As opposed to the case of furfural, when decalin was used as the solvent a higher rate of reactant disappearance was observed than when ethanol and water were used as the solvent. Also, water showed a higher conversion of furfuryl alcohol than ethanol. These differences in behavior are better understood when looking at the product distribution in Figure 6.10.

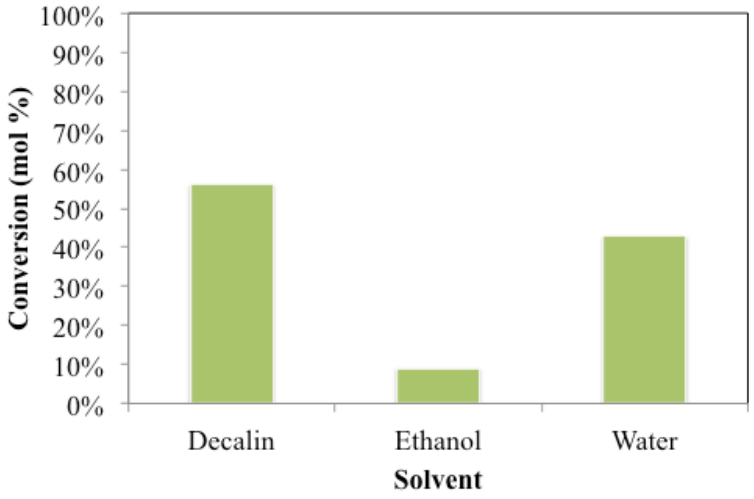

Figure 6.9. Furfuryl alcohol conversion in different solvents. Conditions: initial concentration=0.1M, T=323K, P=2.1MPa, catalyst mass=20mg 5%Pd/C (commercial), reaction time=0.33h

The main products when using decalin as the solvent were not in solution ("others") but probably retained by the catalyst, most likely as oligomers of furfuryl alcohol. It would be expected to observe such behavior in this solvent where reactant-solvent interactions are rather weak and furfuryl alcohol interactions are enhanced, thus promoting oligomerization. When compared to ethanol, the hydrogenation rate

remained constant, but the unaccounted material ("others') was reduced to zero. Since there is a stronger interaction between furfuryl alcohol and ethanol than with decalin it is plausible that oligomerization might be inhibited with this solvent. Water, on the other hand, increased significantly the hydrogenation activity when compared to the other two solvents. Furfuryl alcohol can only undergo ring hydrogenation under these conditions, indicating that water also has an important effect on ring hydrogenation. However this was not observed during furfural hydrogenation, where the main route was aldehyde hydrogenation.

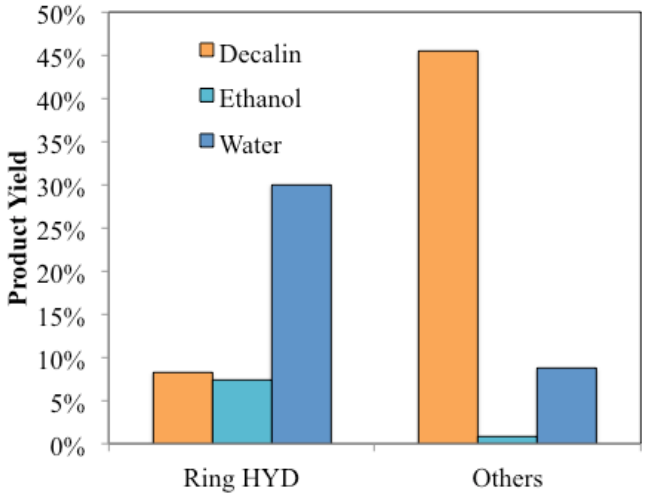

Figure 6.10. Product yield for furfural ring hydrogenation (Ring HYD) and other products in different solvents. Conditions: initial concentration=0.1M, T=323K, P=2.1MPa, catalyst mass=20mg 5%Pd/C (commercial), reaction time=1h

It was shown by Sitthisa that the heat of adsorption of furfural on copper was higher than furfuryl alcohol, denoting a stronger interaction of the former with the metal surface [119]. Thus the surface converage of the catalyst would tend to be dominated by furfural as opposed to the alcohol. In the presence of water, furfural selectively yielded furfuryl alcohol, but the latter was prevented from further

hydrogenation because furfural was dominant on the metal surface. Moreover, when furfural was not present, furfuryl alcohol was freely hydrogenated and water was able to enhance the only possible hydrogenation pathway i.e. ring hydrogenation.

• *Evaluation of transport limitations*

Important information can be obtained by measuring turnover frequencies of a series of catalysts with different metal loadings and considering the Noros-Kowak criterion as explained before. In general, the turnover frequency over catalysts with variable metal loading should remain unchanged in the absence of transport limitations, and when the reaction is structure insensitive. A number of factors could alter the turnover frequency, such as mass and heat transport limitations or catalyst deactivation.

Table 6.2. Turnover frequency for furfural conversion over different Pd/C catalysts

Catalyst	Dispersion (%)	Conversion	Surface Pd Moles/g cat	TOF FAL (s^{-1})
0.5% Pd/C	45.4	15%	$1.8x10^{-5}$	0.22
1.0% Pd/C	25.82	9%	$1.9x10^{-5}$	0.26
1.0% Pd/C	25.82	30%	$1.9x10^{-5}$	0.25
2.5% Pd/C	13.09	6%	$2.6x10^{-5}$	0.30
2.5% Pd/C	13.09	39%	$2.6x10^{-5}$	0.33
5.0% Pd/C	19.54	35%	$6.6x10^{-5}$	0.63
5.0% Pd/C (Commercial)	30.89	12%	$1.2x10^{-4}$	0.86
5.0% Pd/C (Commercial)	30.89	32%	$1.2x10^{-4}$	0.76

In order to evaluate the presence of transport limitations in the liquid phase hydrogenation of furfural, the turnover frequency for reactant conversion was measured over a series of Pd/C catalyst with different metal loading, different dispersion (measured from CO chemisorption), and at different levels of conversion (Table 6.2). The turnover frequency did not systematically increase or decrease as a

function of dispersion, but rather changed in a random manner and not indicating a particular pattern. Although this is not proof for hydrogenation of furfural being a structure insensitive reaction, it does not indicate either a particular dependence of activity on catalyst dispersion. On top of this, the selectivity towards hydrogenation products is not significantly altered over the different catalysts, which supports the hypothesis of the reaction being structure insensitive. Nevertheless a conclusive statement could not be drawn from this set of experiments.

Under the assumption that hydrogenation of furfural is a structure insensitive reaction, the turnover frequency was studied as a function of metal loading, which in Table 6.2 and Figure 6.11 is expressed as surface moles of palladium per gram of catalyst.

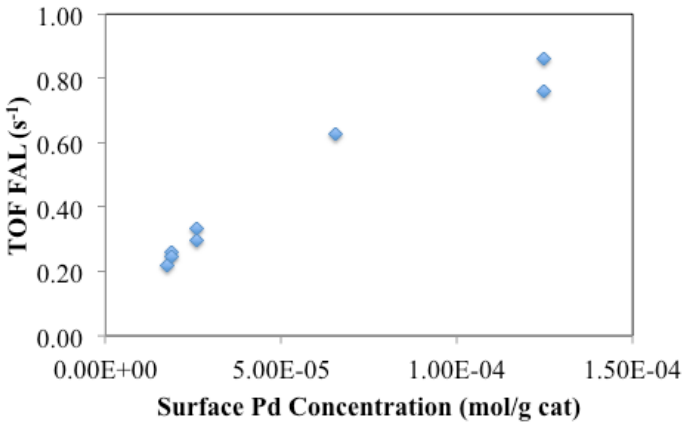

Figure 6.11. Variation of turnover frequency for furfural hydrogenation as a function of catalyst metal loading

The turnover frequency did not decrease as the concentration of palladium in the catalyst increased, therefore mass transport limitations could be initially ruled out (however additional tests were performed in order to further confirm this conclusion). Contrarily, a higher turnover frequency was observed as the palladium

concentration was increased. A reason for this observation could be the presence of heat transport limitations. Hydrogenation is a highly exothermic reaction and it is possible that local increases in temperature could lead to a higher reaction rate. This effect would intensify as the number of reaction sites is higher on the catalyst surface, and result in a behavior like the one observed in Figure 6.11. This effect could be minimized by working with a low palladium content catalyst.

The Noros-Kowak criterion does not provide information about what specific phenomena might be influencing the turnover frequencies, i.e. internal transport limitations, external transport limitations, vapor-liquid transport limitations. In order to support the previous study, two additional tests were performed to test the presence of mass transport limitations. Limitations on hydrogen diffusion from the vapor to the liquid phase can be evaluated by changing the mass of catalyst present in the reactor. An increase in catalyst mass should be followed by an increase in the rate of reaction, unless the limiting step in the process is diffusion of hydrogen from the vapor to the liquid phase. Table 6.2 shows the turnover frequency for different catalysts at two different conversions, where the conversion was varied by changing the amount of catalyst. For every single catalyst, the turnover frequency was not altered by the change in catalyst mass, indicating the absence of this type of limitation. Another important test that provides information about external mass transport limitations is changing the stirring speed. If there exist limitation for the transport of reactants from the bulk liquid phase to the external surface of the catalyst particle, then a change in stirring speed would cause a change in reaction rate. Figure 6.12 shows conversion and product distribution for a series of

experiments with variant stirring speed. It was clear that no effect on rate of reaction was present at different stirring speeds, and therefore external mass transport limitations were ruled out from the system.

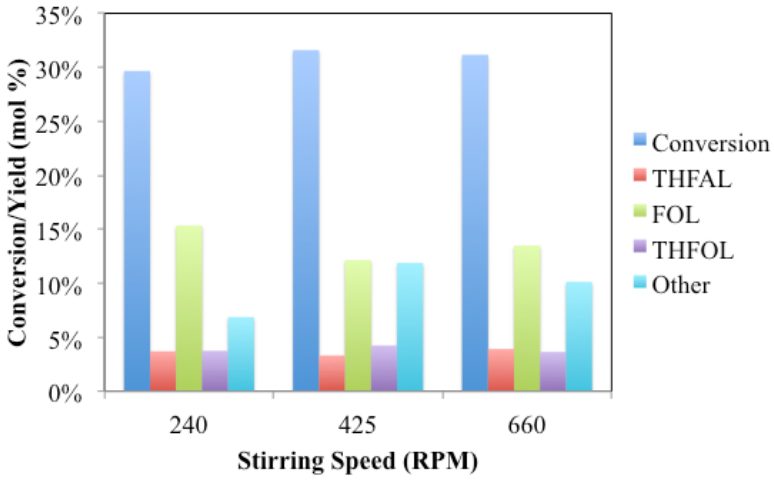

Figure 6.12. Conversion of furfural and product yields at different stirring speeds. Conditions: initial concentration=0.1M, T=323K, P=2.1MPa, catalyst mass=50mg 1.0%Pd/C, reaction time=1h

• *Kinetic model of furfural hydrogenation*

As discussed above, a kinetic model is useful for the estimation of kinetic and thermodynamic parameters (rate and adsorption constants) that provide insight into reaction mechanisms. Based on the preliminary results from the effect of the solvent on hydrogenation of furfural, it would be expected that the parameters predicted by a kinetic model would change when working with different solvents. This information would allow confirming the hypothesis about a transition state modification by the solvent and show how the reaction mechanism would be altered. Because of this it is desired to perform a detailed kinetic model of furfural hydrogenation in two different solvents: water and decalin.

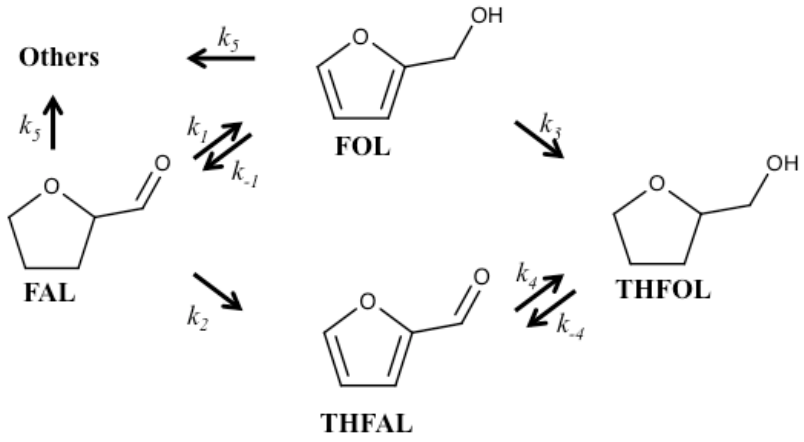

Figure 6.13. Reaction scheme for furfural hydrogenation in liquid phase

The following experimental data will be required for at least 4 different temperatures: conversion and product evolution as a function of time with different initial reactants (furfural, furfuryl alcohol, tetrahydrofurfuryl alcohol and a mixture of furfural and furfuryl alcohol); rate of reaction at early reaction time as a function of initial concentration for different reactants (furfural, furfuryl alcohol, tetrahydrofurfuryl alcohol). The first set of data (as a function of time) will allow to set a model in terms of mole balances for each of the species present in the system and will be the main data set for parameter estimation. The second set of data, will serve as a tool to obtain initial estimates of adsorption constants for each of the species present in the model, that could be input into the fitting data set and provide boundaries for the variation of this parameters. Once the rate and adsorption constants are estimated for each temperature, it will be possible to calculate activation energies, heats of adsorption, activation entropies and entropies of adsorption. Doing this work for the two solvents will allow establishing the

differences and effect that each one has on the reaction mechanism and state of the active species during relevant kinetic steps.

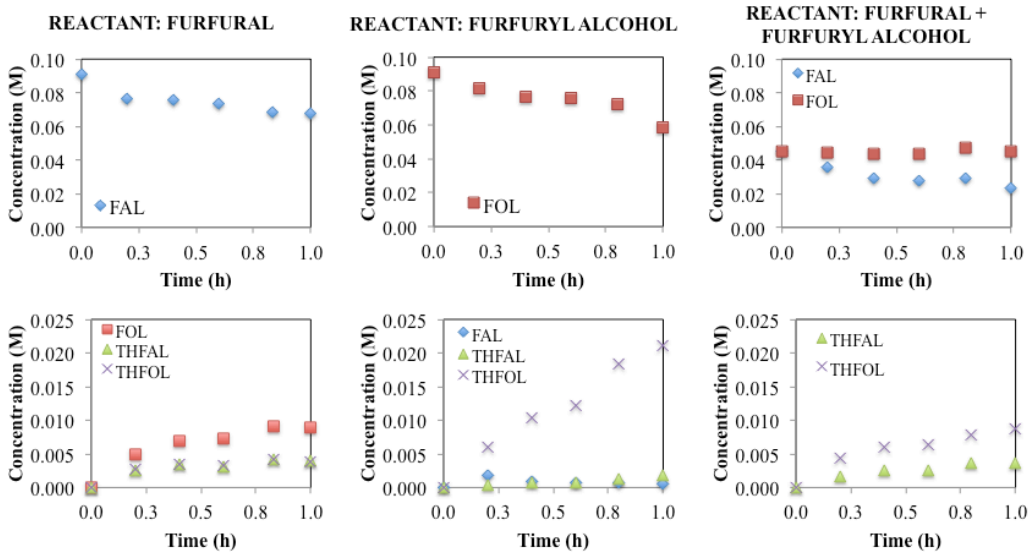

Figure 6.14. Conversion and product evolution as a function of time in hydrogenation of furfural, furfuryl alcohol and a mixture of furfural and furfuryl alcohol. Conditions: initial concentration=0.1M, T=323K, P=2.1MPa, catalyst mass=50mg 1.0%Pd/C

The reaction scheme for the reaction system is shown in Figure 6.13. Hydrogenation of the aldehyde group has been allowed to be a reversible reaction, whereas hydrogenation of the ring was set as a forward reaction alone (this could be supported by the fact that ring hydrogenation is highly favored at low temperatures). Also, formation of condensation products would originate only from furfural and furfuryl alcohol. Figure 6.14 gives a sample of conversion data as a function of time for different feeds and at a temperature of 40°C. No actual modeling has been performed on this data and further experimentation is still required in order to provide the required data for estimation of kinetic and thermodynamic parameters.

6.5. Conclusions

Polar solvents with ability to participate in hydrogen bonding have significant effects on activity and selectivity of furfural hydrogenation in the liquid phase. Water enhanced the rate of ring and aldehyde hydrogenation as compared to decalin. There are two possible explanations for this effect. First, water can act as a hydrogen-shuttle, mediating the transfer of hydrogen from the surface to furfural. Second, water molecules can interact with furfural through hydrogen bonding thus stabilizing activated complexes for hydrogenation and therefore reaction rates. On the other hand, water and ethanol drastically changed product selectivity during furfural hydrogenation. Since hydrogen bonding might be more effective at the aldehyde group, the effect on hydrogenation of this functionality is expected to be higher than for ring hydrogenation. Also, due to strong interaction with the surface, furfural can prevent further hydrogenation of furfuryl alcohol, thus preventing a proportional increase in ring hydrogenation. Further kinetic studies are necessary in order to provide more insight in these interesting solvent effects.

6.6. Remarks for the future

• *DFT calculations*

A good complement for this experimental study would be estimation of activation energies, entropies and heats and entropies of adsorption. A computational study of this kind would provide insight on how the transition state actually looks, which atom is hydrogenated first (for example, carbon or oxygen in the case of the aldehyde group), and also corroborate the parameters estimated from the experiments.

• *Experimental data collection*

The same recommendation done in the case of cresol alkylation is done here. In order to reduce the time required for obtaining reaction data as a function of time, a system of sample collection should be implemented in the reactor in order to measure the concentration of species as a function of time in one single experiment. This would also reduce experimental error from individual experiments.

7. References

[1] Alonso, David. Bond, Jesse. Dumesic, James. 2010. Catalytic conversion of biomass to biofuels. *Green Chemistry*. 12:1493-1513.

[2] Balat, Havva. 2010. Prospects of biofuels for a sustainable energy future: A critical assessment. *Energy Education Science and Technology Part A-Energy Science and Research.* 24:85-111.

[3] Kumar, Parveen. Barrett, Diane. Delwiche, Michael. Stroeve, Pierter. 2009. Methods for Pretreatment of Lignocellulosic Biomass for Efficient Hydrolysis and Biofuel Production. *Industrial & Engineering Chemistry Research.* 48:3713-3729.

[4] Carroll, Andrew. Somerville, Chris. 2009. Cellulosic Biofuels. *Annual Review of Plant Biology.* 60:165-182.

[5] Demirbas, Ayhan. Progress and recent trends in biofuels. 2007. *Progress in Energy and Combustion Science.* 33:1-18.

[6] Chheda, Juben. Huber, George. Dumesic, James. 2007. Liquid-Phase Catalytic Processing of Biomass-Derived Oxygenated Hydrocarbons to Fuels and Chemicals. *Angewandte Chemie International Edition.* 46:7164-7183.

[7] Huber, George. Iborra, Sara. Corma, Avelino. 2006. Synthesis of Transportation Fuels from Biomass: Chemistry, Catalysts, and Engineering. *Chemical Reviews.* 106:4044-4098.

[8] Qi, Zhang. Jie, Chang. Tiejun, Wang. Ying, Xu. 2007. Review of biomass pyrolysis oil properties and upgrading research. *Energy Conversion and Management.* 48:87-92.

[9] Mohan, Dinesh. Pittman, Charles. Steele, Philip. 2006. Pyrolysis of Wood/Biomass for Bio-oil: A Critical Review. *Energy & Fuels.* 20*:*848-889.

[10] Zapata, Paula. Huang, Yi. González-Borja, Miguel. Resasco, Daniel. 2013. Silylated hydrophobic zeolites with enhanced tolerance to hot liquid water. *Journal of Catalysis.* 308:82-97.

[11] Nie, Lei. Resasco, Daniel. 2012. Improving carbon retention in biomass conversion by alkylation of phenolics with small oxygenates. *Applied Catalysis A: General.* 447-448:14-21.

[12] Fernando, Sandun. Adhikari, Sushil. Chandrapal, Chauda. Murali, Naveen. 2006. Biorefineries: Current status, Challenges, and Future Direction. *Energy & Fuels.* 20:1727-1737.

[13] Elliott, Douglas. Hart, Todd. 2009. Catalytic Hydroprocessing of Chemical Models for Bio-oil. *Energy & Fuels.* 23:631-637.

[14] Resasco, Daniel. Crossley, Steven. Molecular Engineering Approach in the Selection of Catalytic Strategies for Upgrading of Biofuels. *AICHE Journal.* 55:1082-1089.

[15] Sharma, R. Bakhshi, N. Catalytic Upgrading of Biomass-Derived Oils to Transportation Fuels and Chemicals. 1991. *The Canadian Journal of Chemical Engineering.* **1991**, 69:1071-1081.

[16] Adjaye, J. Bakhshi, N. 1995. Catalytic Conversion of a Biomass-Derived Oil to Fuels and Chemicals I: Model Compound Studies and Reaction Pathways. *Biomass and Bioenergy.* 8:131-149.

[17] Adjaye, J. Bakhshi, N. 1995. Catalytic Conversion of a Biomass-Derived Oil to Fuels and Chemicals II: Chemical Kinetics, Parameter Estimation and Model Predictions. *Biomass and Bioenergy*. 8: 265-277.

[18] Donnis, Bjørn. Egeberg, Rasmus. Blom, Peder. Knudsen, Kim. 2009. Hydroprocessing of Bio-Oils and Oxygenates to Hydrocarbons. Understanding the Reaction Routes. *Topics in Catalysis*. 52:229-240.

[19] Furimsky, Edward. 2000. Catalytic hydrodeoxygenation. *Applied Catalysis A: General.* 199:147-190.

[20] Fisk, Courtney. Morgan, Tonya. Ji, Yaying. Crocker, Mark. Crofcheck, Czarena. Lewis, Sam. 2009. Bio-oil upgrading over platinum catalysts using *in situ* generated hydrogen. *Applied Catalysis A: General.* 358:150-156.

[21] Pham, Tu. Shi, Dachuan. Sooknoi, Tawan. Resasco, Daniel. 2012. Aqueous-phase ketonization of acetic acid over Ru/TiO_2/carbon catalysts. *Journal of Catalysis.* 295:169-178.

[22] Yu, Wanjin. Tang, Yang. Mo, Liuye. Chen, Ping. Lou, Hui. Zheng, Xiaoming. 2011. Bifunctional Pd/Al-SBA-15 catalyzed one-step hydrogenation-esterification of furfural and acetic acid: A model reaction for catalytic upgrading of bio-oil. *Catalysis Communications.* 13:35-39.

[23] Hakim, Sikander. Shanks, Brent. Dumesic, James. 2013. Catalytic upgrading of the light fraction of a simulated bio-oil over $CeZrO_x$ catalyst. *Applied Catalysis B: Environmental.* 142-143:368-376.

[24] Lohitharn, Nattaporn. Shanks, Brent. 2009. Upgrading of bio-oil: Effect of light aldehydes on acetic acid removal via esterification. *Catalysis Communications.* 11:96-99.

[25] Zapata, Paula. Faria, Jimmy. Ruiz, Pilar. Resasco, Daniel. 2012. Condensation/Hydrogenation of Biomass-Derived Oxygenates in Water/Oil Emulsions Stabilized by Nanohybrid Catalysts. *Topics in Catalysis.* 55:38-52.

[26] Sitthisa, Surapas. Resasco, Daniel. 2011. Hydrodeoxygenation of Furfural Over Supported Metal Catalysts: A Comparative Study of Cu, Pd and Ni. *Catalysis Letters*. 141:784-791.

[27] Zhou, Minghao. Zeng, Zuo. Zhu, Hongyan. Xiao, Guomin. Xiao, Rui. 2014. Aqueous-phase catalytic hydrogenation of furfural to cyclopentanol over Cu-Mg-Al hydrotalcites derived catalysts: Model reaction for upgrading of bio-oil. *Journal of Energy Chemistry.* 23:91-96.

[28] Zhou, Minghao. Zhu, Hongyan. Niu, Lei. Xiao, Guomin. Xiao, Rui. 2014. Catalytic Hydroprocessing of Furfural to Cyclopentanol Over Ni/CNTs Catalysts: Model Reaction for Upgrading of Bio-oil. *Catalysis Letters.* 144:235-241.

[29] Boonyasuwat, Sunya. Omotoso, Taiwo. Resasco, Daniel. Crossley, Steven. 2013. Conversion of Guaiacol over Supported Ru Catalysts. *Catalysis Letters.* 143:783-791.

[30] Guo, Jianhua. Ruan, Renxiang. Zhang, Ying. 2012. Hydrotreating of Phenolic Compounds Separated from Bio-oil to Alcohols. *Industrial & Engineeering Chemistry Research.* 51:6599-6604.

[31] Nie, Lei. De Souza, Priscilla. Noronha, Fabio. An, Wei. Sooknoi, Tawan. Resasco, Daniel. 2014. Selective conversion of m-cresol to toluene over bimetallic Ni-Fe catalysts. *Journal of Molecular Catalysis A: Chemical.* 388-389:47-55.

[32] Yang, Xu-Lai. Pittman, Charles. Zhu, Xi-Feng. 2010. Phenolic Model Reactions with Olefin for Bio-oil Upgrading over Solid Acid Catalyst. *Chemical Journal of Chinese Universities-Chinese.* 31:1398-1404.

[33] Zhang, Zhi-Jun. Wang, Qing-Wen. Yang, Xu-Lai. Chatterjee, Sabornie. Pittman, Charles. 2009. Sulfonic acid resin-catalyzed addition of phenols, carboxylic acids, and water to olefins: Model reactions for catalytic upgrading of bio-oil. *Bioresource Technology.* 101:3585-3695.

[34] Vannice, M. 2005. Kinetics of Catalytic Reactions. Springer Science. New York. Chapter 4.

[35] Singh, Utpal. Vannice, M. 2001. Kinetics of liquid-phase hydrogenation reactions over supported metal catalysts – a review. *Applied Catalysis A: General.* 213:1-24.

[36] Madon, Rostam. Boudart, Michel. 1982. Experimental Criterion for the Absence of Artifacts in the Measurement of Rates of Heterogeneous Catalytic Reactions. *Industrial & Engineering Chemistry Fundamentals.* 21:438-447.

[37] Pangarkar, Kalyani. Schildhauer, Tilman. van Ommen, Ruud. Nijenhuis, John. Kapteijn, Freek. Moulijn, Jacob. 2008. Structured Packings for Multiphase Catalytic Reactors. *Industrial & Engineering Chemistry Research.* 47:3720-3751.

[38] Cybulski, Andrzej. Moulijn, Jacob. 1994. Monoliths in Heterogeneous Catalysis. *Catalysis Reviews Science and Engineering.* 36:179-270.

[39] Nijhuis, Alexander. Beers, Annemarie. Vergunst, Theo. Hoek, Ingrid. Kapeijn, Freek. Moulijn, Jacob. 2001. Preparation of Monolithic Catalysts. *Catalysis Reviews Science and Engineering.* 43:345-380.

[40] Morales-Torres, S. Perez-Cadenas, A. Kapteijn, F. Carrasco-Marin, F. Maldonado-Hodar, F.J. Moulijn, Jacob. 2009. Palladium and platinum catalysts supported on carbon nanofiber coated monoliths for low-temperature combustion of BTX. *Applied Catalysis B: Environmental.* 89:411-419.

[41] Basagiannis, Aristides. Verykios, Xenophon. 2007. Steam reforming of the aqueous fraction of bio-oil over structured Ru/MgO/Al2O3 catalysts. *Catalysis Today.* 127:256-264.

[42] Iojoiu, Eduard. Domine, Marcelo. Davidian, Thomas. Guilhaume, Nolven. Mirodatos, Claude. 2007. Hydrogen production by sequential cracking of biomass-derived pyrolysis oil over noble metal catalysts supported on ceria-zirconia. *Applied Catalysis A: General.* 323:147-161.

[43] Domine, Marcelo. Iojoiu, Eduard. Davidian, Thomas. Guilhaume, Nolven. Mirodatos, Claude. 2008. Hydrogen production from biomass-derived oil over monolithic Pt- and Rh-based catalysts using steam reforming and sequential cracking processes. *Catalysis Today.* 133-135:565-573.

[44] Torres, Walter. Pansare, Sourabh. Goodwin, James. 2007. Hot Gas Removal of Tars, Ammonia, and Hydrogen Sulfide from Biomass Gasification Gas. *Catalysis Reviews Science and Engineering.* 49:407-456.

[45] Pinto, Filomena. André, Rui. Franco, Carlos. Lopes, Helena. Gulyurtlu, Ibrahim. Cabrita, Isabel. 2009. Co-gasification of coal and wastes in a pilor-scale

installation 1: Effect of catalysts in syngas treatment to achieve tar abatement. *Fuel.* 88:2392-2402.

[46] Mullen, Charles. Boateng, Akwasi. 2008. Chemical Composition of Bio-oils Produced by Fast Pyrolysis of Two Energy Crops. *Energy & Fuels*. 22:2104-2109.

[47] De Jong, Krijn. Geus, John. 2000. Carbon Nanofibers: Catalytic Synthesis and Applications. *Catalysis Reviews Science and Engineering.* 42:481-510.

[48] Baronetti, Graciela. de Miguel, Sergio. Scelza, Osvaldo. Fritzler, Miguel. Castro, Alberto. 1985. Pt-Sn/Al_2O_3 catalysts: studies of the impregnation step. *Applied Catalysis.* 19:77-85.

[49] Prado-Burguete, C. Linares-Solano, A. Rodriguez-Reinoso, F. Salinas-Martinez de Lecea, C. 1989. The effect of Oxygen Surface Groups of the Support on Platinum Dispersion in Pt/Carbon Catalysts. *Journal of Catalysis.* 115:98-106.

[50] Pinheiro, Ana. Hudebine, Damien. Dupassieux, Nathalie. Geantet, Christophe. 2009. Impact of Oxygenated Compounds from Lignocellulosic Biomass Pyrolysis on Gas Oil Hydrotreatment. *Energy & Fuels.* 23:1007-1014.

[51] Philippe, M. Richard, F. Hudebine, Damien. Brunet, S. 2010. Inhibiting effect of oxygenated model compounds on the HDS of dibenzothiophenes over CoMoP/Al2O3 catalyst. *Applied Catalysis A: General.* 383:14-23.

[52] Zhao, H. Li, D. Bui, P. Oyama, S. 2010. Hydrodeoxygenation of guaiacol as model compound for pyrolysis on transition metal phosphide hydroprocessing catalysts. *Applied Catalysis A: General.* 391:305-310.

[53] Filley, Jonathan. Roth, Christine. 1999. Vanadium catalyzed guaiacol deoxygenation. *Journal of Molecular Catalysis A: Chemical.* 139:245-252.

[54] Bui, Van. Laurenti, Dorothee. Afanasiev, Pavel. Geantet, Christophe. 2010 Hydrodeoxygenation of guaiacol with CoMo catalysts. Part I: Promoting effect of cobalt on HDO selectivity and activity. *Applied Catalysis B: Environmental.* 101:239-245.

[55] Stagg, S. Romeo, E. Padro, C. Resasco, Daniel. 1998. Effect of Promotion with Sn on Supported Pt Catalysts for CO_2 Reforming of CH_4. *Journal of Catalysis.* 178:137-145.

[56] Chiappero, Martina. Do, Phuong. Crossley, Steven. Lobban, Lance. Resasco, Daniel. 2011. Direct conversion of triglycerides to olefins and paraffins over noble metal supported catalysts. *Fuel*. 90:1155-1165.

[57] Zhu, Xinli. Mallinson, Richard. Resasco, Daniel. 2010. Role of transalkylation reactions in the conversion of anisole over HZSM-5. *Applied Catalysis A: General.* 379:172–181.

[58] Zhu, Xinli. Lobban, Lance. Mallinson, Richard. Resasco, Daniel. 2011. Bifunctional transalkylation and hydrodeoxygenation of anisole over a Pt/HBeta catalyst. *Journal of Catalysis.* 281:21-29.

[59] Ferrari, Maria. Maggi, Rosanna. Delmon, Bernard. Grange, Paul. 2001 Influences of the Hydrogen Sulfide Partial Pressure and of a Nitrogen Compound on the Hydrodeoxygenation Activity of a CoMo/Carbon Catalyst. *Journal of Catalysis.* 198:47-55.

[60] Pham, Tu. Sooknoi, Tawan. Crossley, Steven. Resasco, Daniel. 2013. Ketonization of Carboxylic Acids: Mechanism, Catalysts, and Implications for Biomass Conversion. *ACS Catalysis.* 3:2456-2473.

[61] Zapata, Paula. Faria, Jimmy. Ruiz, Pilar. Jentoft, Rolf. Resasco, Daniel. 2012. Hydrophobic Zeolites for Biofuel Upgrading Reactions at the Liquid-Liquid Interface in Water/Oil Emulsions. *Journal of the American Chemical Society.* 134:8570-8578.

[62] Grabowska, Hanna. Syper, Ludwik. Zawadzki, Miroslaw. 2004. Vapour phase alkylation of *ortho*-, *meta*- and *para*-cresols with isopropyl alcohol in the presence of sol-gel prepared alumina catalyst. *Applied Catalysis A: General.* 277:91-97.

[63] Umamaheswari, V. Palanichamy, M. Murugesan, V. 2002. Isopropylation of m-Cresol over Mesoporous Al-MCM-41 Molecular Sieves. *Journal of Catalysis.* 210:367-374.

[64] Samolada, M. Grigoriadou, E. Kiparissides, Z. Vasalos, I. 1995. Selective O-Alkylation of Phenol with Methanol over Sulphates Supported on γ-Al_2O_3. *Journal of Catalysis.* 152:52-62.

[65] Sad, M. Padró, C. Apesteguía, C. 2008. Synthesis of cresols by alkylation of phenol with methanol on solid acids. *Catalysis Today.* 133-135:720-728.

[66] Karthik, M. Tripathi, A. Gupta, N. Vinu, A. Hartmann, M. Palanichamy, M. Murugesan, V. 2004. Characterization of Co,Al-MCM-41 and its activity in the t-butylation of phenol using isobutanol. *Applied Catalysis A: General.* 268:139-149.

[67] Devassy, Biju. Shanbhag, G. Lefebvre, F. Halligudi, S. 2004. Alkylation of p-cresol with tert-butanol catalyzed by heteropoly acid supported on zirconia catalyst. *Journal of Molecular Catalysis A: Chemical.* 210:125-130.

[68] Sato, Satoshi. Takahashi, Ryoji. Sodesawa, Toshiaki. Matsumoto, Kotaro. Kamimura, Yoichiro. 1999. Ortho-Selective Alkylation of Phenol with 1-Propanol Catalyzed by CeO_2-MgO. *Journal of Catalysis.* 184:180-188.

[69] Velu, S. Swamy, C. 1996. Selective C-alkylation of phenol with methanol over catalysts derived from copper-aluminium hydrotalcite-like compounds. *Applied Catalysis A: General.* 145:141-153.

[70] García, L. Giannetto, G. Goldwasser, M. Guisnet, M. Magnoux, P. 1996. Phenol alkylation with methanol: effect of sodium content and ammonia selective poisoning of an HY zeolite. *Catalysis Letters.* 37:121-123.

[71] Yadav, Ganapati. Kumar, Parveen. 2005. Alkylation of phenol with cyclohexene over solid acids: Insight in selectivity of O- versus C-alkylation. *Applied Catalysis A: General.* 286:61-70.

[72] Gagea, Bodgan. Parvulescu, Andrei. Parvulescu, Vasile. Auroux, Aline. Grange, Paul. Poncelet, Georges. 2003. Alkylation of phenols and naphthols on silica-immobilized triflate derivatives. *Catalysis Letters.* 91:141-144.

[73] Grabowska, H. Mista, W. Trawczynski, J. Wrzyszcz, J. Zawadzki, M. 2001. A method for obtaining thymol by gas phase catalytic alkylation of m-cresol over zinc aluminate spinel. *Applied Catalysis A: General.* 220:207-213.

[74] Velu, S. Sivasanker, S. 1998. Alkylation of m-Cresol with Methanol and 2-Propanol over calcined magnesium-aluminium hydrotalcites. *Research on Chemical Intermediates.* 24:657-666.

[75] Bregolato, M. Bolis, V. Busco, C. Ugliengo, P. Bordiga, S. Cavani, F. Ballarini, N. Maselli, L. Passeri, S. Rossetti, I. Forni, L. 2007. Methylation of phenol over high-silica beta zeolite: Effect of zeolite acidity and crystal size on catalyst behavior. *Journal of Catalysis.* 245:285-300.

[76] Ma, Qisheng. Chakraborty, Deb. Faglioni, Francesco. Muller, Rick. Goddard, William. Harris, Thomas. Campbell, Curt. Tang, Yongchun. 2006. Alkylation of Phenol: A Mechanistic View. *Journal of Physical Chemistry A.* 110:2246-2252.

[77] Jansang, Bavornpon. Nanok, Tanin. Limtrakul, Jumras. 2008. Structure and Reaction Mechanism of Alkylation of Phenol with Methanol over H-Fau Zeolite: An ONIUM Study. *Journal of Physical Chemistry C.* 112:540-547.

[78] O'Connor, Cyril. Moon, Gillian. Bohringer, Walter. Fletcher, Jack. 2003. Alkylation of Phenol and m-Cresol over Zeolites. *Collection of Czechoslovak Chemical Communications.* 68:1949-1967.

[79] Yadav, Ganapati. Thorat, Tushar. 1996. Kinetics of Alkylation of p-Cresol with Isobutylene Catalyzed by Sulfated Zirconia. *Industrial & Engineering Chemistry Research.* 35:721-731.

[80] Santacesaria, E. Grasso, D. Gelosa, D. Carra, S. 1990. Catalytic Alkylation of Phenol with Methanol: Factors Influencing Activities and Selectivities. I. Effect of Different Acid Sites Evaluated by Studying the Behaviour of the Catalysts: γ-alumina, Nafion-H, silica-alumina and phosphoric acid. *Applied Catalysis.* 64:83-99.

[81] Zhu, Xinli. Lobban, Lance. Mallinson, Richard. Resasco, Daniel. 2010. Tailoring the mesopore structure of HZSM-5 to control product distribution in the conversion of propanal. *Journal of Catalysis.* 271:88-98.

[82] Fameth, William. Gorte, Raymond. 1995. Methods for Characterizing Zeolite Acidity. *Chemical Reviews.* 95:615-635.

[83] Sad, M. Padró, C. Apesteguía, C. 2010. Study of the phenol methylation mechanism on zeolites HBEA, HZSM5 and HMCM22. *Journal of Molecular Catalysis A: Chemical.* 327:63-72.

[84] Liu, Xiumei. Liu, Min. Guo, Xinwen. Zhou, Jinxia. 2008. SO_3H-functionalized ionic liquids for selective alkylation of m-cresol with tert-butanol. *Catalysis Communications.* 9:1-7.

[85] Koros, R. Nowak, E. 1967. A diagnostic test of the kinetic regime in a packed bed reactor. *Chemical Engineering Science.* 22:470.

[86] Gunther, William. Duong, Quynh. Roman-Leshkov, Yuriy. 2013. Catalytic consequences of borate complexation and pH on the epimerization of L-arabinose to L-ribose in water catalyzed by Sn-Beta zeolite with borate salts. *Journal of Molecular Catalysis A: Chemical.* 379:294-302.

[87] Nie, Xiaowa. Liu, Xin. Song, Chunshan. Guo, Xinwen. 2010. Bronsted acid-catalyzed tert-butylation of phenol, o-cresol and catechol: A comparative computational study. *Journal of Molecular Catalysis A: Chemical.* 332:145-151.

[88] Yadav, Ganapati. Kamble, Shashikant. 2009. Synthesis of carvacrol by Friedel-Crafts alkylation of o-cresol with isopropanol using superacidic catalyst UDCaT-5. *Journal of Chemical Technology and Biotechnology.* 84:1499-1508.

[89] Nie, Xiaowa. Liu, Xin. Gao, Lei. Liu, Min. Song, Chunshan. Guo, Xinwen. 2010. SO_3H-Functionalized Ionic Liquid Catalyzed Alkylation of Catechol with tert-Butyl Alcohol. *Industrial and Engineering Chemistry.* 49:8157-8163.

[90] Ng, Sai. Harris, H. Prausnitz, J. 1969. Henry's Constants for Methane, Ethane, Ethylene, Propane, and Propylene in Octadecane, Eicosane, and Docosane. *Journa of Chemical & Engineering Data.*14: 482-483.

[91] Nitta, Masahiro. Aomura, Kazuo. Yamaguchi, Katsumi. 1974. Alkylation of Phenols. II. The Selective Formation of Thymol from m-Cresol and Propylene with a γ-Alumina Catalyst. *Bulletin of the Chemical Society of Japan.* 10:2360-2364.

[92] Forissier, M. Bernard, J. 1991. Catalyst Deactivation. Elsevier Science Publishers B.V. Amsterdam, 359-366.

[93] Nevicato, D. Pitault, I. Forissier, M. Bernard, J. 1994. Catalyst Deactivation – Studies in Surface Science and Catalysis Vol. Elsevier Science B.V. 249-256.

[94] Olson, D. Haag, W. Borghard, W. 2000. Use of water as a probe of zeolitic properties: interaction of water with HZSM-5. *Microporous and Mesoporous Materials.* 35-36:435-446.

[95] Malshe, Kusum. Patil, Pratap. Umbarkar, Shubhangi. Dongare, Mohan. 2004. Selective C-methylation of phenol with methanol over borate zirconia solid catalyst. *Journal of Molecular Catalyst A: Chemical.* 212:337-344.

[96] Dixit, Lalji. Prasada, T. 1999. Heats of Adsorption of Hydrocarbons on Zeolite Surfaces: A Mathematical Approach. *Journal of Chemical Information and Modeling.* 39:218-223.

[97] Xu, Weiyin. Miller, Stephen. Agrawal, Pradeep. Jones, Christopher. 2014. Positive Effect of Water on Zeolite BEA Catalyzed Alkylation of Phenol with Propylene. *Catalysis Letters.* 144:434-438.

[98] Ehrhardt, K. Suckow, M. Lutz, W. 1995. Hydrothermal decomposition of aluminosilicate zeolites and prediction of their long-term stability. *Studies in Surface Science and Catalysis.* 94:179-186.

[99] Ravenelle, Ryan. Schuβler, Florian. D'Amico, Andrew. Danilina, Nadiya. van Bokhoven, Jeroen. Lercher, Johannes. Jones, Christopher. Sievers, Carsten. 2010. Stability of Zeolites in Hot Liquid Water. *Journal of Physical Chemistry C.* 114:19582-19595.

[100] Crossley, Steven. Faria, Jimmy. 2010. Shen, Min. Resasco, Daniel. Solid Nanoparticles that Catalyze Biofuel Upgrade Reactions at the Water/Oil Interface. *Science.* 327:68-72.

[101] Alonso, David. Bond, Jesse. Dumesic, James. 2010. Catalytic conversion of biomass to biofuels. *Green Chemistry.* 12:1493-1513.

[102] Weingarten, Ronen. Tompsett, Geoffrey. Conner, Wm. Huber, George. 2011. Design of solid acid catalysts for aqueous-phase dehydration of carbohydrates: The role of Lewis and Bronsted acid sites. *Journal of Catalysis*. 279:174-182.

[103] Lange, Jean-Paul. van der Heide, Evert. van Buijtenen, Jeroen. Price, Richard. 2012. Furfural-A Promising Platform for Lignocellulosic Biofuels, *ChemSusChem*. 5:150-166.

[104] Merlo, Andrea. Vetere, Virginia. Ruggera, Jose. Casella, Monica. 2009. Bimetallic PtSn catalyst for the selective hydrogenation of furfural to furfuryl alcohol in liquid-phase. *Catalysis Communications*. 10:1665-1669.

[105] Wolffenbuttel, B. Nijhuis, T. Stankiewicz, A. Moulijn, J. 2001. Influence of water on fast hydrogenation reactions with monolithic and slurry catalysts, *Catalysis Today*. 69:265-273.

[106] Krishnamoorthy, Sundaram. Tu, Mai. Ojeda, Manuel. Pinna, Dario. Iglesia, Enrique. 2002. An Investigation of the Effects of Water on Rate Selectivity for the Fischer-Tropsch Synthesis on Cobalt-Based Catalysts. *Journal of Catalysis*. 211:422-433.

[107] Akpa, B. D'Agostino, C. Gladden, L. Hindle, K. Manyar, H. McGregor, J. Li, R. Neurock, M. Sinha, N. Stitt, E. Weber, D. Zeitler, J. Rooney, D. 2012. Solvent effects in the hydrogenation of 2-butanone. *Journal of Catalysis*. 289:30-41.

[108] Hibbitts, David. Loveless, Brett. Neurock, Matthew. Iglesia, Enrique. 2013. Mechanistic Role of Water on the Rate and selectivity of Fischer-Tropsch Synthesis on Ruthenium Catalysts. *Angewandte Chemie International Edition*. 52:12273-12278.

[109] Hu, Sung-Cheng. Chen, Yu-Wen. 1997. Partial Hydrogenation of Benzene to Cyclohexene on Ruthenium Catalysts Supported on La2O3-ZnO Binary Oxides. *Industrial & Engineering Chemistry Research*. 36:5153-5159.

[110] Masson, J. Cividino, P. Court, J. 1997. Selective hydrogenation of acetophenone on chromium promoted Raney nickel catalysts. III. The influence of the nature of the solvent. *Applied Catalysis A: General.* 161:191-197.

[111] Wan, Haijun. Chaudhari, Raghunath. Subramaniam, Bala. 2013. Catalytic Hydroprocessing of p-Cresol: Metal, Solvent and Mass-Transfer Effects. *Topics in Catalysis*. 55:129-139.

[112] Singh, Utpal. Vannice, M. 2001. Kinetics of liquid-phase hydrogenation reactions over supported metal catalysts – a review. *Applied Catalyst A: General.* 213:1-24.

[113] Zeitsch, Karl. 2000. The chemistry and technology of furfural and its many by-products. Sugar series. Elsevier. Page 6.

[114] Dunlop, A. Peters, Fredus. 1940. Thermal Stability of Furfural. *Industrial and Engineering Chemistry*. 32:1639-1641.

[115] Dunlop, A. Peters, Fredus. 1953. The Furans. American Chemical Society Monograph Series. Baltimore.

[116] Patil, Sushil. Lund, Carl. 2011. Formation and Growth of Humins via Aldol Addition and Condensation during Acid-Catalyzed conversion of 5-Hydroxymethylfurfural. *Energy & Fuels.* 25:4745-4755.

[117] Lai, S. Vickerman, J. 1984. Carbon Monoxide Hydrogenation over Silica-Supported Ruthenium-Copper Bimetallic Catalysts. *Journal of Catalysis.* 90:337-350.

[118] Wan, Haijun. Vitter, Audrey. Chaudhari, Raghunath. Subramaniam, Bala. 2014. Kinetic investigations of unusual solvent effects during Ru/C catalyzed hydrogenation of model oxygenates. *Journal of Catalysis*. 309:174-184.

[119] Sitthisa, Surapas. Sooknoi, Tawan. Ma, Yuguang. Balbuena, Perla. Resasco, Daniel. 2011. Kinetics and mechanism of hydrogenation of furfural on Cu/SiO2 catalysts. *Journal of Catalysis*. 277:1-13.